EXES

Handbook for Archive Users

C. DeWitt, E. Montiel, M. Rashman

Rev 1.0
Date: 2023 Sep 29

REVISIONS

REV	DATE	DESCRIPTION	APPROVAL
0.0	2022/10/12	Initial Draft	
0.9	2023/09/14	Completed Draft	
1.0	2023/09/29	Final Formats	

C. DeWitt, E. Montiel, M. Rashman
September 2022

EXES Handbook for Archive Users

Table of Contents

1. ESSENTIAL INFORMATION

Table 1: EXES Instrument Overview

Full wavelength range	4.5 – 28.3 μm
Frequently observed ranges	5.3–8.0 μm, 12.8–14.3 μm, 15.8–28.3 μm
Frequency units	wavenumber [cm^{-1}] = 10^4 / λ [in μm]
Array manufacturer	Raytheon Vision Systems
Array size	1024 × 1024
Pixel Size	0.2″ × 0.2″ (25 μm × 25 μm)
Array material	Si:As IBC
Entrance window material	cesium iodide (CsI)
Main instrument configurations	High-medium, High-low, Medium, Low
Main observing modes	Off-slit nodded spectroscopy, On-slit nodded spectroscopy, Mapping
Instantaneous wavelength coverage	0.8% (medium, high-medium), 3.5-4.5% (low, high-low) of operating λ
Spectroscopy slit widths	1.44″, 2.11", 2.65", 3.20"
Spectroscopy slit lengths	> 120″ (low and medium), 1 – 12″ (high-low), 4 – 40″ (high-medium)
Spectroscopy resolutions (R = λ/Δλ)	1,000 – 3,000 (low), 10,000 – 25,000 (medium), 57,000 – 100,000 (high-low and high-medium)
Wavelength calibration accuracy	0.3 - 2.0 km s^{-1}
SOFIA observing cycles in service	Cycles 2-9
Years in service	2014 to 2022
Built by	University of Texas & University of California Davis (PI: Matthew Richter)
Instrument Paper	Richter, M. J., et al., 2018, JAI, 7, 1840013

Table 2: Science-Ready Pipeline Products

Mode	Dimension	File Type	Use
Mapping (Commissioning – Cycle 4; F0158-F366)	2D	*_WVM_*.fits (Level 2)	File that contains the wavenumber (cm^{-1}) and spatial solution (arcsec) along the slit.
		*_UND_*.fits (Level 2)	File that contains the mapping echellogram that has been flat fielded and corrected for array distortion. The units are erg s^{-1} cm^{-2} sr^{-1} (cm^{-1})$^{-1}$.
Mapping (Cycle 5 – Cycle 9; F0386-F866)	2D	*_CCR_*.fits (Level 2)	Echellogram for each map step that has been flat fielded and corrected for array distortion. An additional simple blackbody correction has been applied. The units are erg s^{-1} cm^{-2} sr^{-1} (cm^{-1})$^{-1}$.

		*_CAL_*.fits (Level 2)	The same product as the CCR, but it has been converted to Jy pixel^{-1}.
Nodding (Commissioning – Cycle 4; F0158-F366)	2D	*_WVM_*.fits (Level 2)	Wavenumber (cm^{-1}) and spatial solution (arcsec) along the slit.
		*_UND_*.fits (Level 2)	Echellogram for each nodded pair that have been flat fielded and corrected for array distortion. The units are erg s^{-1} cm^{-2} sr^{-1} (cm^{-1})$^{-1}$.
		*_COA_*.fits (Level 3)	Coadded echellogram from the UND files.
	1D	*_SPC_*.fits (Level 3)	1D extracted spectra in wavenumber (cm^{-1}) and flux units. It also contains a variance array and ATRAN model. For nod on slit data, both beams are included. In high resolution modes, all cross dispersed orders remain separated.
		*_CMB_*.fits (Level 3)	Combined 1D spectra of nod on slit beams and/or multiple SPC files of the same setting. In high resolution modes, all cross dispersed orders remain separated.
		*_MRD_*.fits (Level 3)	This contains the merged order 1D spectrum of high-medium and high-low observations.
Nodding (Cycle 5 – Cycle 9; F0386-F866)	2D	*_UND_*.fits (Level 2)	File that contains the nodded echellogram that has been flat fielded and corrected for array distortion. The units are erg s^{-1} cm^{-2} sr^{-1} (cm^{-1})$^{-1}$.
		*_CCR_*.fits (Level 2)	The same as the UND files with a blackbody slope correction applied. The units are erg s^{-1} cm^{-2} sr^{-1} (cm^{-1})$^{-1}$.
		*_COA_*.fits (Level 2)	Echellogram coadded from the CCR. The units are erg s^{-1} cm^{-2} sr^{-1} (cm^{-1})$^{-1}$.
		*_CAL_*.fits (Level 2)	The COA file converted to Jy pixel^{-1}.
		*_SPM_*.fits (Level 2)	2D spectral image equivalent of the SPC. First plane contains the flux echellogram, which could be helpful for extended sources
		*_COM_*.fits (Level 2)	2D spectral image equivalent of the CMB. First plane contains the flux

			echellogram, which could be helpful for extended sources
		*_MRM_*.fits (Level 3)	2D spectral image equivalent of the MRD. First plane contains the flux echellogram, which could be helpful for extended sources
	1D	*_SPC_*.fits (Level 2)	1D extracted spectra in wavenumber (cm^{-1}) and flux in Jy. It also contains an uncertainty array, PSG model, and an extraction of the blackbody calibration source. For nod on slit data, both beams are included. In high resolution modes, all cross dispersed orders remain separated.
		*_CMB_*.fits (Level 2)	Combined 1D spectra of nod on slit beams and/or multiple SPC files of the same setting. In high resolution modes, all cross dispersed orders remain separated.
		*_MRD_*.fits (Level 3)	This contain the merged order 1D spectrum of high-medium and high-low observations. The unit for this file is Jy.

Other Important EXES resources:
- [EXES REDUX User's manual](#)
- [EXES REDUX developer's manual](#)
- [Python Notebook on Data Inspection](#)
- [Python Notebook on Telluric Correction](#)
- [Python Notebook on Velocity Shifts](#)

2. INSTRUMENT DESCRIPTION

2.1. EXES INSTRUMENT DESIGN

2.1.1. Optics

The **E**chelon-**cross**-**E**chelle **S**pectrograph (EXES) was capable of observing from 4.5 – 28.3 μm (350-2200 cm^{-1}), at high (R ≈ 57,000–100,000), medium (R ≈ 5000–20,000) and low (R ≈ 1000–3000) spectral resolution (R = λ/Δλ). The instrument used a 1024×1024 Raytheon Vision Systems Si:As BIB detector array. High resolution was provided by an echelon—a coarsely-ruled, steeply-blazed aluminum reflection grating—along with an echelle grating to cross-disperse the spectrum. The echelon could be bypassed so that the echelle acted as the sole dispersive element. This yielded a single order spectrum at medium- or low-resolution depending on the incident angle.

EXES was a liquid helium cooled instrument. The cryostat was approximately 24 inches in diameter and 72 inches long. There were two cryogen reservoirs: one for liquid nitrogen and one for liquid helium. These were at the forward end, as mounted on SOFIA, with the entrance window on the aft end toward the telescope. There were three layers of radiation shielding within EXES: a vapor cooled shield tied only to the cryogen fill tubes, one attached to the liquid nitrogen reservoir, and the third attached to the liquid helium reservoir. All optics except for the entrance window/lens were attached to the liquid helium level. Baffling tubes connected to the liquid nitrogen level reduced thermal emission impinging on the internal optics. Within the liquid helium level, the optics were all tied to a rigid optics box constructed out of aluminum, and the detector headerboard was isolated with G10 fiberglass and was actively maintained at a uniform temperature of 7.0 K.

The EXES optics were comprised of an entrance window/lens, fore-optics, three wheels housing the slits, Dekkers and filters, an echelon chamber, and a cross-dispersion echelle chamber. The entrance window/lens (2 inches diameter) formed an image of the SOFIA telescope secondary at the liquid helium cold stop within the fore-optics. The fore-optics, including the entrance window, changed the incoming f/19 beam to f/10. After coming to a focus, the beam expanded through a pupil (at the cold stop) to an ellipsoidal mirror. The light was redirected off two flat mirrors to a focus at the slit plane.

As the beam came to a focus, it passed through the slit/filter cassette. This was composed of three wheels on a common axle containing:

(i)   filters to isolate grating orders
(ii)   Dekker to determine the length of the slit
(iii) slits of different widths

The filter wheel had 12 slots that were loaded with specific filters for each cooldown cycle based on the planned observations. Broader filters that were used for the low-resolution configuration were included in four of the Dekker wheel slots. The Dekker wheel had a total of 11 features, which included continuously variable length slits, fixed length slits, pinholes, and an open position.

The continuously variable slit length was provided by a cutout on the Dekker wheel that got longer as a function of angle. The smallest size was about 4.5 arcsec and the largest about 45 arcsec. Medium and low mode observations were not cross-dispersed and therefore did not need to use

the variable length Dekker aperture. The maximum usable length of the slit in medium or low mode was about 120 arcsec.

The slit wheel of EXES had seven fixed slit widths. The slits were laser-cut to designed values. However, in 2023 the most commonly used slit widths were revised to reconcile disagreement between the design slit width values and the scaling of blackbody fluxes from in-flight calibrations. The revisions changed the nominal widths by about ~10%, but publications before 2023 may refer to their pre-2022 values, even though nothing had changed within the instrument. Table 3 lists the widths of the seven slits available for EXES, after this revision.

Table 3: EXES Slit Widths

Slit #	Width	Comments
Slit 1	0.81″	Rarely used for science
Slit 2	1.08″	Never used for science
Slit 3	1.44″	Rarely used for science
Slit 4	2.11″	Revised from 1.84″ design value
Slit 5	2.65″	Revised from 2.4″ design value
Slit 6	3.2″	Revised from 3.15″ design value
Slit 7	9.43″	Never used for science

After passing through the slit wheel, the beam hit a flip mirror mechanism, which was used to choose between instrument resolution configurations by either directing the beam into the echelon chamber (high-resolution) or into the cross-dispersion chamber (medium- and low- resolution). In the high-resolution configuration, the beam entered the echelon chamber and expanded to an off-axis hyperboloid mirror that served as both collimator and camera mirror for the echelon grating. The dispersed light, focused by the hyperboloid, bounced off a flat mirror into the cross-dispersion chamber.

The cross-dispersion chamber was conceptually similar to the echelon chamber. The light expanded from the input to an off-axis paraboloid that again served as both collimator and camera mirror. The collimated beam was sent to the cross-dispersion grating, which dispersed the light in the plane of the grating. The camera mirror sent the light to the detector. When EXES was operated in single-order, long-slit spectral configurations—the medium- and low-resolution science configurations—the light never entered the high-resolution echelon chamber.

There was a wheel in front of the detector, which provided a lens for imaging the pupil through the instrument, and a dark slide for isolating the detector. This wheel was available for including transmissive optics to adjust the plate scale on the detector, if desired.

2.1.2. Detector

The detector was a Raytheon Vision Systems Si:As BIB array (blocked impurity band) with 1024x1024 pixels and two sets of four reference pixel columns located on either side of the photosensitive part of the array. The detector's pixels were 25 μm × 25 μm. The EXES detector array was identical to the three that are flown on JWST/MIRI, but the readout electronics are different. The detector material was bonded to a SB 375 multiplexer. The array was mounted in a separate enclosure to reduce scattered light. The headerboard was thermally isolated from the rest of the optics box to permit active temperature control of the array to the optimum temperature, 7.0 K. The raw detector array counts were between 11000 and 3500 DN, with increased integration reaching smaller DN values, and saturation occurring near 3500 K. Detector linearity was measured to be less than 5% at net DN values of 5000, and in most instances, the depth detector was used below 3000 net DN. Consequently, no linearity correction was applied to the mission data.

The minimum integration time while using the full 1024×1024 frame was one second. There was no risk of saturating the detector in the high-resolution modes, but for medium and low configurations, the background flux could easily exceed the array non-linearity in one second, particularly at wavelengths longer than 8 μm. One solution to this was to go into a subarray which reduced the number of rows and restricted the spatial coverage. The most common choices were to subarray to 512 or 256 rows, which permitted observations with background fluxes 2× and 4× higher than full frame modes, respectively. The drawback was that the effective slit length was reduced by the same amount, but this was of little consequence in the majority of cases when point sources were observed.

For a few projects, even subarrays were insufficient to reduce the flux adequately and in these rare cases, the detector bias voltage was reduced from its standard value 2V to lower the sensitivity. This method was successfully employed for the observation of Sakurai's object and its calibrator, Callisto (Woodward et al 2020). There was also an early science program to observe protostellar ices (AOR_ID =86_0005) that also used a lowered bias, but these data were deemed to have been unusable at that time due to the instability of the fringes. Table 4 lists the entirety of cases where a lowered bias was used for science observations.

Table 4: Data Taken with Reduced Detector Bias Voltage

Program	Target	Mode	Wavenumber (cm⁻¹)	Voltage (V)
06_0095	Sakurai's object	LOW	547	0.7
06_0095	Callisto	LOW	547	0.7
86_0005	Vega	LOW	1412, 1444, 1476	Unknown
86_0005	W3 IRS 5	LOW	1412, 1444	Unknown
86_0005	NGC 7538 IRS 1	LOW	1412, 1444, 1476	Unknown

2.2. INSTRUMENT CONFIGURATIONS AND OBSERVING MODES

This document will refer to instrument configurations and observing modes. Instrument configurations are the setup of the EXES motorized mechanisms, including the spectrograph fold mirror, slit, Dekker, and echelle grating angle. Observing modes refer to how the telescope was moved during data collection.

Past EXES documents and publications may mix the nomenclature that is adopted for this document, like "High-resolution mode" or "medium-resolution mode", but for clarity, this document will follow the above convention. Figure 1 shows the relationships between the configurations and modes that are possible with EXES.
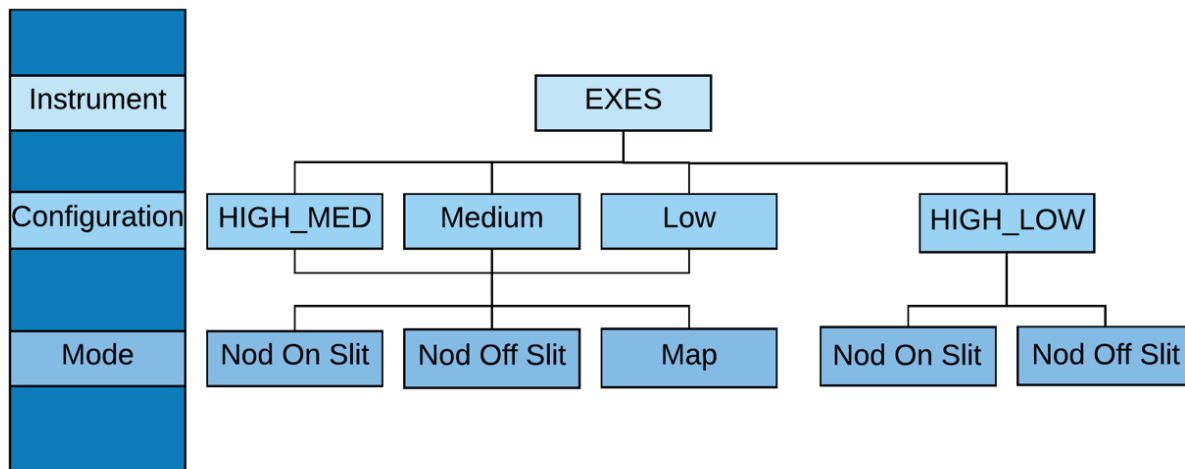

Figure 1 *EXES instrument configurations and observing modes.*

2.2.1. Instrument Configurations

EXES had three spectral resolution ($R = \lambda/\Delta\lambda$) regimes—high, medium, and low— with the exact resolving power depending on wavelength, grating angle, and slit width. Generally, the resolution will be higher at shorter wavelengths in each regime.

2.2.1.1. *High-Medium and Low Configurations*

The high-resolution configurations, which used the echelon grating along with the echelle grating to cross-disperse the spectrum, achieve R = 59,000 – 100,000. If the cross-disperser echelle angle was 35–65°, then the configuration is called high-medium (INSTCFG = "HIGH_MED"); if the angle is 10–25°, then it is called high-low (INSTCFG = "HIGH_LOW"). For these high-resolution configurations, there were non-continuous spectral coverage for $\lambda > 19$ μm due to the orders being larger than the EXES array. The size of the gaps gets larger with wavelength. The gap width is the same for high-medium and high-low mode. Table 5 describes the coverage gaps for four wavelength ranges of the high-medium and high-low configurations.

The position of the coverage gaps could be adjusted with the "dispersion screwdriver", which tilted the camera/collimator mirror of the echelon spectrograph chamber. Some observations required

these shifts to cover a particular spectral feature, but whether these shifts were employed will have no practical impact for the end user of the data. The dispersion driver was unneeded for science programs after Flight 400, and thus was unused for remaining Flights F514-F866.

The maximum plate scale was 0.201″ pixel^{-1} but this value was foreshortened by anamorphic magnification from the echelle cross-dispersion grating. High-medium configurations used the largest grating angles, and the plate scale could be as small as 0.16″ pixel^{-1}. High-low configurations were usually about 0.19″ pixel^{-1}. The pipeline automatically updates the keyword "PLTSCALE" for data products and propagates the correct values.

Table 5: High-Medium/High-Low Configuration Coverage Gaps between Orders

Wavenumber (cm^{-1})	Wavelength (μm)	Coverage (%)	Gap (%)
1886 – 525	5.3 – 19	100	0
500	20	94	6
400	25	77	23
354	28.3	67	33

2.2.1.2.   *Medium and Low Configurations*

The medium and low configurations arose from bypassing the echelon and only using the echelle grating. Similar to high-medium, medium used steeper angles on the echelle grating to achieve R = 5,000– 20,000. The low configuration, again similar to high-low, used shallower angles to achieve R = 1,000–3,000. The medium and low modes had continuous coverage at all wavelengths, but the longest wavelengths used for medium or low modes during the mission were 17 μm and 18.2 μm, respectively, where high-resolution also would have had continuous coverage. The plate scale for medium and low configurations are not affected by anamorphic magnification and are always 0.201″ pixel^{-1}.

EXES also had configurations for field imaging and pupil imaging, but these were only used for instrumental alignment at the beginning of each flight series. The field imaging configuration was used to measure the angle of the slits with respect to the guider camera and telescope control drives so that the telescope could control motions that were parallel and perpendicular to the slit. These alignment observations were done using narrow band filters centered between 4.7 -5.3 μm to limit the count rate and avoid saturating the detector. No imaging or pupil imaging products were used directly for science programs, and they are not included in the archive.
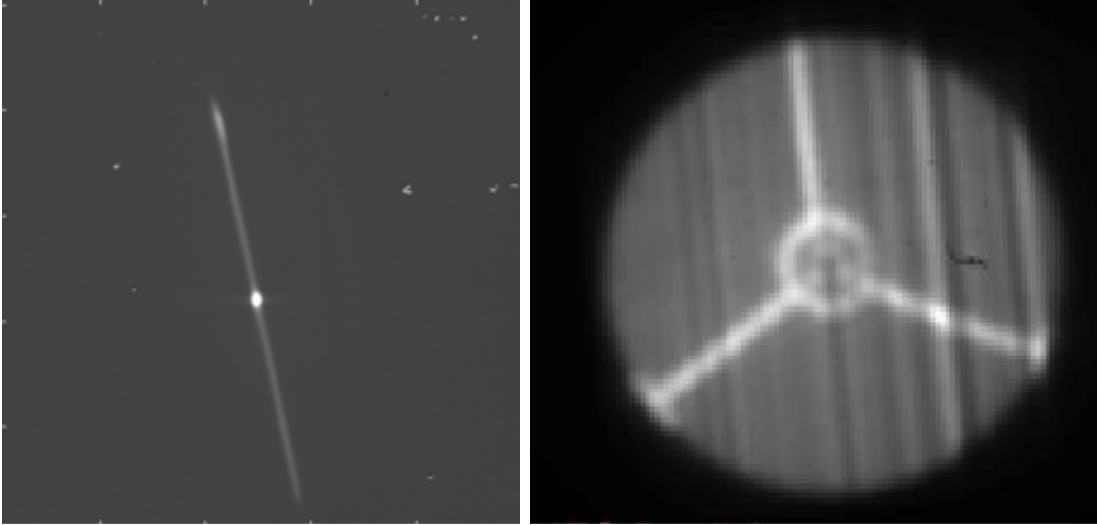
Figure 2 *(Left) EXES field imaging configuration, used for defining the slit boresight and angle with respect to the telescope, usually during the first observation on the first flight of an observing series. Once located, the boresight did not change much during the flight series, aside from ~1 arcsec changes due to instrument /guider flexure. (Right) EXES pupil image, with secondary supports in view. The internal EXES cold stop blocked scattered light from the perimeter of the secondary mirror.*

2.2.1.3. Trade-offs Between High-Medium and High-Low Configurations

The difference between high-medium and high-low modes was the degree of cross-dispersion set by the echelle grating angle. High-angles provided the most dispersion, splaying the orders as far as the operable limits of the grating and maximizing the height of the slit to between $5 - 40''$, depending on the wavelength and order.

When the slit height was about $4\times$ the PSF size, it was usually beneficial to nod point sources on the slit, which would increase the fraction of time integrating on source from 50% to 100% when compared to nodding off slit. The S/N was expected to increase by a factor of $\sqrt{2}$. This mode of observation was the most efficient possible for EXES in high-resolution.

High-low sources used the echelle grating at low angles to maximize the number of orders recorded on the detector. EXES observed with a $1.5 - 3.5''$ fixed Decker length when in these modes, which meant light losses were just as high as from the slit width dimension.

There was maximal blaze efficiency at usually only one high-medium order and one high-low order, and the instrument team always selected the best or near the best echelle order that met the needs of the observation. Generally, when the goal was to maximize spatial coverage or sensitivity, high-medium was selected. High-medium mode was used on sources > 20 Jy and typically > 100 Jy.

When the goal was to maximize spectral coverage, high-low mode was selected. High-low mode was only attempted for sources with F > 50 Jy, with 100s of Jy sources being far more typical.

Figure 3 shows the optimum high-med order for 741 cm⁻¹ (13.5 µm) and 1496 cm⁻¹ (6.8µm). Other echelle orders between these were achievable but had high costs due to the lowered grating efficiency.
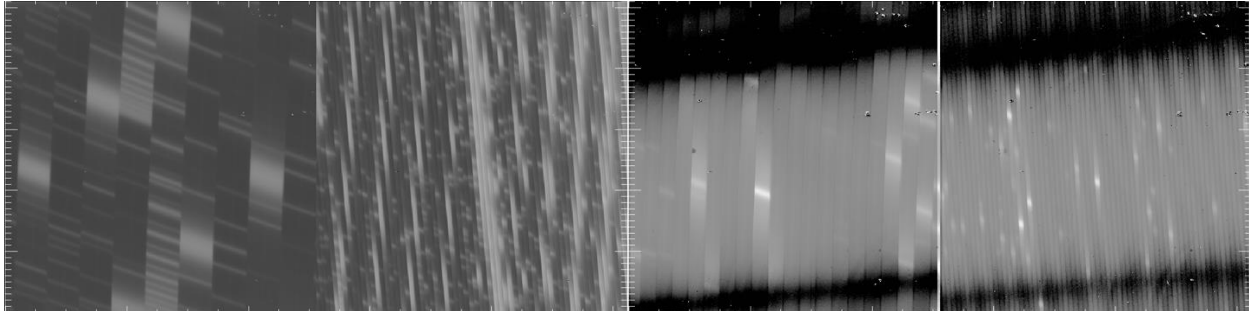

Figure 3 *From left to right: 741 cm⁻¹, 4ᵗʰ order; 722cm⁻¹, 1ˢᵗ order; 1496cm⁻¹, 8ᵗʰ order; 1496cm⁻¹, 4ᵗʰ order. The images above show the sky emission spectra before nod-subtraction and order rectification.*

2.2.2. Observing Modes

There were three science observing modes possible with EXES: Nod On Slit, Nod Off Slit, and Map. Each is discussed below.

- **Nod On Slit:** The telescope was nodded along the slit at distances that kept the target within the slit length. The nod throw was typically half the slit length. Typically, the nod period was set to between 30 – 120 seconds.
- **Nod Off Slit:** The telescope was nodded from the target to a blank sky position. This was used for extended sources, or generally when the slit length was shorter than 10 arcsec, (e.g., when the PSF was larger than four times the slit length.) Like Nod_on_slit mode, the nod interval was typically set to between 30 – 120 seconds.
- **Mapping:** The telescope was moved perpendicular to the slit while EXES took spectra on a grid of telescope positions, which were always one-dimensional stripes. At the end of the slit scan of the target, the telescope was moved to a chosen off-sky position to observe three integrations of the sky for the purpose of background subtraction.

The integration time per step was typically between 2-6 seconds in mapping mode. EXES did not use the secondary chopper for any observing modes.

3. INSTRUMENT PERFORMANCE

3.1. COORDINATES, POINTING, AND PEAK-UP

Every observation began with the source acquisition, where the telescope was pointed to the planned coordinates contained in the AOR of the observation. The header keywords "OBSRA" and "OBSDEC" record this position. The pointing accuracy of the initial acquisition was expected to be accurate to 1″ (Temi et al. 2018).

3.2. POINT SOURCES

If the target was a point source (or at least point-like), then the instrument team refined the telescope pointing by moving the telescope by sub-arcsecond motions parallel and perpendicular to the slit, until the flux from the target to the detector was maximized. This was called the peak-up procedure. Based on the flux sensitivity to these iterative peak-up positions, the boresight could be located over the flux peak to within ~0.25″.

Peak-up nods were saved files with ".peakup." in the raw filename. They can be reduced by the pipeline with the same flat field used for the regular nodded files. In most cases, the peak-up integration time was negligible, and inclusion of those files could even contribute noise and are usually omitted from the reductions in the archive.

While relative centering on point sources after peak-up should be accurate to within 0.25″ of the IR peak, the precision of the RA and DEC header values for the observation are unchanged.

Sometimes the boresight centering would drift over long integrations, and nod-pair strengths would fall with time. The choice to keep integrating or re-acquire the target with peak-up nods was made by the observing team based on the severity of the flux loss and the remaining observing time available. Some IR-only targets were located at several arcseconds offset from their planned coordinates, due to when proposers mistakenly used submm coordinates that were at an offset to the mid-IR coordinates.

3.2.1. Extended sources

Extended sources did not permit boresight refinement with the peak-up nod procedure. For these observations, the pointing accuracy was the 1″ uncertainty in the initial acquisition. It is possible to utilize the archive of FPI guider images taken during the observations to make a refined measurement of the RA and DEC of the EXES boresight (SIBSXFPI, SIBSYFPI), and thereby derive the accurate mid-IR coordinate, but this is beyond the scope of this manual.

3.2.2. Observations with More Elaborate Peak-up Procedures

A small number of observations needed more complicated procedures to ensure the correct target in the slit. These special cases with two-step procedures are noted in the header history for those observations.

- The Orion IRc2 survey (05_0043) was always centered on the flux peak at 1280-1370 cm^{-1} (7.3-7.8 μm) to avoid confusion with other sources that dominate the BNKL at the longer survey wavelengths. (See Nickerson et al. 2023).

- The target wavelength for Europa (05_0153) was 6.1 μm, where its continuum was too weak for EXES to detect. Instead, a procedure was adopted to peak-up at 19 μm by rotating the filter and leaving the other mechanisms in place. After Europa was confirmed to be centered, the 6.1 μm was rotated back in and the science observation proceeded (see Sparks et al. 2019).

- The embedded HMYSO W51A IRS2E is close to a second bright mid-IR peak, IRS2W. The peak-up procedure therefore confirmed 2E was reached by offsetting to IRS 2W and then back to IRS 2E.

3.3. IMAGE QUALITY

The point-spread function (PSF) size is needed for understanding the beam and dilution in extended source observations or to estimate the slit loss factors for correcting the fluxes of point sources. The image quality of EXES observations was usually dominated by the wavelength of the observation and by the telescope's performance, which could vary during the flight due to turbulence, weather, and telescope elevation. The average image quality generally improved over the mission due to advances in the temperature/focus compensation, a flexible body compensator for the secondary mirror, and active mass dampers for the primary mirror.

While telescope control and observing conditions usually dominated the imaging performance, in EXES Flights 743-750 a manufacturing defect caused the CsI entrance window into EXES to deform under the vacuum pressure. The image size on those flights was degraded to FWHM ~ 4″, and temporal variations and asymmetries were observed in the spatial PSF shape.

Since EXES was a slit fed spectrograph, there were limited opportunities to measure the true 2D image quality. However, observations of point sources with sufficiently long slits could be used to estimate the image quality, by assuming radial symmetry for the PSF. Figure 4 shows an example of a spatial profile from an EXES observation in the high-medium configuration.

Table 6 lists the representative PSF sizes which are measured using the 1D spatial profile along the slit height of the 2D spectra (COA or CAL) for observations during a flight series.
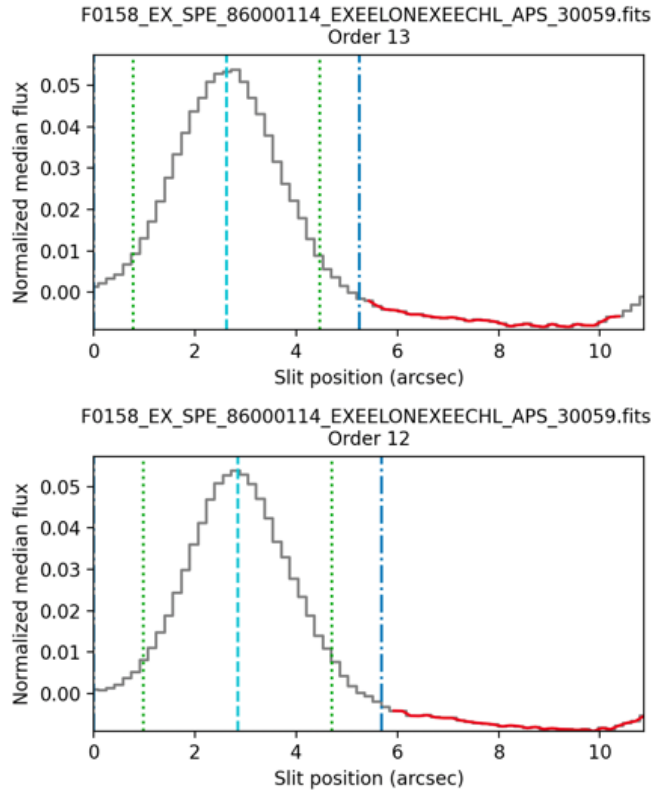
F0158_EX_SPE_86000114_EXEELONEXEECHL_APS_30059.fits
Order 13

F0158_EX_SPE_86000114_EXEELONEXEECHL_APS_30059.fits
Order 12

Figure 4 *Pipeline spatial profiles for a point source observed with EXES in a high-medium configuration can be used to estimate the image quality.*

Table 6: PSF Size by Flight Series and Wavelength, Estimated from 1D Spatial Profiles

Flights	Flight Series	Dates	6μm (″)	14μm (″)	25μm (″)
158-159	Commissioning	Apr 2014	2.4-3.5	2.5	3.0
194-198	OC3A	Feb-Mar 2015	2.2	2.5	2.9-3.2
235-237	OC3H	Sep 2015	2.2	2.4	2.9-3.2
288-291	OC4C	Mar 2016	2.3	2.6	3.2-3.4
362-366	OC4M	Jan 2017	2.5-3.0	2.2	-
386-391	OC5C	Mar 2017	2.3-3.5	-	2.9-3.2
398-400	OC5F	May 2017	2.1-2.9	-	2.8
514-523	OC6L	Oct-Nov 2018	2.1-2.4	2.6	-
553-560	OC6S	Apr 2019	2.1-3.0	2.1-2.3	2.5-3.1
658-661	OC7K	Feb 2020	1.7-1.9	2.0-2.1	2.7-2.8
743-750	OC8N	Jun 2021	4	4	4
797-799	OC9G	Dec 2021	1.7	2	2.6
829-838	OC9K	Feb-Mar 2022	1.7	1.9	2.6
859-866	OC9O	Apr-May 2022	1.6	1.9	2.5

Note − "-" indicates that there were no suitable observations for spatial PSF measurements.

3.4. WAVENUMBER / WAVELENGTH SCALE ACCURACY

Only data taken after Flight 386 (March 2017) was included in the post-mission reprocessing. Table 7 - Table 9 contain the wavelength accuracies for the reprocessed data (Flights 386-866).

The wavenumber scale of EXES data is calibrated using the vacuum wavenumbers of atmospheric sky lines that fell in the wavelength range of the observation. Additional details of the method and the known systematic errors are located in Section 4.3. Below are the 1-σ velocity uncertainties listed by mode and wavelength. Velocity uncertainties can be converted to wavenumber or wavelength via:

$$\sigma_{wn} = \sigma_v * wn / c$$
$$\sigma_\lambda = \sigma_v * \lambda / c$$

where $c = 2.998 \times 10^5$ km s^{-1}.

Table 7: 1-σ Wavenumber Errors in High-Medium and High-Low Configurations

Central wavenumber (cm^{-1})	Central wavelength (μm)	σ_v error (km s^{-1})
354 – 525	19.0– 28.3	0.5 - 1.0
525 – 642	15.6 – 19.0	0.15 - 0.24
700 – 900	11.1 – 14.3	0.16 - 0.22
1200 – 1400	7.14 – 8.3	0.16 - 0.19
1400 – 1900	5.3 – 7.14	0.3

Table 8: 1-σ Wavenumber Errors in Medium Configuration

Central wavenumber, (cm^{-1})	Central wavelength (μm)	1-σ error (km s^{-1})
535-1111	9.0-18.7	1.0
1362-1835	5.5 – 7.3	0.5

Table 9: 1-σ Wavenumber RMS Errors in Low Configuration

Central wavenumber, (cm^{-1})	Central wavelength (μm)	1-σ error (km s^{-1})
1430-1700	5.9-7.0	2.0
547	18.3	3.0

3.5. INTENSITY AND FLUX ACCURACY

Only data taken after Flight 386 (March 2017) were included in the post-mission reprocessing, and earlier data on the IRSA archive is unlikely to have correct flux scaling because of erroneous calculations in the pipeline versions used at that time. It should be emphasized that this early data

is still "scientifically ready" for most applications. <u>Table 10</u> and <u>Table 11</u> summarize the intensity/flux calibration status of IRSA archive contents. More details can be found in Section <u>4.4</u>.

3.5.1. Extended Sources and 2D Flux Accuracy

The EXES flux calibration procedure is designed to scale 2D intensities of extended targets to the known flux of an internal blackbody source. Extended source observations are fully flux-calibrated by the pipeline in Level 2 and Level 3 products. The data taken on flights F158-F366 was last reduced in 2014-2017 with an older pipeline and does not produce accurate intensities. Data taken on F386-F400 has intensities scaled too high due to the flat fielding procedure. Based on the empirical behavior of point source fluxes from the reprocessed data of this period (Section <u>4.5</u>), the intensity can be corrected with a factor of ×0.8, and the resulting intensity uncertainty will be approximately 10%. Data taken on F514-F866 should have the best possible intensity accuracy available for EXES data. Intensity values should be assigned an uncertainty of 10% at all wavelengths.

Table 10: Intensity Calibration Status of the Data in the IRSA Archive by Flight

Flight Numbers	Dates	Flux Calibrated?	Intensity Error
F158 – F366	Apr 2014 – Jan 2017	No, due to early pipeline errors	N.A.
F386 – F400	Mar 2017 – May 2017	Scaled ×1.25 too high	10%*
F514 – F866	Oct 2018 − May 2022	Yes	10%

After scaling by ×0.8.

3.5.2. Point Source Flux Accuracy

Point source fluxes are all underestimated in the 1D extracted pipeline products because of light losses at the slit. Slit throughputs varied wildly, between 50% - 90%, because the losses varied with the slit width and slit height and the imaging conditions during the integration. Section <u>4.5</u> provides guidance for estimating slit losses to produce more accurate point source fluxes.

When these slit loss corrections are performed, the resulting point source fluxes were found to be accurate to 13% for configurations with a slit height > 5" (which includes all HIGH-MEDIUM MEDIUM and LOW configurations as well as HIGH_LOW configurations with WNO0 < 530 cm^{-1}) and 17% for configurations with slit height less than 5", which includes all HIGH_LOW configurations between 530 – 2000 cm^{-1} (5-19 μm).

It should be noted that the majority of the EXES science program goals did not require absolute fluxes for point source observations. The spectroscopic features under investigation were often absorption lines, which are usually analyzed after the continuum is normalized to 1.0. In cases where the absolute point source flux is needed, such as emission line analysis, there are frequently archival flux measurements available (such as ISO/SWS or Spitzer) that are sufficient.

Table 11: Point Source Flux Calibration for the IRSA Archive by Flight Series

Flight Numbers	Dates	Flux Calibrated?	Flux Error (Slit height < 5")	Flux Error (Slit height > 5")
F158 – F366	Apr 2014 – Jan 2017	No, due to early pipeline errors	N.A.	N.A.
F386 – F400	Mar 2017 – May 2017	Scaled ×1.25 too high	13%*	17%*
F514 – F866	Oct 2018 − May 2022	Yes	13%	17%

* After scaling by x 0.8.

3.6. SPECTRAL RESOLUTION

Spectral resolution, defined as $R = \lambda/\Delta\lambda$, depends on central wavenumber, instrument configuration, and slit width. To a smaller degree it also depends on whether the source is a point source or an extended source. Point sources experienced diffraction at the slit edges, which tended to sharpen the slit image on the grating and boost the spectral resolution. The resolution boosting effect became stronger at long wavelengths. In Table 12 the point source resolution was measured at three wavelength regimes of the EXES wavelength operating range. Resolution values were calculated by applying Gaussian broadening to transmission models to data until a best matching R value was reached. If resolution values better than 3% are needed, this approach on the data set of interest should be used for derivation.

The representative values below are included in the pipeline reductions and used to broaden the transmission model to the appropriate R. They are also recorded in the header keyword RP.

Table 12: Point Source Resolutions for High-Medium and High-Low Configurations

Slit width (″)	R = $\lambda/\Delta\lambda$
354 - 637 cm^{-1} (15.7-28.3 μm)	
1.44	-
2.11	94000 +/- 2500
2.65	74845 +/- 2500
3.20	61981 +/- 2500
667 - 909 cm^{-1} (11-15 μm)	
1.44	-
2.11	92000 +/- 2500
2.65	73253 +/- 2500
3.20	60663 +/- 2500
1000 -1888 cm^{-1} (5.3-10 μm)	
1.44	105000 +/- 2500
2.11	90000 +/- 2500
2.65	71660 +/- 2500
3.20	59344 +/- 2500

3.6.1. Resolution for Extended Sources in High-Medium and High-Low Configurations

The spectral resolution of extended emission sources is unaffected by diffraction resolution boosting because the on-axis light diffracted away from the slit gets filled in by diffracted off-axis emission. As a consequence, spectral resolution for extended sources will match the resolutions measured against sky emission lines or a laboratory gas cell.

Table 13 has the resolutions for extended sources by slit, which were measured at 1330 cm^{-1} and 735 cm^{-1} (7.5 and 13.5 μm) with a C_2H_2 gas cell from the ground. The values were not seen to change with wavelength, but wavelengths longer than 13.5 μm were untested for extended emission resolution because of a lack of available gas cell features or sky emission lines that were sufficiently narrow. The resolutions in this table supersede the header keyword RP values, when the target is an extended source (which are only applicable for point source observations).

Table 13: Extended Source Resolutions for High-Medium and High-low Configurations

354-1888 cm^{-1} (5.3-28.3 μm)	
Slit width (″)	R = λ/Δλ
1.44	105600 +/- 2500
2.11	85500 +/- 2500
2.65	71600 +/- 2500
3.20	57300 +/- 2500

3.6.2. Resolutions of Medium and Low Configurations

Medium and low modes have continuously variable resolution values that depended on the echelle grating angle, which could take any value between 0-70°. In reality, there were only a limited number of medium and low-resolution observations which were repeatedly observed for different targets.

The resolution was derived for every case and the "RP" keyword value in the header was updated accordingly. In cases where the target source was point-like, the resolution value was determined by matching the broadening of the transmission. If it was an extended source, the resolution was measured on sky emission lines. Table 14 contains a subset of the medium resolution determinations.

Table 14: A Subset of the Medium Resolution Determinations

Slit Width (″)	Wavenumber (cm^{-1})	Source Type	R = λ/Δλ
2.65	1748 – 1830	Point source	R=13600+/-150
2.65	1486	Point source	R=10600+/-150
2.65	1447	Extended source	R=9250 +/- 250
3.2	1447	Extended source	R=7750 +/- 250
3.2	1430	Extended source	R=9700 +/- 800

Low resolution configuration was used even less frequently than medium configuration, and in this case, even the target names can be named in one table. The "RP" value is corrected and

included in the headers for these files. All low configuration targets were point sources. Table 15 contains all the low-resolution mode targets taken in the post-mission reprocessing interval.

Table 15: All Low-Resolution Mode Targets Taken in the Post-Mission Reprocessing Interval

Slit Width (″)	Wavenumber (cm⁻¹)	Targets	R = λ/Δλ
2.65	1430 -1700	Cyg OB2-12 / Vega	R=2200 +/- 250
2.65	547	Sakurai's Object / Callisto	R=1500 +/- 250
3.2	1345	IC 5117, NGC 6886, etc.	R=1900 +/- 250

4. DATA

4.1. DATA PRODUCTS DESCRIPTIONS

4.1.1. EXES filename conventions

Raw files in the archive have the following naming convention:

> *[targetname].[sci/flat/peakup/dark].[FN].fits*

`[targetname]` is a file stem name chosen by the observing team. Some examples of raw data filenames are:

```
jupiter.flat.80037.fits
acma.sci.05022.fits
ngc2071.sci.30064.fits
```

where [`sci/flat/peakup/dark`] indicate the type of file. "`sci`" may either be a "`stare`" at the sky, "`nod`" or "`map`". "`dark`" indicates that the beam to the detector was blocked internally by either the lens wheel mirror or the slit wheel mirror or both at the same time. These files are used to find the detector reset levels and to measure scattered light internal to the spectrograph. "peakup" files are nodded observations used to adjust the boresight to maximize the flux through the slit for point sources. As discussed in Section 3.1, they are usually excluded from the reductions.

[`FN`] is the 5-digit file number, which was sequentially taken on each flight. About 100 data files were taken with EXES during a typical full-length SOFIA flight. The first flight of each series started the file number with 10000 and the value on each subsequent flight was incremented by 10000. On the few occasions when a 10th flight in a series was reached, the [`FN`] of the 10th flight file numbers would start with 05000 or 95000. The [`FN`] is carried over to the reduced products, but the stem of the raw filename is dropped to follow the naming conventions of the Redux pipeline.

Raw data can be retrieved by selecting "Level 0" products on the IRSA archive pages.

Reduced products from the SOFIA REDUX pipeline for EXES are named according to the following convention:

> *FILENAME = F[flight]_EX_SPE_AOR-ID_SPECTEL1|SPECTEL2_Code_FN1[-FN2]*.fits,

where *flight* is the SOFIA flight number, *EX* is the instrument identifier of EXES, *SPE* specifies that the file is a spectrum, *AOR-ID* is the AOR identifier for the observation, *SPECTEL1|SPECTEL2* is the keyword specifying which gratings were used, *Code* is three letters identifying the product type (listed in Section 4.1.4), and *FN1* is the file number which corresponds to the raw data input file. *FN1-FN2* is used if there are multiple input files for a single output file, where *FN1* is the file number of the first input file and *FN2* is the file number of the last input file.

SPECTEL1 can take a value of "EXEELON" which means the high-dispersion echelon grating was used in either the high-low or high-medium mode (and data is cross-dispersed) or NONE, when the echelon was bypassed for a single order spectrum in the LOW or MEDIUM resolution mode. *SPECTEL2 will only have a value of* EXEECHL, indicating that the echelle grating was used, either as a cross-disperser for HIGH_LOW or HIGH_MED, or as the primary disperser for LOW and MEDIUM modes.

This document will refer to file types by their 3-letter code – e.g. FLT, COA, or MRD to explain content and use of the data.

4.1.2. Pipeline Versions

During the operating lifetime of SOFIA, all EXES data was reduced and delivered to the SOFIA archive using an IDL-based pipeline "EXES_REDUX" (Clarke et al. 2015). The IDL pipeline was continually improved by the instrument team during the mission, but the changes were generally undocumented and the version number was not incremented. Data with header keyword `PIPEVERS = 1_0_2` means that a version of the IDL pipeline was used.

Near the end of the SOFIA mission, the EXES pipeline was rewritten in Python, and it was also called "EXES_REDUX". Data with header keyword `PIPEVERS= 3_0_0dev` used the Python version of REDUX.

All EXES data taken from Cycle 5 - Cycle 9, Flights F386-F866, was reprocessed after the mission using the Python version of REDUX.

4.1.3. Pipeline physical units and common conversions

All EXES data uses wavenumbers and is in the telecentric frame of reference (i.e., in relation to the telescope at the time of observation). Atmospheric lines are assumed to be at their vacuum rest frequencies.

Wavenumbers in cm^{-1} can be converted to microns (μm) with this formula:

$$\lambda = 10000/wn \ [cm^{-1}]$$

or to Gigahertz GHz by:

$$\nu = 30 \times wn \ [GHz]$$

EXES intensity units (the flux per solid angle) are in ergs s^{-1} cm^{-2} sr^{-1} $(cm^{-1})^{-1}$ and are used in the CCR and COA files.

To obtain Jy arcsec^{-2} instead, multiply ergs s^{-1} cm^{-2} sr^{-1} $(cm^{-1})^{-1}$ by 78.4.

1D extracted fluxes are always in Jansky (Jy), where 1 Jy = 10^{-23} erg s^{-1} cm^{-2} Hz^{-1}.

The pipeline optionally creates an intermediate file with the code "CAL" when 2D intensity planes are converted to 1D fluxes. CAL files look like the COA file, but they are scaled so that each pixel

value has been integrated over its solid angle, to obtain the pixel flux in Jy. For more details of the conversion, see the CAL file description in the following section (Section 4.1.4).

4.1.4. Pipeline Products description

The Python version of REDUX (`PIPEVERS=3.0.0dev`) produces the following products during the 1D spectral extraction phase:

4.1.4.1. SPM, SPC

The SPM is the first of the new 2D spectral images produced by the pipeline. It is a multi-extension FITS file. The first seven extensions contain the 2D: flux, error, mask, flat, wavenumber calibration, spatial calibration (e.g., position along slit width), and order mask. These come directly from the coadded (*COA*, intensity units: ergs s^{-1} cm^{-2} sr^{-1} (cm^{-1})$^{-1}$), or the version converted to flux units (*CAL*, flux units: Jy/pixel). The eighth plane is the PSG complete atmospheric transmission (wavenumber, total transmission, and individual molecules; see Section 4.1.6) for the observation. The remaining number of extensions are determined by the number of orders, which are: flux, error, flat, wavenumber position, slit position, spatial map, spatial profile, aperture mask, spectral flux, spectral error, transmission, and response. These extensions are a combination of 1D and 2D arrays, and the spectral flux units are either in intensity (ergs s^{-1} cm^{-2}(cm^{-1})$^{-1}$) or flux (Jy) depending on the choices made earlier in the pipeline.

The corresponding 1D product is the SPC and is comprised of a single extension. It has a "traditional" multi-dimensional array, which contains the wavenumber, flux, error, total transmission from the PSG model, and response. Similarly, the flux plane units for these are either in ergs s^{-1} cm^{-2}(cm^{-1})$^{-1}$ or Jy, which again depend on the choices made earlier in the pipeline.

For nod on slit observations, the positive and negative beams remain independent. For high resolution observations, the cross dispersed orders remain unmerged. Finally, the choice in units established here will remain the same for the remaining generated pipeline products (e.g., for a single source, SPM/SPC, COM/CMB, and MRM/MRD will always have the same units).

4.1.4.2. COM, CMB

The COM is similar to the SPM, but both/either the positive and negative beams and/or multiple individual observations have been robustly combined into a single spectrum. It is still multi-extension, and cross-dispersed orders remain unmerged (high-resolution modes only). The first two extensions are the 2D flux and error. The third plane, like in the SPM, is the complete PSG atmospheric transmission model for the observation. The remaining extensions, which are determined by the number of orders, are: the flux, error, flat, wavenumber position, spectral flux, spectral error, transmission, and response.

The corresponding 1D product is the CMB and is comprised of a single extension. It has a "traditional" multi-dimensional array, which contains the wavenumber, flux, error, total transmission from the PSG model, and response.

4.1.4.3. MRM, MRD

The MRM is the final new 2D spectral image product and is made only for high-resolution mode observations. It is when the multiple cross dispersed orders have been merged into a single spectrum. It is also multi-extension and they are: flux, error, wavenumber position, spectral flux,

spectral error, PSG atmospheric transmission, and response. Note that the PSG transmission extension in this file is [*,12] where wavenumber has been dropped from the array (use the wavenumber position extension).

The corresponding 1D product is the MRD and is comprised of a single extension. It has a "traditional" multi-dimensional array, following the format of the MRD generated by the IDL pipeline, which contains the wavenumber, flux, error, total transmission from the PSG model, and response.

- *Cycles 2 – 4:* The data from these cycles have only been processed with early versions of the IDL version of the pipeline. The 1D products are the SPC, CMB, and MRD.

Pipeline Product that are 2D Echellograms:
- *Cycles 5 – 9:* RDC, FLT, UND, CCR, COA, and CAL
- *Cycles 2—4:* RAW, WVM, FLT, UND, and COA

All EXES 2D echellograms have dimension NAXIS1 × NAXIS2 = 1024 × 1024 unless the sub-array mode was used for an observation, where NAXIS2 has been reduced.

4.1.4.4. RDC/RAW

The first products created by the pipeline from the flat/sci/dark files taken in-flight are either RAW (commissioning – Cycle 4; IDL) or RDC (Cycle 5 – 9; Python). These files are bias subtracted, and have their headers reformatted to be compatible with passing through the remaining steps of the pipeline. The IDL RAW flies are single extension and the first half of the third dimension are the observations, while the second half contains the variance plane. The Python RDC files are multi-extension. The first plane contains the observations, the second plane the uncertainty, and the third plane the bad pixel mask. These products are "Level 2" in both versions of the pipeline.

4.1.4.5. WVM and FLT

The WVM (commissioning – Cycle 4; IDL) was a single extension FITS file that contained an echellogram with the wavenumber calibration and slit height. It was a "Level 2" product. The WVM was folded into the sixth and seventh extensions of the Python FLT file.

The FLT made by the IDL pipeline was a singe extension FITS file containing the undistorted echellogram of the EXES blackbody source. Note that this echellogram is not rotated for high resolution mode. The FLT in the Python version of the pipeline became a multi-extension FITS file containing: the distorted flat, the standard deviation of the distorted flat, the undistorted flat, the standard deviation of the undistorted flat, the illumination, wavelength calibration, slit height, and order masks. The undistorted flat observations are rotated for high resolution observations. The illumination echellogram simply highlights which parts of the EXES array did or did not receive signal. The order mask extension is an echellogram that notes which orders landed where for cross-dispersed observations. The FLT is a "Level 2" product for both versions of the pipeline.

4.1.4.6. UND

The UND product is the 2D echelleogram of an observation that has been nod/sky (mapping) subtracted and corrected for the distortions from the optics (e.g., undistorted). The images have been resampled onto a regular grid of spatial and spectral elements and the dispersion and spatial

axes aligned with the rows and columns. The UNDs made by the IDL version of Redux are single-extension FITS files. They contain the flux (first half of the 3D array) and variance (second half of the 3D array). The UNDs for high resolution modes have not been rotated. For the Python version of SOFIA Redux, these are multi-extension FITS files, and the extensions are: flux, error, mask, flat, wavenumber calibration, spatial calibration (e.g., position along slit height), and order mask.

The individual nod subtracted pairs have not yet been coadded (see COA). This means that flux, error, and mask extensions have the array size of $1024 \times$ NAXIS2 $\times$ number of nod pairs, while the remaining extensions are simply $1024 \times$ NAXIS2. The units are EXES "intensity" units: ergs s^{-1} cm^{-2} sr^{-1} $(cm^{-1})^{-1}$. There is a UND file for every individual observation taken for a particular setting. These are "Level 2" products in both versions of the pipeline.

4.1.4.7.   CCR

The CCR is a new product generated by the Python pipeline where a blackbody correction has been applied to every pixel in the 2D echellogram. The data and uncertainty are multiplied by this 2D array, which is from the wavenumber map (extensions 6 and 7 for the FLT and UND products, respectively) and blackbody temperature set point ("BB_TEMP" header keyword) and then normalized by a uniform blackbody set to the central wavenumber ("WNO0" header keyword) and BB_TEMP. There is a CCR file for every individual observation for a particular setting.

4.1.4.8.   COA

The COA product is the 2D echellogram of an observation where the number of nod pairs that comprise a UND have been coadded together. IDL Redux creates COA files that are single-extension FITS files, which contain the coadded flux and coadded variance. For high resolution observations, the FITS files are not natively rotated but will be displayed rotated in the IDL version of Redux.

Note, from Cycles 5 – 9, it is possible that multiple UNDs have been coadded together into a single COA file. To see which option in the pipeline has been selected, check whether there is a COA for every UND file, or if a single COA exists. The file name in the single COA will give the range of files (e.g., 10018—10025) that comprise it. In the Python version of Redux COAs there are multi-extension FITS files and the extensions are: flux, error, mask, flat, wavenumber calibration, spatial calibration (e.g., position along slit height), and order mask. The units are EXES "intensity" units: ergs s^{-1} cm^{-2} sr^{-1} $(cm^{-1})^{-1}$. COAs in the IDL pipeline are "Level 3", while they are "Level 2" for the Python pipeline.

4.1.4.9.   CAL

The CAL product is an optional 2D echellogram generated by the Python version of SOFIA Redux. It is identical to the COA except it has been converted from intensity units to flux units, Jy $pixel^{-1}$.

4.1.5.   Recommended Files for Getting Started

The files that are useful for science analysis depend on whether the data was taken in nodded mode or map mode. It also depends on whether the target is a point source or an extended source.

Nodded observations of point sources: have no loss of information when extracted to 1D. Use the 1D extracted spectra files, MRD, MRM (orders merged), or CMB, COM (orders unmerged).

Nodded observations of extended sources: 1D spectra may still be sufficient, but there is loss of spatial information, and the user may wish to perform their own extraction using the 2D COA or CAL echellogram files. See Appendix B and C for guidance.

The pipeline's order merging routine does not work well for sources with a weak or absent continuum (for example, for observations of H_2 emission from shocked gas in supernova remnants and Herbig Haro objects). Figure 5 shows the 1D EXES order-merged and order-unmerged spectra of the bow shock HH7. The H_2 S(4) line is well detected in the order-unmerged data, but merging artifacts make it difficult to see in the order-merged data. Only use the order-unmerged 1D products CMB or COM for sources without a continuum.
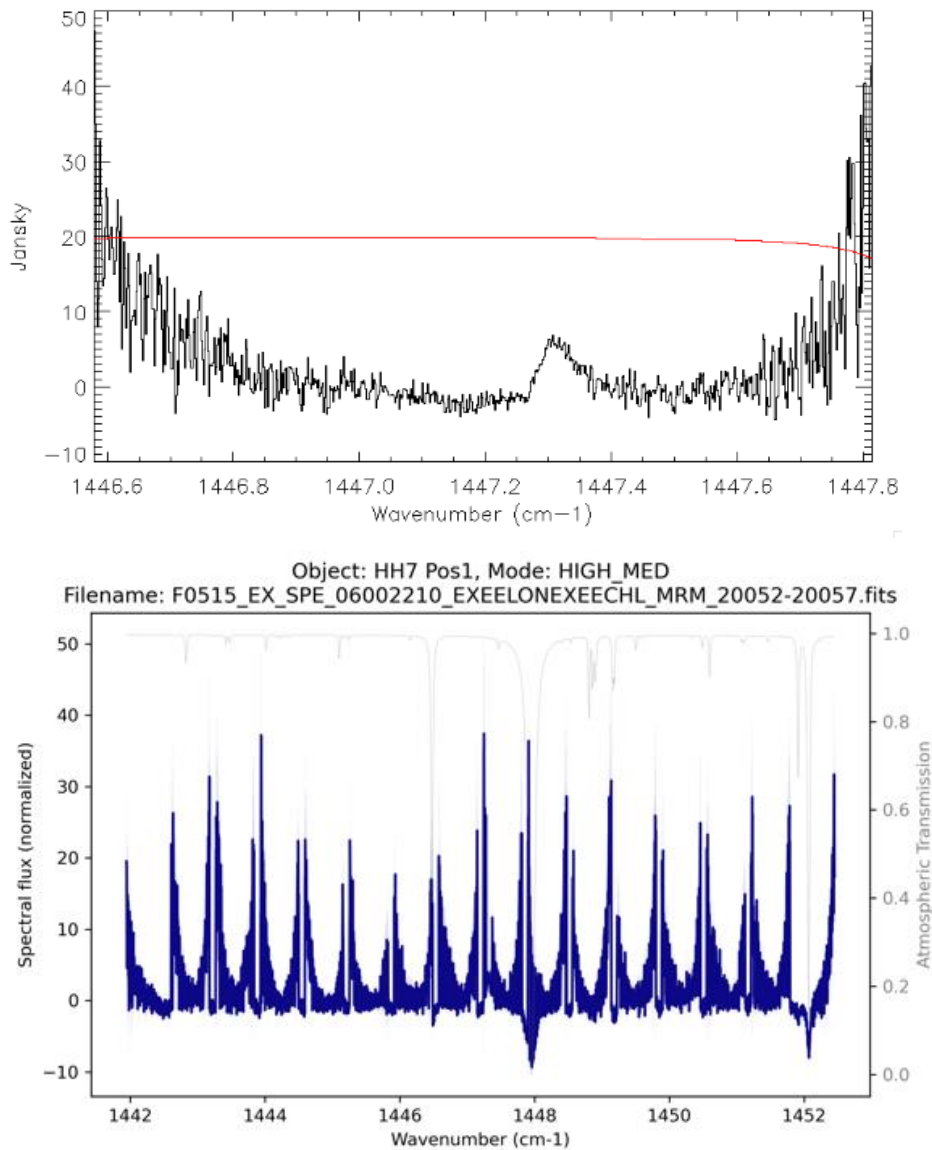
Figure 5 *(Top) The unmerged 1D spectrum of HH7 has well detected H_2 S(4) in order 4 in the CMB order unmerged file. (Bottom) The order-merged version of this observation is unusable because the pipeline merging gets confused by the curved over shape.*

4.1.6. Mapped Observations of point sources or extended sources

The REDUX pipeline cannot combine or extract EXES map files. The end point of these reductions is the 2D echellograms: CCR/CAL files for `PIPEVERS = 3_0_0dev` and UND/WVM files for `PIPEVERS = 1_0_2`. See Appendix <u>B</u> and <u>C</u> for more information about extractions from the 2D data products.

4.1.7. Telluric transmission models

1D data products include an atmospheric transmission model which has been interpolated to the wavenumber scale of the data and convolved to the appropriate spectral resolution. Data reduced with the python-based pipeline (`PIPEVERS = 3_0_0dev`) uses Planetary Spectrum Generator (PSG, <u>Villanueva et al. 2018</u>). Data reduced with the IDL pipeline (`PIPEVERS = 1_0_2`) uses ATRAN (<u>Lord 1992</u>).

The PSG model grid uses a set of default column densities for flight altitudes between 36000-45000 at 1000 ft spacings and telescope elevations from $30 - 70°$ at $5°$ spacings. The pipeline uses the SOFIA altitude and telescope elevation from the data headers and performs a bilinear interpolation of the transmission models; however, no attempt is made to optimize the molecule overburden values to make the transmission model fit the data.

The ATRAN model is single array with the total transmission of the atmosphere. The PSG model includes a total transmission array as well as arrays with the transmission broken down to the contribution from different atmospheric molecules: H_2O, CO_2, O_3, N_2O, CO, CH_4, O_2, N_2, NO_2, HNO_3, and collisionally induced absorption (CIA). CO, N_2, and CIA are included by the PSG defaults, but they are not important absorbers in the EXES wavelength range. For most EXES observations, only one or two of the eight active MIR species need to be considered.

ATRAN models do not include NO_2 and HNO_3 but these molecules are important sources of absorption at many EXES wavelengths. <u>Figure 6</u> shows a PSG transmission model with color codes for different molecules.
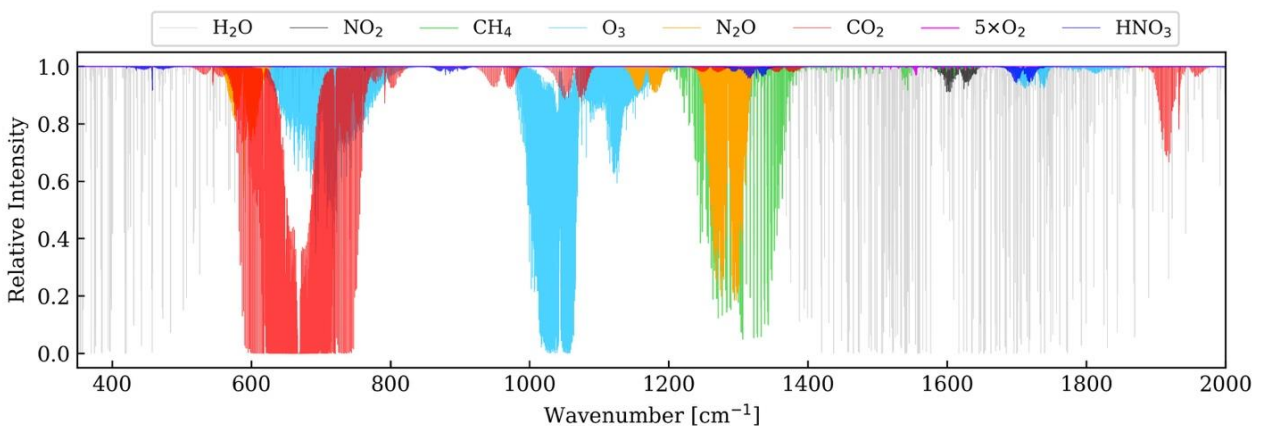

Figure 6 *PSG transmission model of Earth's atmosphere that shows where specific molecules cause telluric interference. Figure courtesy of Dr. Jialu Li, University of Maryland.*

The 1D spectral products only include the total transmission model, in the fourth array.
PSG also generates the transmission by molecule on the same wavenumber scale and the arrays can be accessed in the MRM file, in MRM extension = 5.

The contents of the 12 transmission models are detailed in Table 16.

Table 16: Transmission Spectra by Molecule in the MRM, Extension 5 file.

Extension	Content	Comments
[*,0]	Total transmission	
[*,1]	H_2O	
[*,2]	CO_2	
[*,3]	O_3	
[*,4]	N_2O	
[*,5]	CO	This molecule has no significant absorption between 5.3-28.3 µm.
[*,6]	CH_4	
[*,7]	O_2	
[*,8]	N_2	This molecule has no significant absorption between 5.3-28.3 µm.
[*,9]	NO_2	
[*,10]	HNO_3	
[*,11]	CIA	Collisionally induced absorption. CIA can be neglected between 5.3-28.3 µm.

4.1.8. Sky radiance spectra

Sky radiance spectra are produced by extracting only the B-side of nodded data and omitting the sky subtraction step. Sky radiance spectra usually give the clearest view line emission from the atmosphere and thus their main use is for wavelength calibration, by aligning sky emission lines to their known frequencies.

Sky radiance spectra are distinguished from sky-subtracted object spectra by a different file naming convention to prevent confusion. There is a one-to-one correspondence between the end-product of sky subtracted and radiance reductions, summarized here:

Sky subtracted spectra ↔ Sky radiance spectra
SPC ↔ SSP
MRD ↔ SMD
COA ↔ SCO

Sky radiance files also include thermal emission from the telescope optics in addition to the sky emission lines and sky thermal background. There is no obvious way to separate or distinguish the contribution from the telescope.
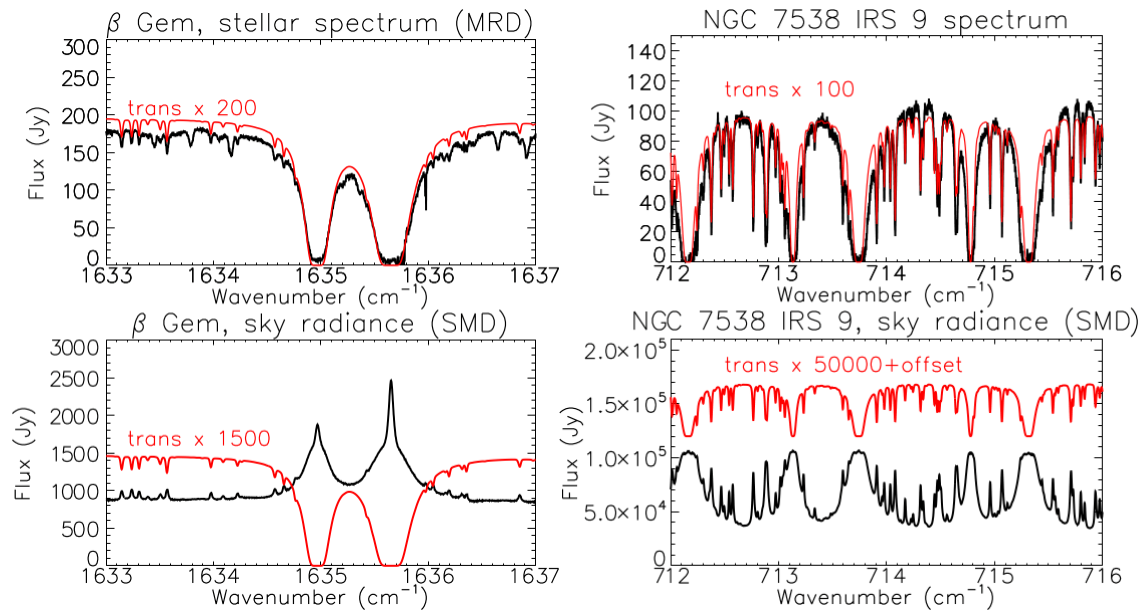
Figure 7 *(Top row) Two examples of nod-subtracted data with the transmission model scaled and overplotted in red. (Bottom row) The corresponding sky radiance spectra have much higher fluxes than the nod-subtracted data, and the line shapes differ due to different line formation properties of absorption and emission.*

If the standard wavelength solution quality (as characterized in Section 4.1) is sufficient for the science, then sky radiance files can be ignored. However, they can be useful if there is a need to evaluate wavenumber outliers due to systematic errors, by comparing the measured and theoretical wavenumbers of sky lines. Sky variance and regular nod subtracted data reductions are rectified and wavelength calibrated in the same way, so any frequency offsets seen in the sky emission spectra will also be present in the nod subtracted reductions. Another potential purpose is to check to see whether there are uncatalogued atmospheric lines in the spectrum that may be underpredicted in the transmission model.

Figure 7 shows two spectra observed at the same spectral setting at the same altitude of 43000 ft. The PSG transmission model that was matched to the observation parameters is about the same for both observations and shows moderate levels of absorption from nitric acid, HNO_3. However, the spectrum toward AFGL 2591 clearly has deeper HNO_3 lines than the PSG model. The sky radiance files corroborate the elevated HNO_3 levels and might be useful for evaluating the degree of telluric interference, because the sky radiance has such high S/N in comparison to the target continuum. The telluric radiance line strengths are correlated to the transmission, but it is beyond the scope of the manual to derive the relationship.
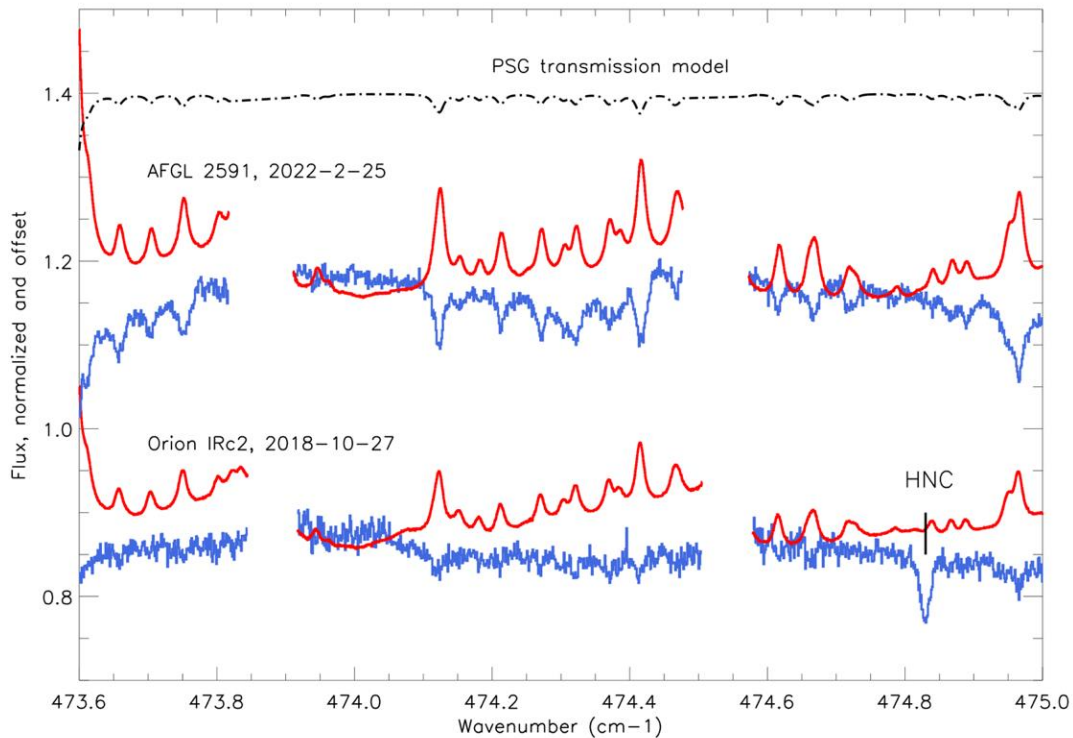
Figure 8 *The PSG model does not capture strongly variable atmospheric constituents like HNO₃. Here the radiance spectra may be of use to assess the telluric interference because the atmospheric emission from HNO₃ is correlated to the transmission in the nod subtracted data. Orion IRc2 was well represented by the PSG model. For AFGL 2591, the column of nitric acid in the sky was much worse, even though both observations took place at 43000 ft altitude. The Orion IRc2 spectrum has a source line of HNC. This inspection shows it does not suffer significant telluric interference.*

4.2. POINTING, SLIT ROTATION, NOD COORDINATE

4.2.1. Slit angle, LOS rewinds

EXES did not have a field de-rotator and could not control its slit angle. SOFIA was an alt-az mounted telescope and thus saw regular field rotation, but it also had a Line-of-Sight (LOS) mechanism which could stabilize the rotation of field (ROF) for intervals of between about 3 minutes to 1 hour at a time, with the exact duration set by the plane heading and the target location. When the LOS mechanism limit was reached, it would "rewind", and the telescope ROF and slit angle of EXES would be rotated by ~3°.

Individual EXES data files in nod or maps mode were always taken within the LOS time span and therefore the slit position angle was fixed at a single value, which is specified in the header keyword TELVPA (telescope vertical position angle). TELVPA is defined as the angle the slit was pointing in degrees East of North.

Though individual nods have only one TELVPA, pipeline reductions regularly combine nodded observations with different slit angles in order to obtain the highest possible signal to noise at the

slit center. The combined data (found in the COA and all subsequent files) will have a record of which files were coadded, but it does not record all the TELVPA values. The TELVPA of the files that contributed to a COA can be located in the headers of the CCR files.

Combining different TELVPA values has no impact on point sources, but extended sources may have spatial smearing at the slit extremes. This is usually negligible, but not in all cases.

For example, the PDR ρ Oph (AOR = 09_0211_2), was observed in HIGH_MEDIUM at 1447 cm^{-1} for three nodded files on F832. Table 17 shows the slit angles and exposure times recorded in the header for each of the individual nodded files (CCR) and the 2D coadded file (CAL). Note that the COA keyword only records the TELVPA value of the first nodded file.

Table 17: Slit Angles for Nodded ρ Oph Observations, AOR = 09_0211_2

Filename (abridged)	TELVPA	EXPTIME
F0832_EX_SPE_0902112_***_CCR_40097.fits	267.980°	256s
F0832_EX_SPE_0902112_***_CCR_40098.fits	267.983°	256s
F0832_EX_SPE_0902112_***_CCR_40099.fits	269.957°	256s
F0832_EX_SPE_0902112_***_CAL_40097-40099.fits	267.980°*	768s

The CAL file TELVPA keyword only lists the slit angle of the first nodded file.

Files 40097 and 40098 share the same TELVPA (to the precision of the telescope housekeeping), but prior to file 40099, the LOS had to be reset, which rotated the slit by +2°.

The amount of spatial smearing is small in this case: a 2° angle change moved the ends of the 10 arcsec slit (SLTH_ARC = 9.757 arcsec) by only 0.17 arcsec, which is negligible when compared to a FWHM ~2" PSF.

Reach et al. (2019) and Neufeld et al. (2019) both observed H_2 emission from shocks with EXES and found the slit rotations of the coadded data to be an acceptable tradeoff for obtaining high S/N in the line profiles. However, Soam et al. (2021) observed H_2 emission from PDR IC 63, where the slit angle changed by nearly ~70° over the observation of the 587cm^{-1} H_2 S(1) line. In that instance, the authors chose a customized procedure to place the data onto an RA/DEC grid before extracting to a 1D spectrum.

Mapped observations of point sources and extended sources are not combined by pipeline, so they have only one TELVPA per file (CCR or CAL). Users who want to coadd maps will need to take the slit angle into account.

4.2.2. Equatorial Reference Frame vs Science Instrument Reference Frame

4.2.2.1. Nodded Observations

EXES had limited control of the telescope in order to send nod and map commands. These motions were commanded in either the Equatorial Reference Frame (ERF), where telescope motions were

defined in terms of relative East and North or in the Science Instrument Reference Frame (SIRF), where telescope motions were defined in terms of parallel (p) and perpendicular (q) to the slit direction. Commands were specified in relative values in arcsec for both reference frames.

If the slit length of the configuration was long enough, then a point source could be nodded along the slit, to maximize observing efficiency.

To nod a source on slit (INSTMODE = NOD_ON_SLIT), the nod motions had to be specified in SIRF, and recorded in the header keyword "NOD_PQ = '**XX**" P 0.00" Q., where **XX** is the parallel nod throw. The nod throw is converted into relative East and North motions in arcsec and recorded in the header keyword "NOD".

Nodding off slit (INSTMODE = NOD_OFF_SLIT) could be done in SIRF or ERF. If the observation was an isolated point source and the slit was simply too short for nodding on slit, then it was convenient to define the nod in SIRF as "NOD_PQ = '0' P **XX**" Q, where the perpendicular was usually **XX** = 15.0" to get to clear sky away from the source. Some extended sources or targets in crowded fields required a specific offset sky position to ensure clear backgrounds, and then the nod would be commanded in ERF, and the header keyword NOD in arcsec East, North would define the motion. When nodding off slit, the telescope was sent to the sky position first (B), followed by the on-source position A. The nodding sequence would proceed by alternating BABA. Ground-based observatories commonly use the nod sequence "ABBA", but this was not used by EXES.

The end products of the REDUX pipeline for all nodded observations are the 1D spectra files, e.g., CMB/COM (for unmerged orders) and MRD/MRM files (for merged orders).

4.2.2.2.   *Mapped Observations*

Mapped observations are defined by the initial offset from the target coordinate, the number of map steps, and the step size and direction. Maps could only be executed in the SIRF reference frame, because it only makes sense to scan the slit perpendicular to its spatial dimension.

The header keyword TSTEP_PQ = '0.00" p **0.XX**" q is the map step size and direction, in parallel p and perpendicular q. p is always 0.00. The map step is converted to relative East and North with the keyword TSTEP = **YY**" E   **ZZ**" N. The header keyword OFFSETPQ specifies the starting position of the map in parallel and perpendicular directions, in arcsec. In this case, parallel doesn't have to be 0 valued, because it may be useful to direct the map stripe to be off-centered from the target. (For example, if observing Venus with an angular diameter of 20", a 12" slit would need to be positioned twice to cover both hemispheres.) The OFFSETPQ perpendicular offset, q, will always have an opposite sign to the step direction. The OFFSET header keyword is the conversion of OFFSETPQ to relative E and N, in arcsec. NPOINTS specifies the number of map steps in the file. At the end of every file, the telescope is moved back to the OFFSETPQ position, and three sky integrations are taken for the purpose of sky subtraction of the whole file.

"CCR" or "CAL" products are the end products for maps or slit scans with the REDUX pipeline, and differ only in the units, which are erg s^{-1} cm^{-2} SR^{-1} (cm^{-1})$^{-1}$ and Jy pixel^{-1}, respectively. The structure of each CCR/CAL file is: [wavenumber, spatial row, map step number]

To produce a simple continuum map from a file, one can take a mean over all the spectral dimension (or a subset of wavenumbers in order to isolate line frequencies or exclude noisy regions), leaving a data cube with size NAXIS2 × NPOINTS. Figure 9 shows an example of a CCR map file of Jupiter taken in medium configuration at 1300 cm^{-1}. The right panel shows the file with the spectral dimension averaged (collapsed). The pixel size in the map is 0.201" × 0.95". The slit direction is a fixed value from the file- TELVPA = 242.088°, East of North. The row index in NAXIS2 increases in this slit angle direction.
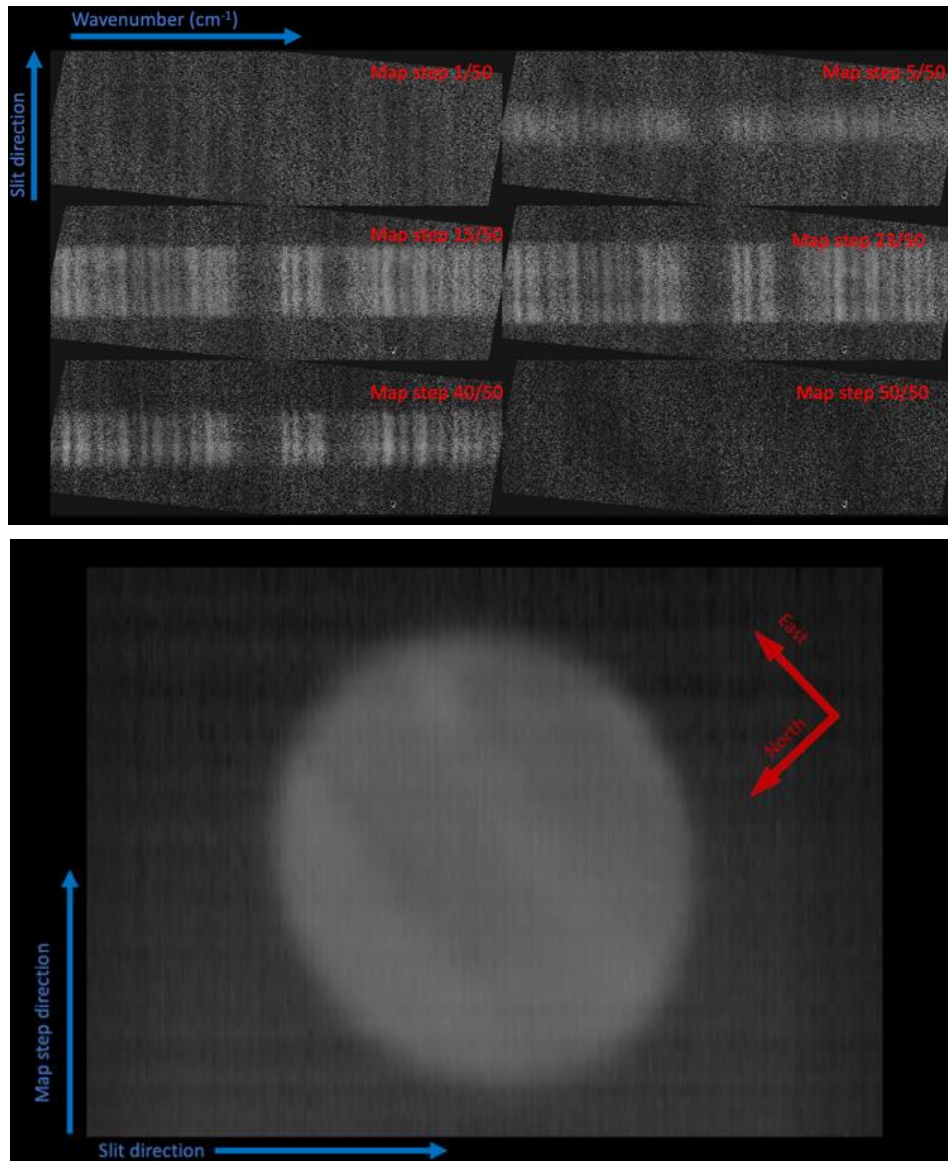
Figure 9 *(Top) 2D spectral planes from a 50 step Jupiter CCR file. (Bottom): reconstructed image when the spectral dimension is averaged. The observation was taken in medium configuration, 1300cm^{-1} (7.7 mm), and the emission is from methane in Jupiter's atmosphere.*

4.3. WAVELENGTH CALIBRATION

Wavenumber solutions were set using the expected frequencies of atmospheric sky lines. Line centers were taken from transmission models made with Planetary Spectrum Generator for PIPEVERS=3_0_0dev or ATRAN for PIPEVERS = 1_0_2.

4.3.1. Wavelength calibration of high-resolution configurations

The wavenumber solution of the high-resolution modes is controlled by four pipeline parameters:

- *WNO0:* The bulk wavenumber shift of the spectrum.
- *HRFL:* Focal length of the high-resolution chamber. According to the instrument design, this length is 100 cm.
- *HRR:* The High-Resolution "R" value is the tangent of the input angle onto the high-resolution grating, and it controls the dispersion (wavenumbers per pixel) value. The grating R value is not to be confused with the spectral resolution, R= $\lambda/\Delta\lambda$. Optical alignment changes or deliberate moves of the dispersion screwdriver will alter HRR. For EXES the value is usually between HRR = 9.7 – 10.1, or about 84.3°.
- *DETROT:* This parameter defines the detector alignment with respect to the high-resolution dispersion axis. It is approximately 0.1 radians (~5.7°). When the wavenumber solution veers off at high or low order extremes of a setting, this parameter is adjusted to put things right.

Even after optimizing these parameters, there are still optical distortions that cause systematic wavelength shifts in some areas of the detector. These systematic offsets are observed to change the dispersion value as a function of the column number along the order.

Figure 10 illustrates the typical behavior of the systemic errors in the wavenumber scale for high resolution modes. The measured wavenumbers of numerous sky emission lines are shown in terms of the velocity offset from their theoretical frequencies, against the column number (which runs along the orders). The data used for this example is an SSP file from a 722 cm^{-1} high-low observation. The "S" shape of the offset curve is typical for the systematic behavior at all wavelengths where the measurements can be made.
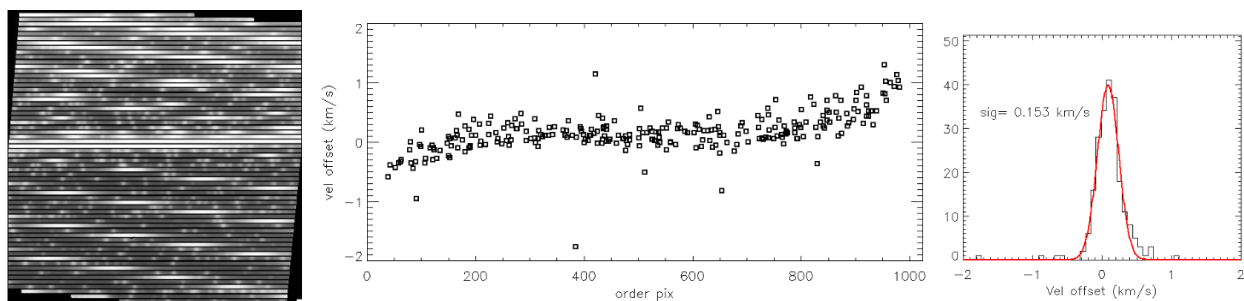
Figure 10 *Example of characterization of the wavecal quality for a commonly used setting: high-low (1st order) at WNO0 = 722cm^{-1}. The right frame is a flat-fielded, rectified sky spectrum (nod-subtraction turned off), with many bright O_3 and CO_2 lines that are used to measure the accuracy of the wavelength solution. The middle panel shows the offset of the measured vs expected line position, expressed in velocity. The line fit offsets are plotted against the pixel position along the order, left to right, which reveals that systematic velocity offsets are largest at the extremities of the orders.*

This grating setting has a small amount of overlapping coverage between adjacent orders. When the spectrum is order-merged, the order extremities are usually screened out because the blaze efficiency and S/N is lower in those regions. The histogram in the right panel shows the wavelength solution scatter for the order-merged spectrum, which is 0.153 km s^{-1} in this example. Table 7 - Table 9 show the 1-σ velocity errors in the wavenumber scale arranged by instrument configuration and wavenumber, with Table 7 showing the values for the HIGH configuration.

4.3.2 Medium and low-resolution configurations

The wavelength solution for medium and low-resolution configurations was determined with just two parameters, XDFL (the cross-dispersion focal length) and the wavenumber center, WNO0. In reality, the cross-dispersion chamber has a fixed focal length close to 100 cm, and the echelle grating angle determines the dispersion per pixel. However, it was convenient to treat the XDFL as the varying parameter and empirically adjust the wavelength scale to the telluric lines on an individual reduction basis. The 1-σ errors in the wavenumber scale for MEDIUM and LOW configurations are in Table 8 and Table 9.

4.4. INTENSITY AND FLUX CALIBRATION

Flux calibration for EXES is accomplished in the flat fielding process. Before every observation, a flat field spectrum was taken with the filter, gratings, Dekker, and slit in place by rotating a pick-off mirror aligned to a blackbody source in front of the entrance window. The blackbody source was temperature-controlled with 0.1 K precision, and completely filled the EXES pupil. The spectral flat field frame was assigned the appropriate flux per solid angle using the Planck function (as function of wavelength and the blackbody temperature). The calibrated flat field frame was used to scale the on-sky data into physical 2D intensity units, ergs s^{-1} cm^{-2} SR^{-1} (cm^{-1})$^{-1}$, which is independent from assumptions about the solid angle of the pixels. The blackbody temperature precision was cross-checked with a non-contact thermometer gun and found to match the blackbody temperature sensors to within 2 K over the set-point range 250K – 320K.

However, the flat field pick-off mirror was found to have a non-negligible contribution to the flux through its emissivity, ε (where ε = 1-reflectivity). The total flux of the flat field frame is then (1-ε)B(λ, T$_{bbsource}$) + εB(λ, T$_{ambient}$), where B is the Planck function, ε is the mirror emissivity, T$_{bbsource}$ is the blackbody temperature (saved in header keyword BB_TEMP), and T$_{ambient}$ is the temperature of the ambient environment around the calibration unit. These values have been measured in flight data to be ε = 0.1 and T$_{ambient}$ = 295K. When flat fields at a particular setting were repeated at different altitudes in the flight, there was less than 5% variation in the counts, which suggests that T$_{ambient}$ changes very little during the flight despite the cooling expected in the Nasmyth tube after the telescope door was opened.

The calibration system and strategy changed twice during the mission, which has some significant impacts on the flux calibration. The calibration source originally used a ZnSe lens in front of the blackbody source in order to ensure the calibration beam overfilled the EXES pupil. This lens contributed a large emissivity; at the same time, it was recognized that the angular size of the blackbody without the lens was sufficient to fill the pupil. Thus, the calibration source system was

flown without the lens for F362-F866. If early EXES data F158 – F291 is reprocessed, it is recommended to use these parameters to obtain correct flux/intensity scaling:

$$\varepsilon = 0.4, \quad T_{ambient} = 295K.$$

The other major change in calibration was in how flat fields are constructed. From Flight F158 through F400, the flat field was computed as "black – sky", where an off-source sky integration taken immediately after the blackbody was subtracted from the frame. This procedure removed scattered light internal to the spectrograph (see Section 4.5.1) from the flat frame, which made it a better match for the sky-subtracted data to which it was applied.

However, the sky frame flux includes telescope and sky thermal emission that is ~20% of the brightness of the blackbody source, causing the flat fielded data to be overcorrected. This failing was eventually recognized and after F514, flat fields were computed as "black-dark", where the "dark" component was a measurement of the instrument's internal scattered light pattern.

Using the findings for point source fluxes in OC5C and OC5F, the consequence of flat fielding with "black – sky" for data taken from F158 – F400 seems to be that intensities and fluxes are overestimated by a factor of ×1.25. Therefore, a correction factor of ×0.8 should be applied to intensities and fluxes for all data taken on or before F400, reprocessed with PIPEVERS = 3.0.0dev (the Python pipeline). The errors in the flux calculations for the earlier pipeline, PIPEVERS = 1.0.2 are not easily summarized and for data that was not included in the post-mission reprocessing before F386, intensity and flux values are not characterized. Table 18 lists the status of the intensity calibration of data in the IRSA archive by flight.

Table 18: Intensity Calibration for Data in the IRSA Archive by Flight

Flight Numbers	Calibrated in IRSA?	Method	ε	$T_{ambient}$	Intensity Error
F158-F291	No	Black - sky	0.4	295K	N.A.
F362-F366	No	Black - sky	0.1	295K	N.A.
F386-F400	Yes*	Black - sky	0.1	295K	10%*
F386-F866	Yes	Black - dark	0.1	295K	10%

* All intensities and fluxes from F386-F400 should be scaled by ×0.8.

4.4.1. Flux/Intensity Accuracy for Extended Sources

Extended sources overfilled the slit and filled the instrument pupil in the same way as the blackbody calibration source. Hence, the intensity values of the pixels in the 2D spectra (in the COA and CAL files) should be accurate without the additional considerations that affect point sources.

For 1D spectral products, the CAL 2D plane has been summed over a specific set of spatial rows set by the user in the pipeline. To interpret the integrated flux in the 1D spectra of extended sources, the beam size Ω must be determined, which depends on the slit width and the aperture radius chosen in the pipeline extraction steps. The header keyword SLTW_ARC is the slit width in arcsec. The header keyword APRADO**XX** is the radius of the extraction aperture, where **XX** is the order

number. Therefore, the beam area used for the extracted flux is $\Omega = 2*APRAD*SLTW\_ARC$, in $arcsec^2$.

Even though the blackbody scaling was crucial to all flux calibrations, its accuracy could only be tested for a limited set of observations: Venus and Mars, both observed near $1387cm^{-1}$ (7.2 µm). The EXES 2D fluxes of these targets matched to within 3% of the detailed thermal model for Mars (Global Circulation Model) for widely spaced observations on F365, F516, and F558 (J. Alday, private communication). Venus was observed on F366, and the temperatures derived on the clouds at 7.2 µm match the literature values from Encrenaz et al. (2013) to within 5%.

The blackbody calibration source was tested on the ground and in flight and found to be repeatable to better than 5% at all wavelengths, which suggests the blackbody unit is quite consistent, and that changing ambient temperatures in flight did not have a significant effect on the calibration. Using this limited set of information, assigning a 10% intensity error contributed from the blackbody scaling process for extended emission observations is suggested.

4.4.2. Flux Calibration for Point Sources

4.4.2.1. Pipeline Conversion of Intensity to Flux

After coadding nod pairs, the pixels in intensity units are converted to integrated fluxes by multiplying by their solid angle on the sky. The solid angle, Ω_{pixel} is the product of the angular slit width, "SLTW_ARC", and the spatial plate scale, "PLTSCALE", with a factor to convert square arcseconds to steradians and another factor to convert the flux units to Jansky:

$$\Omega_{pixel} = SLTW\_ARC \text{ x } PLTSCALE \text{ x } (4.848 \text{ x } 10^{-6})^{-2} /(2.998 \text{ x } 10^{-13})$$

$$COA \text{ file} \leftrightarrow CAL \text{ file}$$
$$erg \text{ } s^{-1} \text{ } cm^{-2} \text{ } sr^{-1} \text{ } (cm^{-1})^{-1} \text{ x } \Omega_{pixel} = Jy \text{ } pixel^{-1}$$

Once the pixels are in Jy units, the target flux can be measured by simply summing the spatial rows of the CAL file.

4.4.2.2. Slit Losses and Throughput Factors

The EXES flux calibration of point like sources systematically underestimates the total flux because the pipeline does not account for slit losses. Slit losses depend on the aperture dimensions, image size, and stability; the slit throughput factor was estimated to vary between ~50-90% over the various instrument configurations and imaging conditions. For an estimate of the slit throughput factor, the fraction of the intensity of a normalized 2D PSF model that is inscribed by a rectangle with the dimensions of the slit can be computed. The dimensions of the slit are known from the header keywords for the slit width, SLTW_ARC and the slit height, SLTH_ARC (both in arcsec).

The most accurate approach is to use the FWHM from the data itself because it reduces the uncertainty from variable imaging and guiding. However, this requires that the source has strong enough continuum and a long enough slit to enable measurement of the PSF FWHM. The Redux pipeline measures the spatial profile FWHM for each order, and writes it to header keywords,

APFWHM**XX**, where **XX** is the order number. For data that is unsuitable for measuring the spatial profile, a characteristic FWHM value for the wavelength and flight number from Table 6 in Section 3.3 can be adopted.

A IDL tool, `slitloss.pro` was written for making the slit throughput computation and is available for download at https://github.com/SOFIAObservatory/Recipes/blob/master/slitloss.pro

`slitloss.pro` takes user provided inputs for the PSF size (FWHM), slit width, and slit height and returns the slit throughput factor. The program assumes symmetric 2D Gaussians. This is a simplification, but there was rarely adequate data to constrain a more realistic PSF model, which would probably vary with observing conditions.

To correct the flux from a 1D extracted pipeline spectrum, divide the spectrum by the throughput factor that is output by `slitloss.pro`.

Two examples using `slitloss.pro` are shown below and illustrated in Figure 11.

Example 1: Vega, high-medium, 1496cm^{-1} (AOR =06_0056_17)

Vega is a strong continuum source and the instrument configuration high-medium means the slit was long enough for the pipeline to measure the spatial profile. Using the header information of any of the 1D extracted files, one can find the header keywords APFWHM**XX** (where **XX** is the order number). This is the Gaussian fit to the spatial profile in each order. Here we adopt a typical value from APFWHM16 = 2.254″ as the FWHM of the spatial profile. The slit height and width dimensions can be located in the keywords SLTH_ARC = 8.704″ and SLTW_ARC = 3.2″ respectively.

To use `slitloss.pro` from the IDL command line, enter the following command:

```
print, slitloss(psf = 2.25, slitw=3.2, slith = 8.7)
>> 0.851
```

The program returns the slit throughput estimate, 0.851.

The median EXES flux from the 1D spectrum MRD file was 65.5 Jy. The corrected flux is therefore 65.5 / 0.851 = 77 Jy. The ISO/SWS spectrum is an exact match for this flux value, 77 Jy.

Example 2: ο Ceti (Mira), high-low 1495cm^{-1}, (F661, AOR = 07_0014_4)

For this example, the slit height in short wavelength, high-low configurations is far too short to measure the spatial profile. Instead, the user will have to adopt a typical value for F661 from Table 5 of FWHM = 1.8″. The slit height and slit width dimensions in the header: SLTH_ARC = 1.74″ and SLTW_ARC = 2.11″, respectively.

At the IDL command line, type:

```
print, slitloss(psf = 1.8, slitw= 2.11, slith = 1.74)
>> 0.514
```

The program prints the estimated slit throughput, 0.514.

The median flux from the 1D extracted spectra is 1350 Jy, so the estimate of the total flux is 1350 Jy / 0.514 = 2626. The ISO/SWS flux of Mira at this wavelength is 2850 Jy, so the EXES estimate is lower by -8%. However, source type of Mira is notorious for large amplitude pulsations.
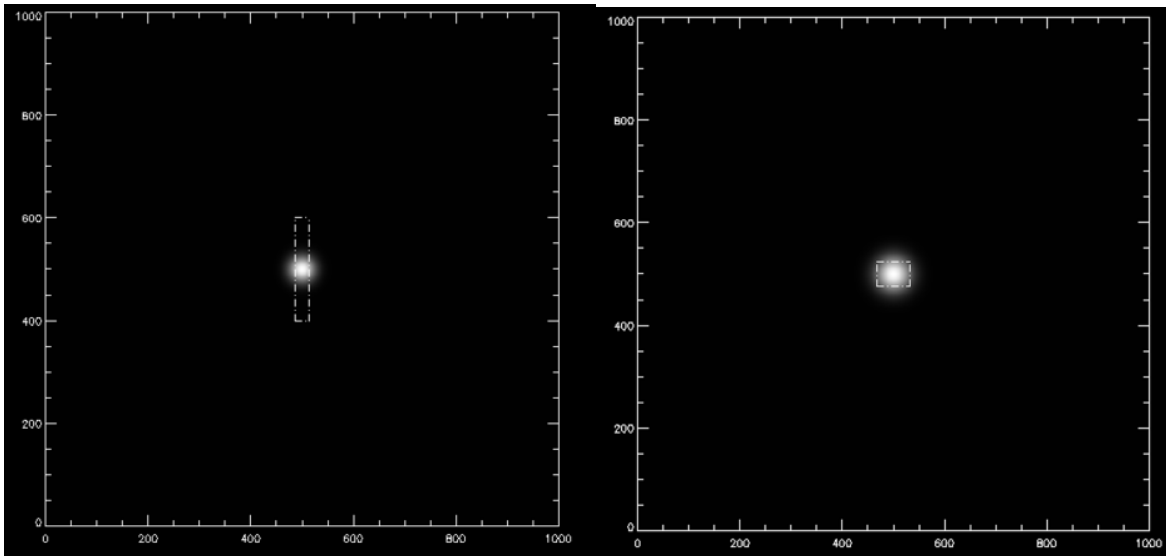
Figure 11 *Depictions of the loss calculations for the examples above. Vega had a FWHM 2.25" PSF, slit width = 3.2" and slit height = 8.7". The throughput is estimated to be ~85%. (Right). o Ceti (Mira) had FWHM = 1.8" (adopted from Table 5), slit width = 2.65" and slit height = 1.74". The throughput is estimated to be 51%.*

4.4.2.3. Point Source Flux Errors

To characterize the point source flux calibration accuracy, EXES data that was taken in standardized configuration, with a relatively large sample size, and targets with adequate flux stability were examined. This set of qualities was surprisingly hard to find in the pool of EXES programs, but 06_0056/07_0063, which observed a set of 10 red giant branch stars and telluric calibrators at 1496cm^{-1} (6.8 μm) met the criteria best. The observations were taken over four flight series between Oct 2018 and April 2022. All targets had ISO/SWS fluxes.

Eight targets were observed in high-medium mode and two were observed in high-low mode to take advantage of their brightness and obtain more spectral coverage. The observations share the same spectral resolution and slit width, but the throughput corrections are always higher for the high-low observations because the slit height is smaller. The slit throughput for the high-low observations was estimated to be 0.62. The throughput for the high-medium observations is estimated to have been 0.84-0.93, depending on the image quality.

Figure 12 shows the slit-loss corrected EXES fluxes compared to ISO/SWS fluxes for this sample. The investigation revealed that a multiplier, ×1.7 is required to match the slit-loss corrected fluxes to ISO/SWS measurements. The factor is not understood at this time. It does not seem to be due to incorrect flux scaling in the 2D planes, which were found to match the (albeit few) intensity standards Mars and Venus at a nearby wavelength (7.2 μm vs 6.8 μm).

Underestimated slit losses also are unlikely, because in the RGB observations, the EXES and ISO fluxes for high-low and high-medium observations fall on the same line, when the procedure from Section 4.4.2.2 is applied using the measured spatial profiles as the PSF size.
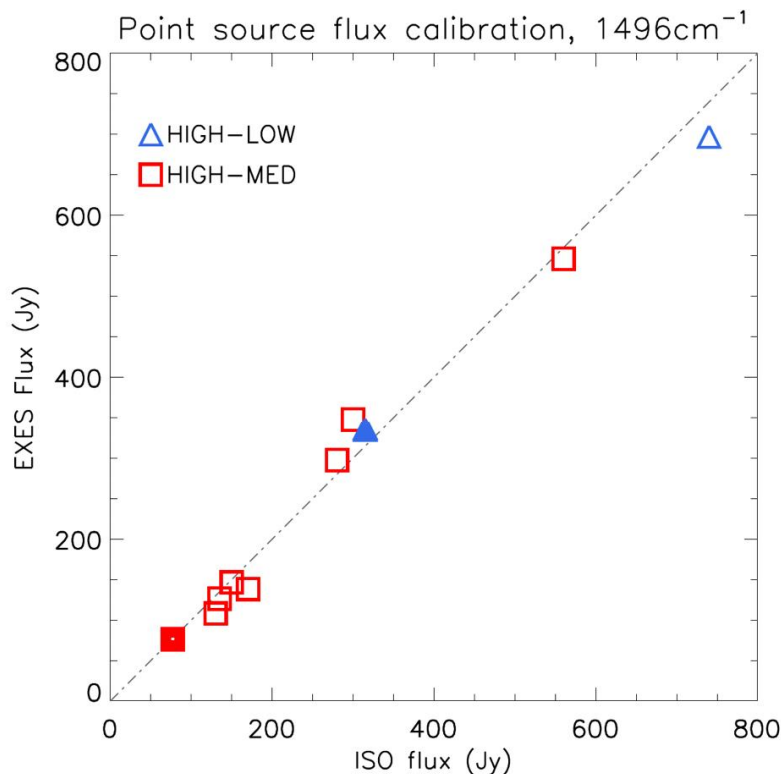
Figure 12 *Slit loss corrected EXES fluxes vs ISO/SWS fluxes stars observed in the programs 06_0056/07_0063, using the 1.7× correction factor. The filled points are Vega and Sirius, observed as telluric calibrators for the program. The open points are late M giants.*

If the slit losses of the high-medium mode were actually 1.7× higher than implied by the PSF measurements (accounting for the multiplier), then the high-low mode slit losses would be ~1.7^2 higher. This is not supported by the data. The fractional flux difference (F_{EXES}-F_{ISO})/F_{ISO} of these 10 sources shows a standard deviation of 10%. To obtain a better constrained error estimate and to verify the 1.7× correction factor, all of the Cycle 5-9 archive was combed for usable point source observations, in all configurations and wavelengths. The inclusion criteria were:
1) Point sources with strong continuum
2) Mid-IR Flux measurement (ISO/SWS, Spitzer, etc.)
3) Low mid-IR variability

Point sources that passed these criteria included: hot calibrator stars like Sirius and Vega, massive protostars which are point-like at the wavelength of observation, and red giant branch stars. Point

sources that could not be used included low mass protostars, asymptotic giant branch stars, M-supergiants, asteroids, and the Jovian moons.

Asteroids may seem like good flux calibration standards, but the STM (Standard Thermal Model) models used to predict their fluxes were found to be accurate to only 50%. SOFIA/FORCAST made regular use of asteroids for spectral flux calibration, but the strategy hinged on obtaining contemporaneous MIR photometry to fit the broad SED. This auxiliary data is unavailable for the EXES observations of asteroids, and leaves the true fluxes too poorly known for use as flux standards.

Even with "problem" sources excluded, the target pool still leaves much to be desired in terms of source variability, and it is expected that some of the flux offsets measured are simply due to this fact. The data points also are largely taken for wavelengths < 8 μm, with only five targets observed at longer wavelengths that meet the inclusion criteria. Observations with "short" slits (SLTH_ARC < 5") and "long" slits (SLTH_ARC > 5") were differentiated because the shorter slit observations are impacted more by uncertainties with the PSF size, in part because there is insufficient spatial coverage to measure a spatial profile width, which requires reliance on "typical" series PSF sizes from Section 3.3 (Table 6). Figure 13 shows EXES flux vs ISO/SWS flux for long and short slits for observations between F514-F866. All the flight series appear to hold to the same line using the ×1.7 correction factor.

Figure 14 shows histograms of the fractional flux offsets, $(F_{EXES}-F_{ISO})/F_{ISO}$, for the data included in Figure 13. The standard deviations of these histograms were used as an estimate of the 1-σ point source flux errors for the case of long slit configurations (> 5") 0.13, and short slit configurations (< 5") 0.17. Because there were so few qualified point source observations to represent long wavelengths, these were plotted separately in the left panel of Figure 15. There are insufficient points to measure 1-σ errors, but the flux scaling using the 1.7× correction factor appears to be applicable for 13-14 and 20-26 μm observations.

OC5C/OC5F (F386-F400) used the "black – sky" flat field structure, which causes the flat fields to systematically over correct the data.

It appears that the fluxes shown in Figure 15 can be corrected by multiplying the EXES flux measurements by 0.8, based on a fit to slope of the red points. However, the real factor may be something more subtle, since the wavelengths represented in the plot are predominantly from 5.5 – 8 μm. After such correction the scatter in the fractional offsets is no worse than data from later flight series, and it is suggested that the same 1-σ errors can be adopted, after F386 – F400 data is scaled by ×0.8. Figure 21Table 19 summarizes the point source flux calibration errors and status by flight number.
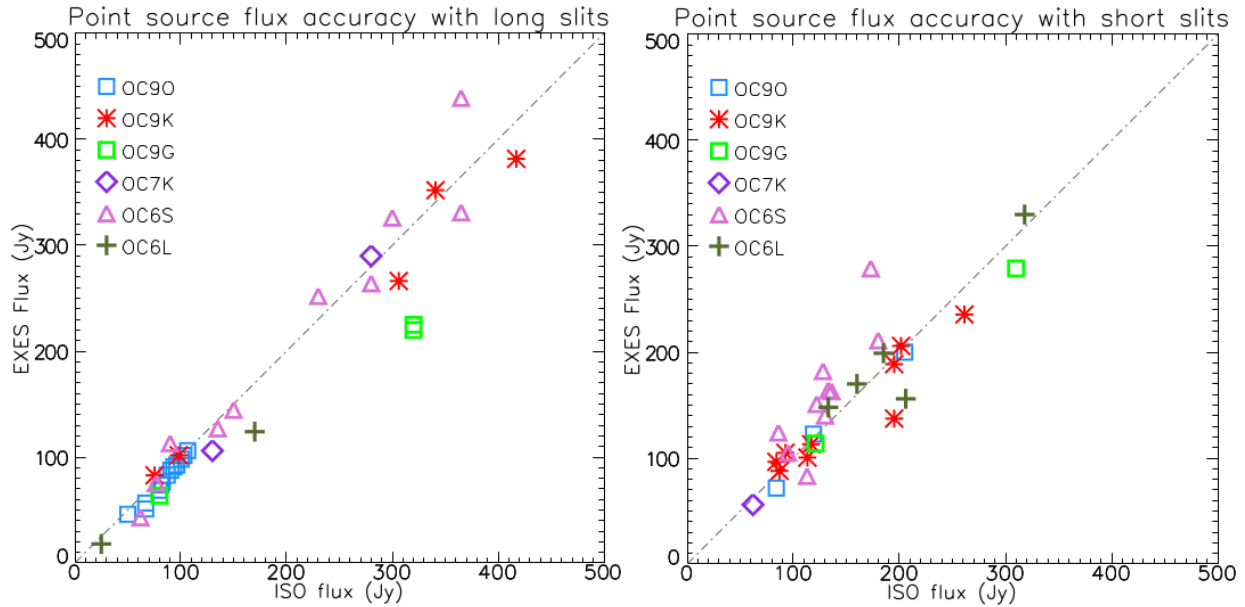
Figure 13 *EXES Flux measurements vs ISO/SWS values for point source observations, using the x1.7 correction factor for: (Left) "Long slit" (>5") configurations. (Right) Short slit (< 5") configurations. The correction factor seems to be standard for all series and wavelengths, F514-F866.*
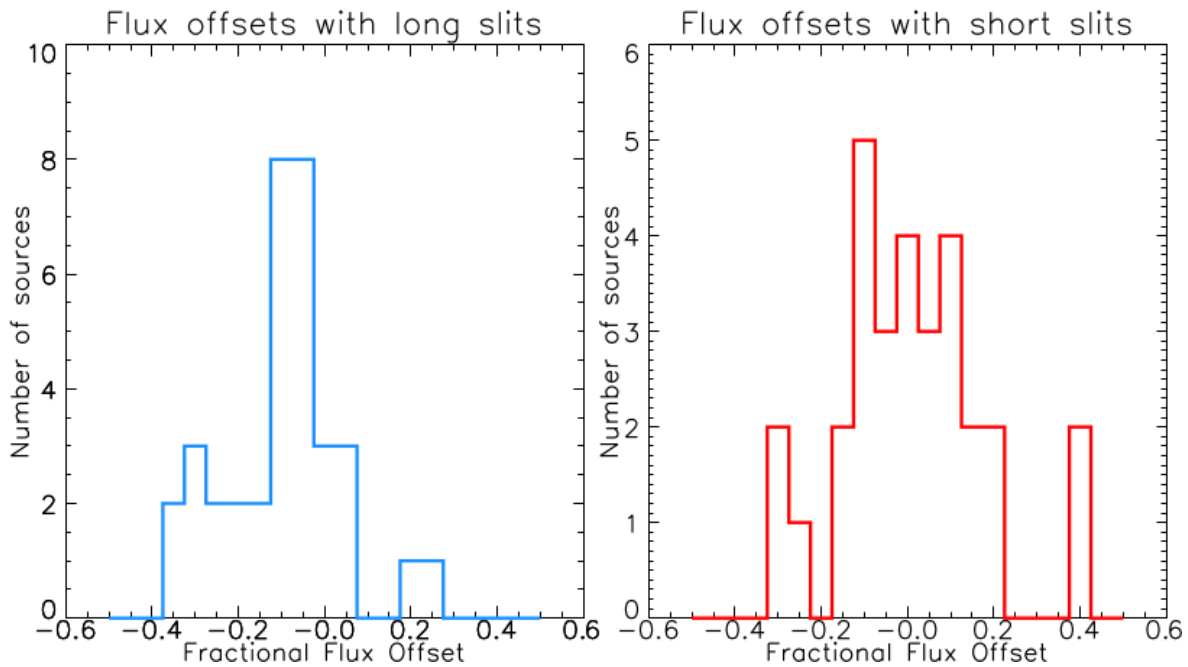

Figure 14 *Histograms of the fractional flux offsets, $(F_{EXES}-F_{ISO})/F_{ISO}$ for the data in Figure 12. The standard deviation of the left is 0.13, and 0.17 for the right, which we adopt for the 1-s error for point source fluxes with EXES.*
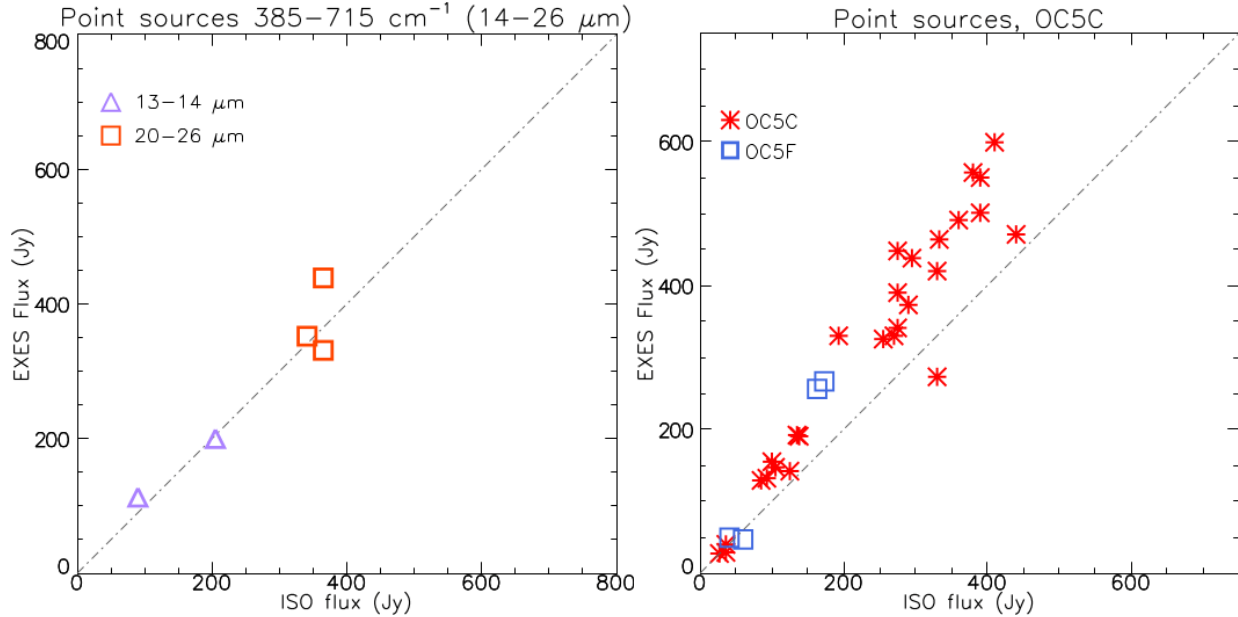
Figure 15 *(Left) There were very few acceptable flux standards for wavelengths longer than 14 mm, but what there is suggests that the 1.7x factor holds at these wavelengths. (Right) During the flights in OC5C and OC5F (F386-F400), flat fields were constructed from blackbody-sky integrations, instead of the blackbody-dark model employed after F514.*

Table 19: Point Source Flux Calibration for Data in the IRSA Archive by Flight

Flight Numbers	Calibrated in IRSA?	Method	ε^1	$T_{ambient}$	Flux Error (> 5")	Flux Error (< 5")
F158-F291	No	Black - sky	0.4	295K	N.A.	N.A.
F362-F366	No	Black - sky	0.1	295K	N.A.	N.A.
F386-F400	Yes[2]	Black - sky	0.1	295K	13%[2]	17%[2]
F386-F866	Yes	Black - dark	0.1	295K	13%	17%

[1]*Calibration mirror emissivity, see Section 4.4;* [2]*All fluxes from F386-F400 should be scaled by ×0.8.*

4.5. DATA ARTIFACTS

4.5.1. Detector Array Summary

When the EXES detector reset, the pixels went to values of 10500-11000 ADU. Integrations caused the array to count downward from this level to the saturation limit of about 3500 ADU. Non-linearity of about 5% took effect around 6000 DN or in terms of net DN, about 5500-6000. Observations were designed not to exceed 3000 net-DN and so strong non-linearity was seldom encountered. Linearity corrections have been derived for the array based on lab measurements, but when included in the pipeline it was found to have negligible effect, so the linearity correction was not used for data reductions to save computation time.

The photosensitive part of the array had 1024 × 1024 pixels. There were 4-pixel columns of reference pixels on either side of the array for the purpose of removing electronic effects from the data. In the raw data files, the reference columns are located on the right side of the array in columns 1024-1031, despite their physical location in the physical array. Thus, in the full frame raw data[1], the planes have 1032 × 1024 pixels (NAXIS1 × NAXIS2).

The reference columns were not found to be helpful for improving noise and are customarily cropped from the data at the first reduction step in the pipeline. Intermediate products from the pipeline retain the 1024 columns taken from the photosensitive part of the array.

The array read patterns consisted of a set of non-destructive reads, ending in a destructive read. This enabled experimentation with "Sample-up-the-ramp" and Fowler read methods, but it was determined for EXES that the highest signal to noise was achieved using only the destructive read differenced from a frame with the array reset values, which was taken from the first integrations of a set of dark files. Thus, most planes of the raw data were unused in the processing because they were the series non-destructive reads prior to the destructive read/reset.

The data taking strategy of EXES was to perform sky subtraction using A and B nodded data that was two minutes apart. Map files measured the sky background once per file which could be as long as 10 minutes. In either case, the sky subtraction step also took the role of removing any static array reset patterns which differed from the stored reset frame used by the pipeline. This accounts for why pattern burn-in and odd-even row gains do not have a notable effect on the final data.

4.5.2.   Bad Pixels

The EXES array had very few bad pixels – excluding the eight columns of reference pixels, the permanently dead pixels made up fewer than 0.3 % of the array. The bad pixel mask (BPM) did not change appreciably over the mission and the single version of the BPM included with the downloadable redux pipeline is suitable for reducing all mission data, except for F158 and F159, which requires its own BPM.

4.5.3.   Scattered Light Background

The EXES detector could see light from the spectrograph optics even when the direct light path into the detector chamber was blocked. This scattered light level is very stable and is fully removed from on sky data when the A-B sky subtraction is performed. It is also fully removed from the flat field, either when the blackbody is "sky subtracted" for F158-F400 or when it is "dark subtracted" for F514 – F866. The internal scattered light did not change appreciably with wavelength, but some faint arc features could change with configuration and over time, which is why, when constructing flat fields from black – dark, the closest available dark frame was used.

Beginning in F514, EXES took regular "dark" frames at least once per flight, but dark frames were taken infrequently during F158-F400, which meant that sky subtracted flats had to be tolerated, which interfere with accurate flux scaling. The scatted light background for EXES was reduced

---

[1] The exception was for the two commissioning flights in 2014 (F158 and F159). At that time, the raw data files were 1024 × 1024 pixels, preserving the reference columns at the expense of eight photosensitive columns from the array edges. In this case, the pipeline keeps the 1024 columns. The reference columns are masked out in the flat field procedure.

substantially when additional baffling was installed near the detector box entrance prior to F658 from approximately 3.3 DN s^{-1} to 0.4 DN s^{-1}. The internal scattered light background looks structurally different before and after the baffling was installed. The scattered light background before and after the baffling change can be seen in Figure 16.
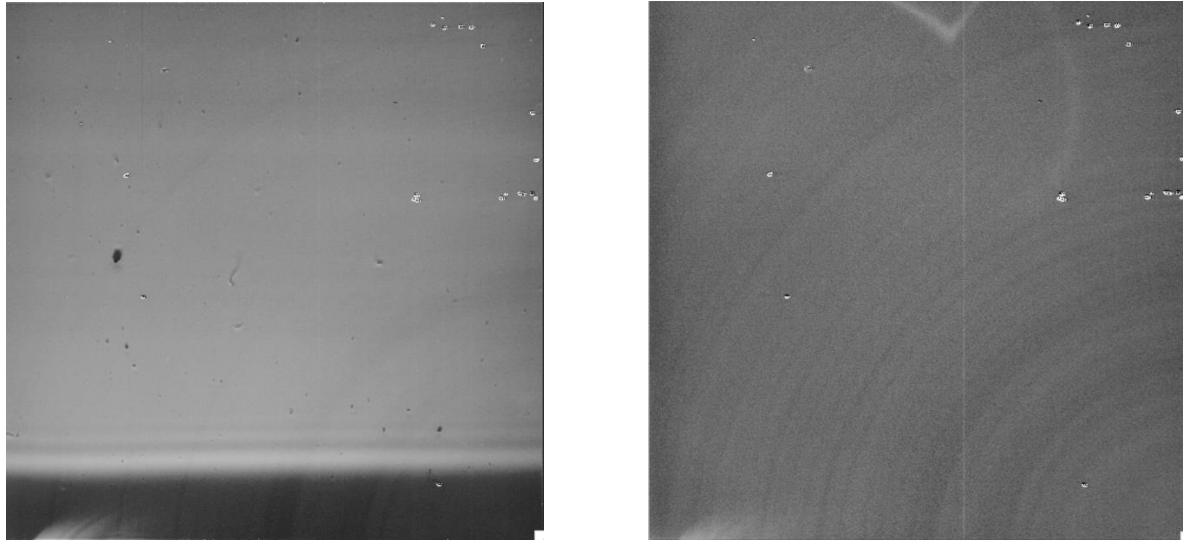

Figure 16 *(Left) The "dark" background in data frames from F158 – F560 was about 3.5 DN s^{-1}. (Right) After additional baffling was installed, the background rate dropped to 0.3 DN s^{-1}.*

In either case, the background levels are removed during ordinary A-B nod subtraction and for any method of flat field construction.

4.5.4. Detector Related Artifacts

In this section common and uncommon array artifacts or defects are described. Most of these will not be encountered by the user of the "science-ready" products, but the descriptions of the artifacts are included for users who will inspect the raw data and earlier steps from the pipeline products.

4.5.5. Memory Rolls

Occasionally the EXES detector would reset with all the columns permutated by several pixels. The most common "rolls" were four or eight pixels that placed the four reference columns on either side of the array or all eight on the left in the raw data. If unaddressed, the data will not match the bad pixel mask and wrong parts of the array may be cropped out.

An effort was made to fix any raw data on the archive with this issue, but files may have been missed if they were observed on F158-F366, which were not uniformly reprocessed after the mission. The best way to deal with this glitch is to shift the array columns back into place and resave the raw file (rather than modifying BPMs or ignoring this issue). Use the bad pixel mask included with the pipeline to confirm the correct position of the columns.

Frequency: Uncommon
Severity: Moderate, if unaddressed.

Fix: This was fixed by shifting raw data back into place. If this is done there is no impact on the science data. All affected files within the scope of the post-mission reprocessing (F386 – F866) have been fixed.

4.5.6. Gain Differences Between Odd and Even Rows.

It is normal for raw EXES data to show count offsets between even and odd rows of ~ 200 DN (Figure 17). For the most part, the offset is eliminated in the first processing step where the detector planes are converted to net data counts. (RDC files for PIPEVERS =3.0.0dev or RAW files with PIPEVERS=1.0.2). However, there may still be subtle offsets between odd and even rows before nod-subtraction and flat division. These offsets are due to small differences in array gain between the odd rows and even rows. These gain offsets are usually corrected in flat fielding, and do not impact the final data products.
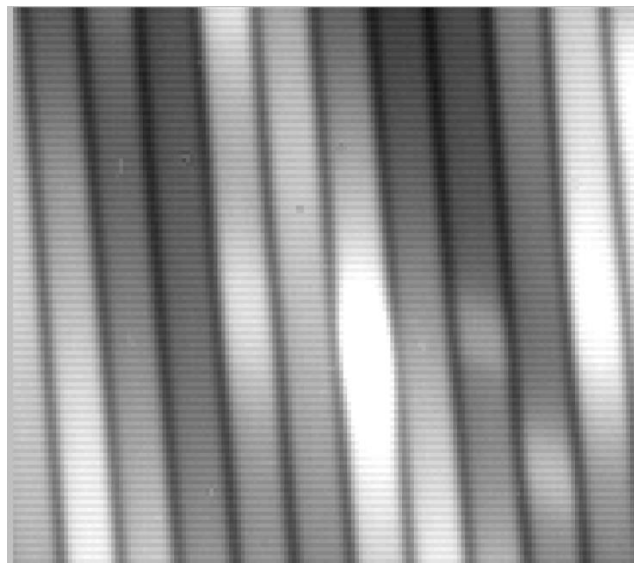
Figure 17 *Example of row gain differences between odd and even rows in an RDC file before sky subtraction.*

Even in the rare instances that some gain offsets remain, the oversampling of the PSF and the spectral resolution element means that the data can be binned by 2× and eliminate the residual odd-even effect.

Frequency: Common
Severity: Low
Fix: None required

4.5.7. Detector Burn-in and Latency

Occasionally the observation of a bright target would cause a persistent pattern to remain on the detector. The use of subarray mode and the return to full frame format also leaves a burn in pattern at the row borders of the subarray. These latency patterns tend to decay slowly over subsequent array reads and tended to remain until the detector anneal was performed, where the array temperature was heated above 25 K. These burned in patterns are removed in the sky subtraction pipeline step.

Frequency: Occasional
Severity: Low
Fix: None required

4.5.8. "Herring Bone Noise"

Electrical pickup from the motors and the blackbody power supply caused visible ripples in the background in nod-subtracted frames (Figure 18 and Figure 19). To avoid this, the EXES motors were powered off during science integrations.
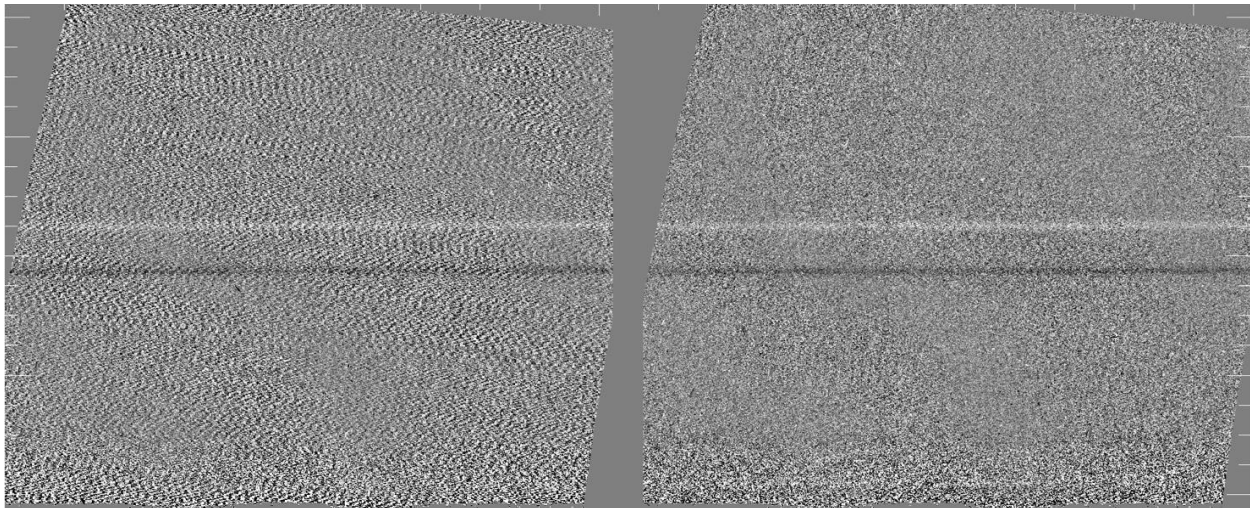
Figure 18 *(Left) Medium configuration spectra affected by herring bone noise when motor hold currents were left active during an exposure. (Right) A different frame taken after motor boxes were powered off.*
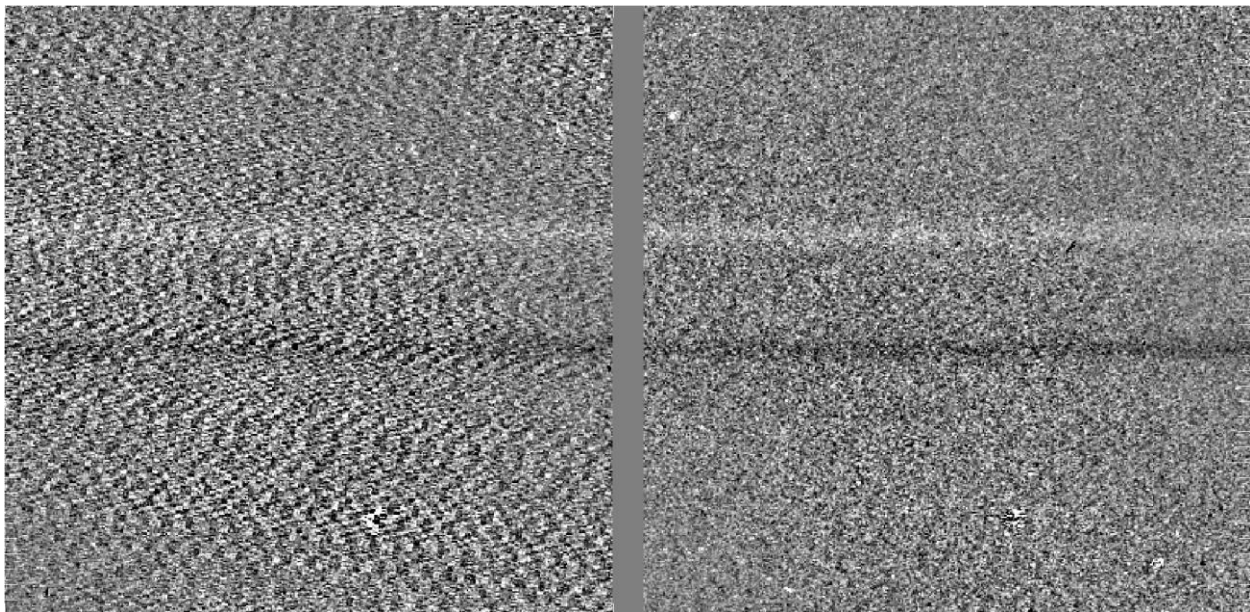
Figure 19 *Zoomed in view of Figure 18.*

Most of the Flight 362 science data was affected because the data taking commands failed to power off the motors. In later flights, herring bone noise can be occasionally seen in peak-up nod files or sky stares, where the data are not used for science products and the motors were left powered on for the sake of operational efficiency.

Frequency: Rare, except for F362 and earlier series
Severity: Low/Medium
Fix: None required. The data is usable but produces lower S/N spectra.

4.5.9. Tree Rings / First Read Issues
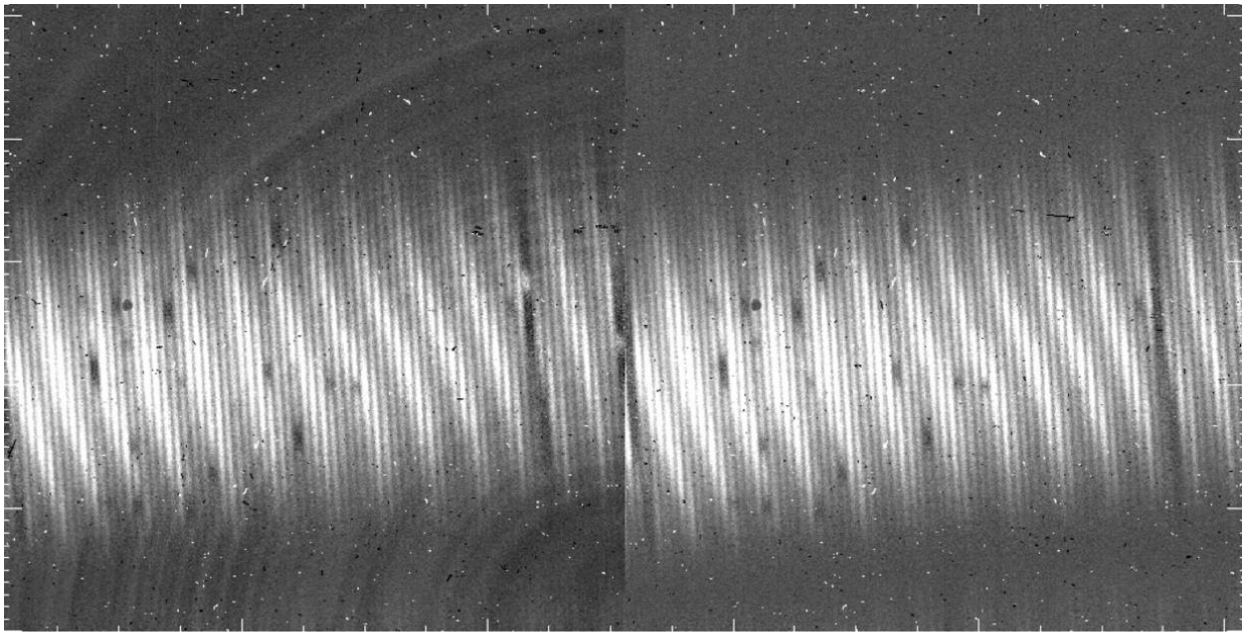
Figure 20 *(Left) An example of the first nod pair of a file which is marred by tree rings. (Right) This panel shows the same nod pair after the problematic 1st and 2nd B-side (sky) integrations were thrown away.*

The detector array often showed a pattern of noise that was called tree rings for the first integrations of a new file. When processed to nod-subtracted frames, the first nod-pair difference exhibits a background of concentric rings as seen in the left panel of Figure 20. This effect was only impactful for settings where the background count rate was very low. Therefore, only high-resolution modes of shorter wavelengths, >1250 cm-1 (<8.0 μm) required this correction.

The fix for this issue was to discard the first one or two integrations of a file, which allows the first nod pair to be used. A typical nodded file used four integrations per nod side and ran for four nod pairs. Discarding two integrations amounted to a 6.25 % loss to the total integration time in a file. This meant the B side of the nod has slightly reduced integration time, but removal of the problematic background pattern was deemed to be of higher importance.

The severity of this issue varied from flight series to flight series. In general, the fewest integrations possible were discarded that would reduce the tree ring appearance. High resolution data at longer

wavelengths (< 1200 cm^{-1}) or medium and low mode data did not require throwing away integrations because of their higher background count rates.

Frequency: Common
Severity: Medium
Fix: Throw away 1st or 1st and 2nd integrations in each nod file. Customarily done for all data included in post-mission reprocessing (F386 – F866). May not have been applied consistently in earlier data.

4.5.10. Amplifier Glitch

A transient effect in the raw data where one or two out of the four amplifier columns is elevated in DN to the other three (or two). The pattern repeats every four columns. It can also be seen to change abruptly at a particular row in the raw data. This effect can only be seen in the nod-subtracted data, because the amplitude is small compared to the sky background (Figure 21).
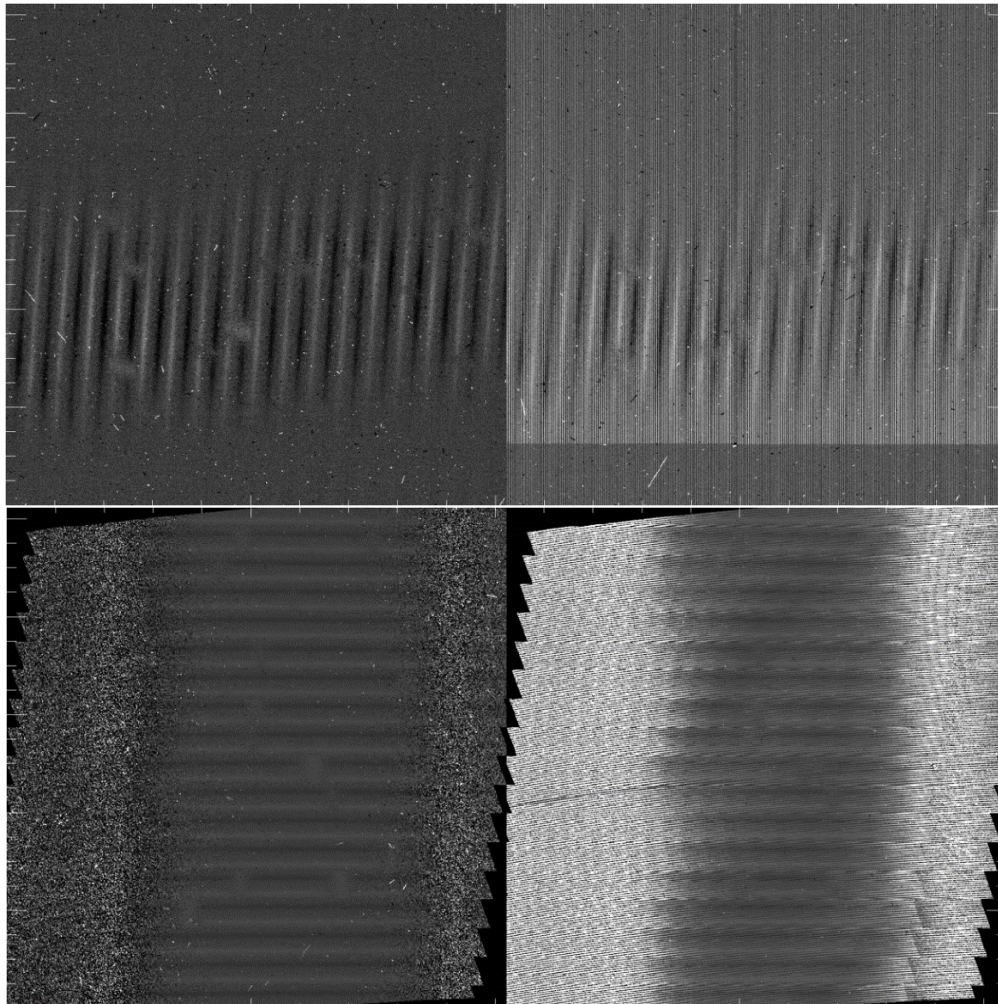
Figure 21 *(Top) A normal nod-pair and nod-pair affected by an amplifier glitch, before rectification. The data is nod-on-slit in high-medium mode at 1748 cm^{-1} (5.72mm). In this instance, it is the 2rd amplifier that has a raised reset level relative to the 1st, 3rd and 4th. The offset level changes again between y = 124 and y=125. (Bottom) The same nod-pairs following the rectification, which can be seen in the CCR files.*

Frequency: Occasional for Flights F829-F866
Severity: Medium/Severe
Fix: Affected data was discarded from reductions, or occasionally included where the glitch location didn't impact the data. Fixing the planes at the RDC file stage and rerunning the pipeline is possible, but is cumbersome and must be done on an array plane-by-plane basis. The offsets from the affected amplifier column are constant with respect to the other three amplifier columns, so the median values can be equalized on each affected sector of the array.

4.6. SKY SUBTRACTION RESIDUALS

Sky emission lines are generally far brighter than the science targets and do not always cancel out during nod subtraction. This section shows some of the variety of sky line residuals in EXES data and some of the procedures used by the pipeline to improve the cancellation. Sky line residuals tend to cancel with longer integrations and greater numbers of nod-pairs. Fainter science targets will always be more affected than brighter targets. Because the strength and shape of sky lines changes over time, the time span between sky subtraction is usually linked to how well it cancels. Nodded data is sky-subtracted at intervals of 2 minutes or less, but mapped observations sample the sky background just once per map file, which can take 5-10 minutes to execute. Nodded observations therefore tend to have lower sky line residuals than mapped data. However, when mapped targets were exceptionally bright, like Mars and Jupiter, emission residuals can go unnoticed.

4.6.1. Residuals in Nod-On-Slit vs Nod-Off-Slit Modes

Data taken with nod-on-slit mode has the potential to fully cancel the residual emission for any integration length, as long as the A and B side observations of the target are well-balanced. Therefore, the sky line residuals usually only have to be considered for nod-off-slit and mapped data.

In Figure 22, a sequence of nod-pairs viewed at the UND step is shown to illustrate the variety that residual emission can take over a short time period. The strong, broad lines are CO_2. The residual CO_2 emission is strongly negative in pair 1 and strongly positive in pair 4. In nod pair 3, the CO_2 lines actually have both faint positive residuals in the line wings and negative residuals in the line core at the same time. The narrow line residuals in Figure 22 are due to O_3. They show a negative/positive pattern across the line width due to small shifts in the line center between the A and B beams. This could be due to atmospheric motions, but it is more likely due to flexure changes in the spectrograph chamber.

Figure 23 shows a segment of MRD for a long integration of Orion IRc2 in high_low, nod-off-slit mode (05_0043_31). The strongest CO_2 line obviously contains residual negative emission because it goes below 0. The weaker telluric lines in the rest of the range seem to have cancelled, but it would be hard to be certain. (The triangular lines with no counterpart in the red transmission model are due to real source absorption caused by HCN.)

In contrast to the nod-off-slit observation of IRc2, the nod-on-slit observation of NGC 7538 IRS 1 in Figure 24 shows no signs of residual emission, and the continuum shape is well-fit by a telluric model, and drops to zero flux in the middle of the strong CO_2 as expected. (There are also HCN lines in the spectrum.)
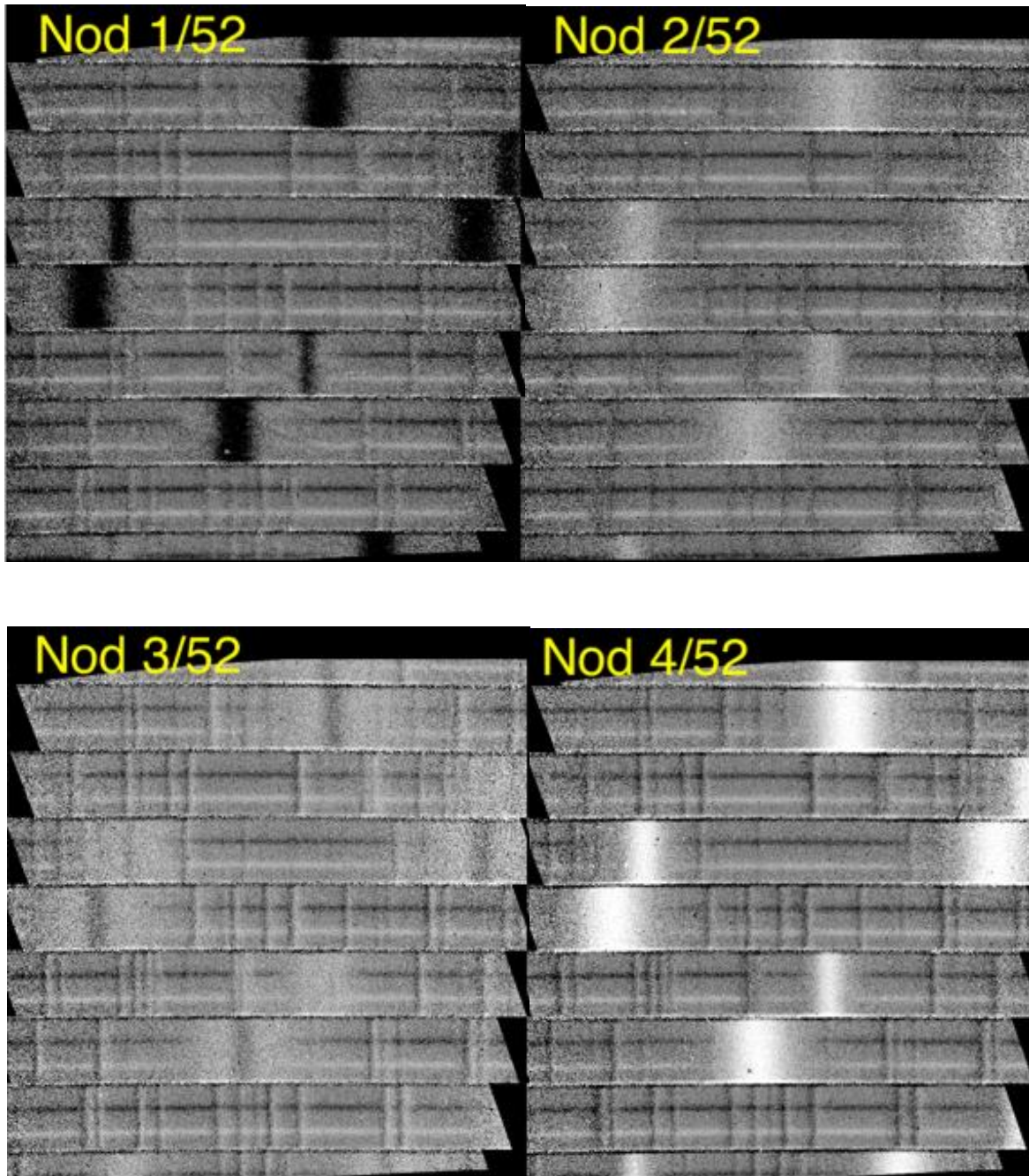
Figure 22 *The first four nod pairs of a 56-nod sequence for the high-medium, 714 cm^{-1} (14 mm) observation of NGC 7538 IRS 9 (AOR_ID=75_0024_16). The strong, broad CO_2 lines are the most prominent atmospheric lines, showing a variety of degrees of non-cancellation. The CO_2 lines in Nod 3/52 show both faint positive residuals from the line wings and negative residuals in the line core at the same time. The narrow lines are due to O_3. The residuals of O_3 can have a negative /positive residual on the left and right edges of the line. This is probably due to tiny shifts caused by flexure in the spectrograph chamber.*
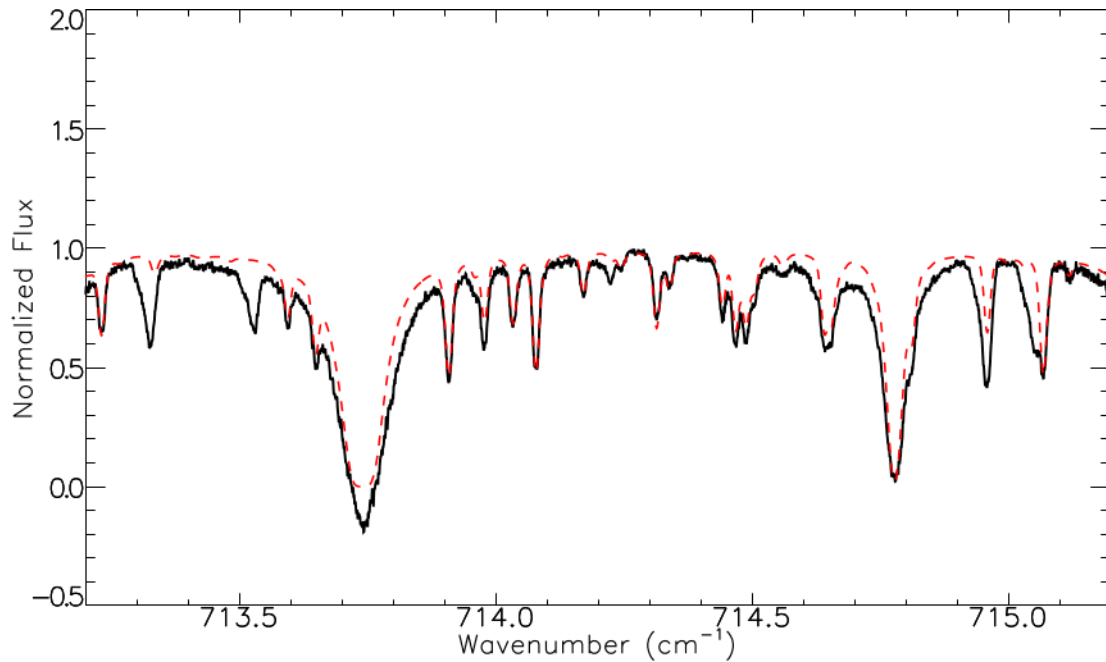
Figure 23 *Orion IRc2 observed in High-low config, nodding off slit. Red – telluric model. Nod-off-slit observations are more susceptible to nod residuals, particularly from strong features like the broad CO_2 lines, which here are seen to go below 0 flux, which is unphysical and can only be due to nod-residuals. Altitude 43000 ft Airmass = 1.3.*
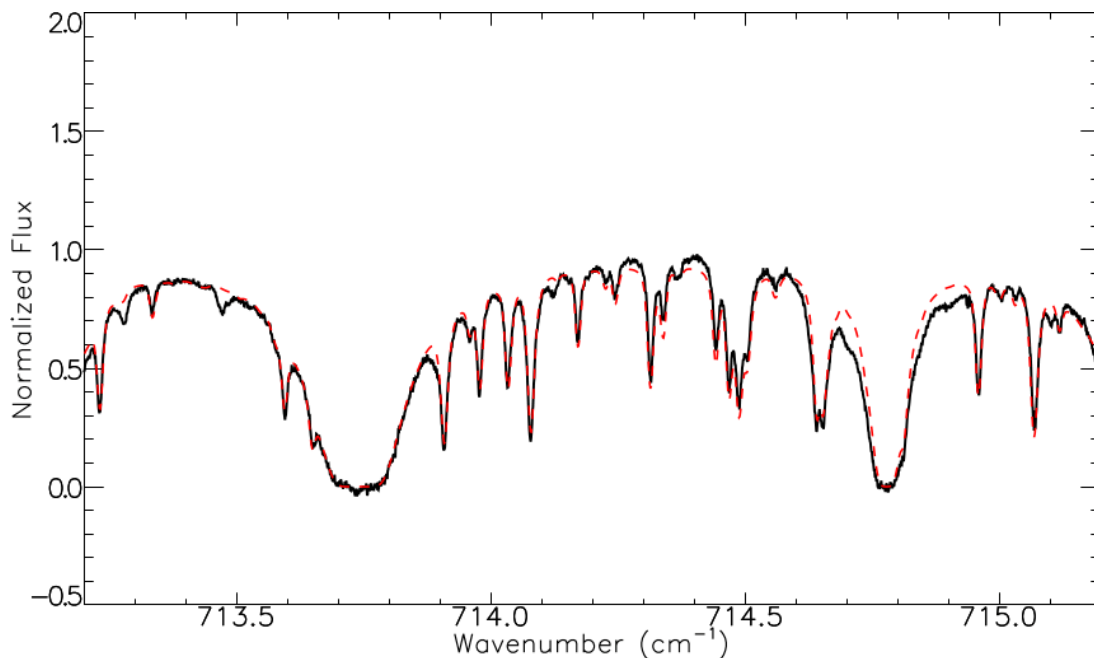
Figure 24 *NGC 7538 IRS 1 was observed at the same wavelengths as Orion IRc2 shown in <u>Figure 23</u>, but used nod-on-slit mode instead of nod-off-slit mode. Nod-on-slit observations usually do not have strong residual emission because the beams can be forced to cancel. Here NGC 7538 IRS 1 shows that even observed at lower altitude and higher airmass, the CO_2 lines go to zero where they are supposed to. Altitude 41000 ft Airmass = 2.1.*
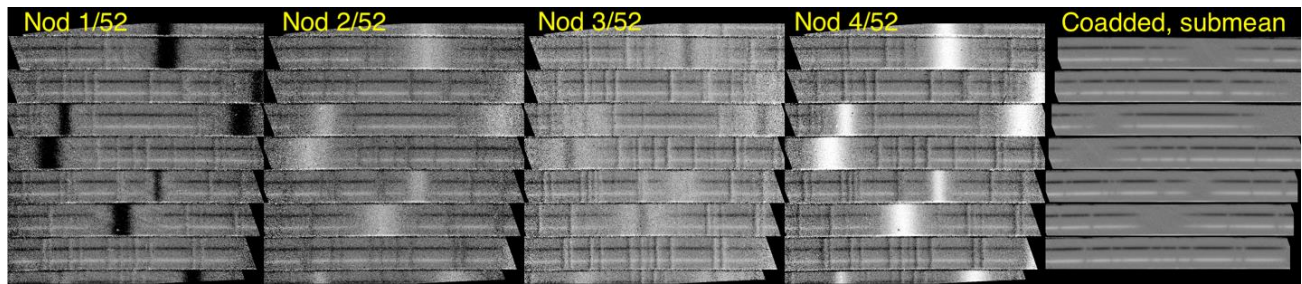
Figure 25 *Residual removal with "submean" in the coadd nods step.*

With enough nod iterations, residuals tend to cancel out, but when they do not, and the data is taken in "INSTMODE =NOD_ON_SLIT", they can be suppressed by the pipeline procedure called "submean" where the channel residuals are zeroed out based on the assumption that A and B beams are equal and opposite valued. This is illustrated in Figure 25, where the final 2D spectrum has been cleaned of residuals with this pipeline routine. Wherever possible, submean has been used for nod-on-slit mode data in the IRSA archive.

4.6.2. Background subtraction

For data taken in nod-off-sky mode it is sometimes possible to subtract a background region in a clear region along the slit to remove telluric residuals. At minimum this requires a slit that is larger than the PSF size, but this can be complicated if the source emission is extended.

Figure 26 and Figure 27 show how this procedure was applied to the medium configuration observation of IC 443B at 1447cm^{-1} (6.91 μm).
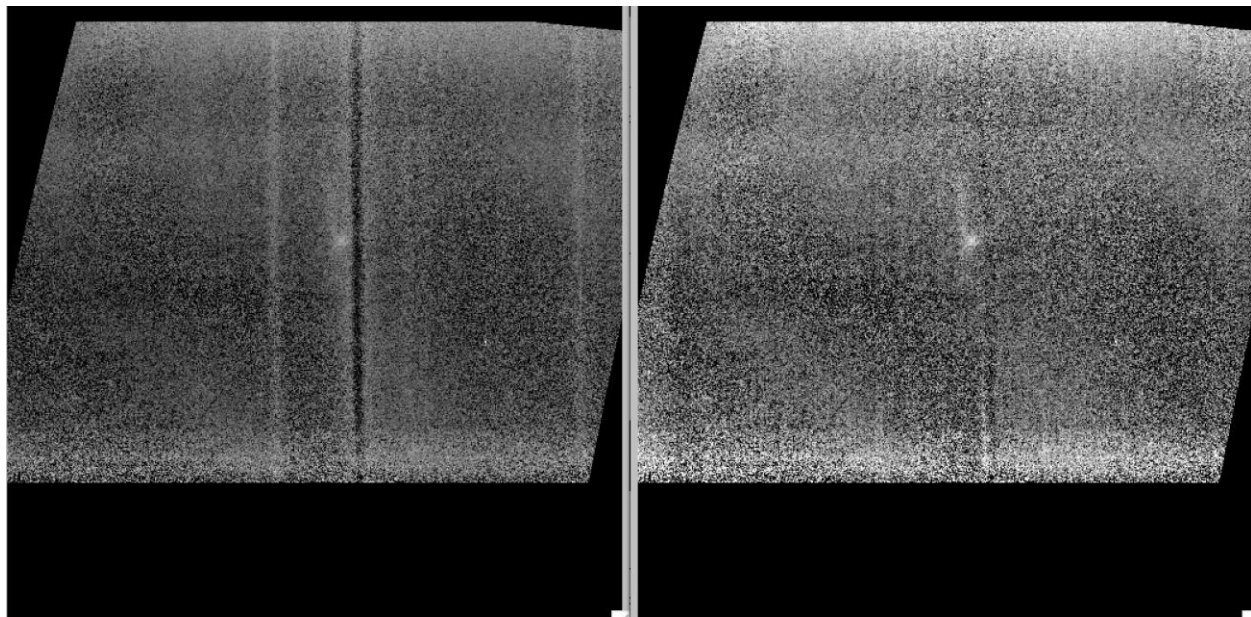
Figure 26 *A medium configuration observation of the supernova remnant IC 443 B has H$_2$ emission close to a strong negative atmospheric residual. Subtracting a background aperture away from the emission is effective at removing the residual, revealing more structural detail in the source.*
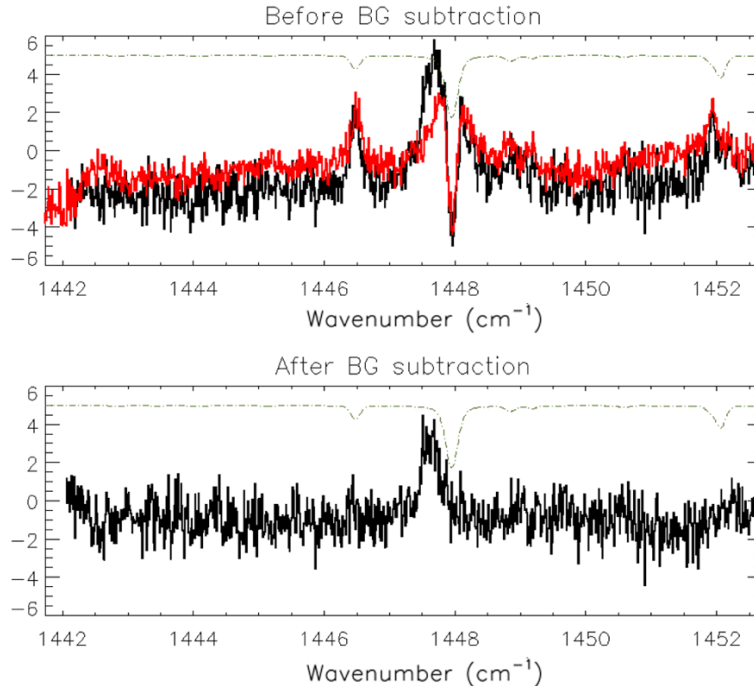
Figure 27 *The 1D spectral extraction of the emission clump from IC 443 B before and after background subtraction.*

Unfortunately, if an observation is taken with a short slit in nod-off-slit mode, and there is insufficient space to extract a background, there are few options to remove the residual emission, short of modelling and subtracting the residual pattern.

4.6.3. Off-sky contamination

Occasionally, off sky coordinates were not completely clear of emission, and cancelled emission from the on-source target. This was a rare occurrence; however, there was a recurrent case when observing massive YSOs in complicated star forming regions, where forbidden line emission was found to be much more extended than the dusty continuum of the protostars. The off-sky coordinates were clear of continuum emission, but at the frequencies of the forbidden emission lines, there would be a tangled mess of emission and spurious absorption (high-ionization potential lines are unlikely to form an absorption line because of the required gas densities.)

Figure 28 and Figure 29 show the example of Orion IRc2 at 534 cm^{-1} where the bright [S III] line appears as a reverse P-Cygni line. The echellogram (COA) even shows negative values, which are certainly unphysical and are due to [S III] emission in the off-source sky position.

4.7. FRINGING

Like most other IR spectrographs, EXES suffers from fringing in all its modes and at all wavelengths.

4.7.1. Fringing in the HIGH_LOW and HIGH_MEDIUM configuration

In the high-resolution configurations between $1250 - 1850$ cm^{-1} ($5.4 - 8$ μm), the most prominent fringes have a spacing of about 0.5-0.6 cm^{-1}, with maximum amplitudes up to 20% of the continuum.
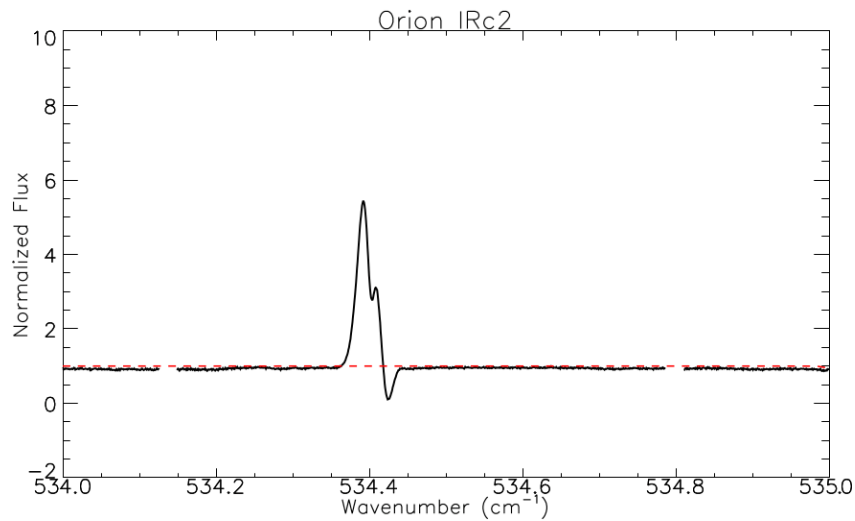
Figure 28 *The 18.7 μm [S III] emission toward Orion IRc2 is probably in the foreground Orion Nebula (M42) and extends over both the on source and off source positions, resulting in an inverse P-Cygni like appearance. The high ionization potential of the [S III] line makes it very unlikely the line could be seen in absorption, and over-subtraction from the off-source beam is far more likely.*
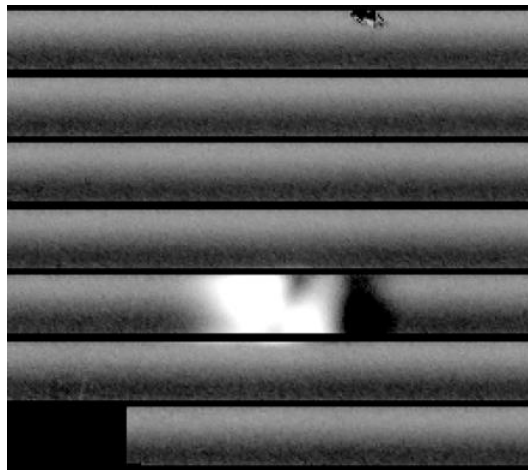
Figure 29 *The 2D spectrum of the [S III] line emission even shows negative values, which is not-physically possible and must be due to oversubtraction from the B (off-source sky) coordinate.*

The periods, phase, and amplitudes are usually stable across different observations. Therefore, if a telluric calibrator shares the same instrument configuration and slit width, then it is likely to be effective for fringe suppression, particularly if observed in the same flight series. However, the vast majority of observations don't have suitable telluric calibrators and users must often use their own telluric correction strategies, which usually don't address fringing.

One strategy is to perform baseline corrections for each emission / absorption line. Generally, this means finding regions with pure continuum at lower and higher frequencies than the line of interest and fitting a line or other low order polynomial to divide out and level the feature before extracting the line parameters. In Barr et al. (2020), the authors chose linear baseline corrections for each of

the ~200-300 H_2O absorption lines toward HMYSOs AFGL 2591 and AFGL 2136, because linear corrections are less sensitive to the placement of the continuum than higher order polynomials.
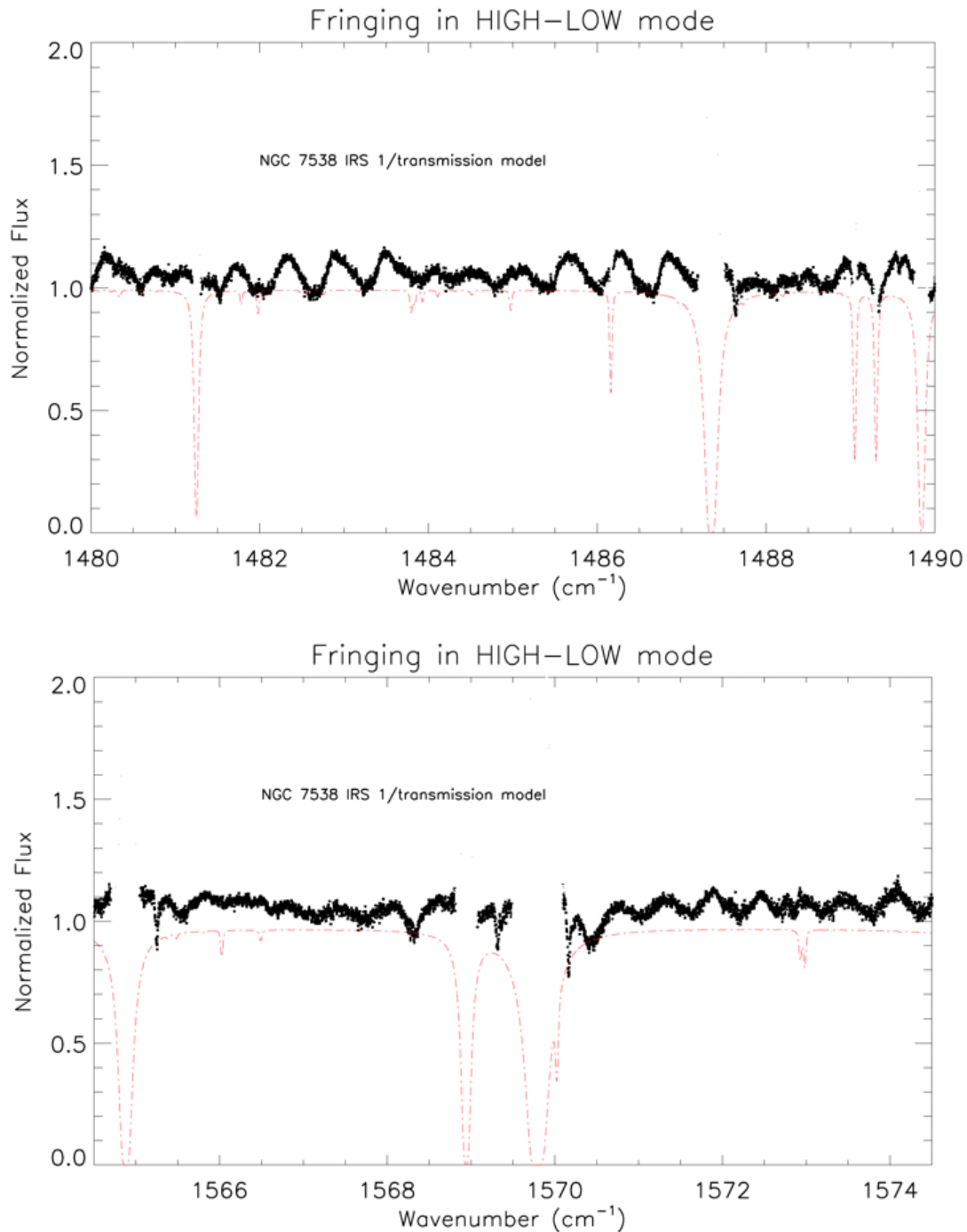
Figure 30 *(Top) Segment of a high-low spectrum (R = 59000) centered at 1485cm^{-1} (6.73 μm) for NGC 7538 IRS 1. The fringe amplitude can be up to 18% of the continuum level. (Bottom) Segment of a high-low spectrum (R=59000) centered at 1570cm^{-1} (6.37 μm) for NGC 7538 IRS 1. The amplitude of the fringing is about 10% of the continuum.*

The spectral regions between 550-800 cm^{-1} (12 – 17 μm) likely have fringing, but due to the densely spaced atmospheric lines of O_3 and CO_2, the periods and amplitude are difficult to characterize. At wavenumbers below 550 cm^{-1} (λ > 17 μm), the baselines appear to be shaped by more than just fringing. Some settings show baseline variations that seem to be tied to the relative position along an order, like an upward curl or droop. Fortunately, most of the spectral lines of interest are far narrower than the erratic but broad continuum variations; simple polynomial fits to the baseline around the lines will be effective for analysis.
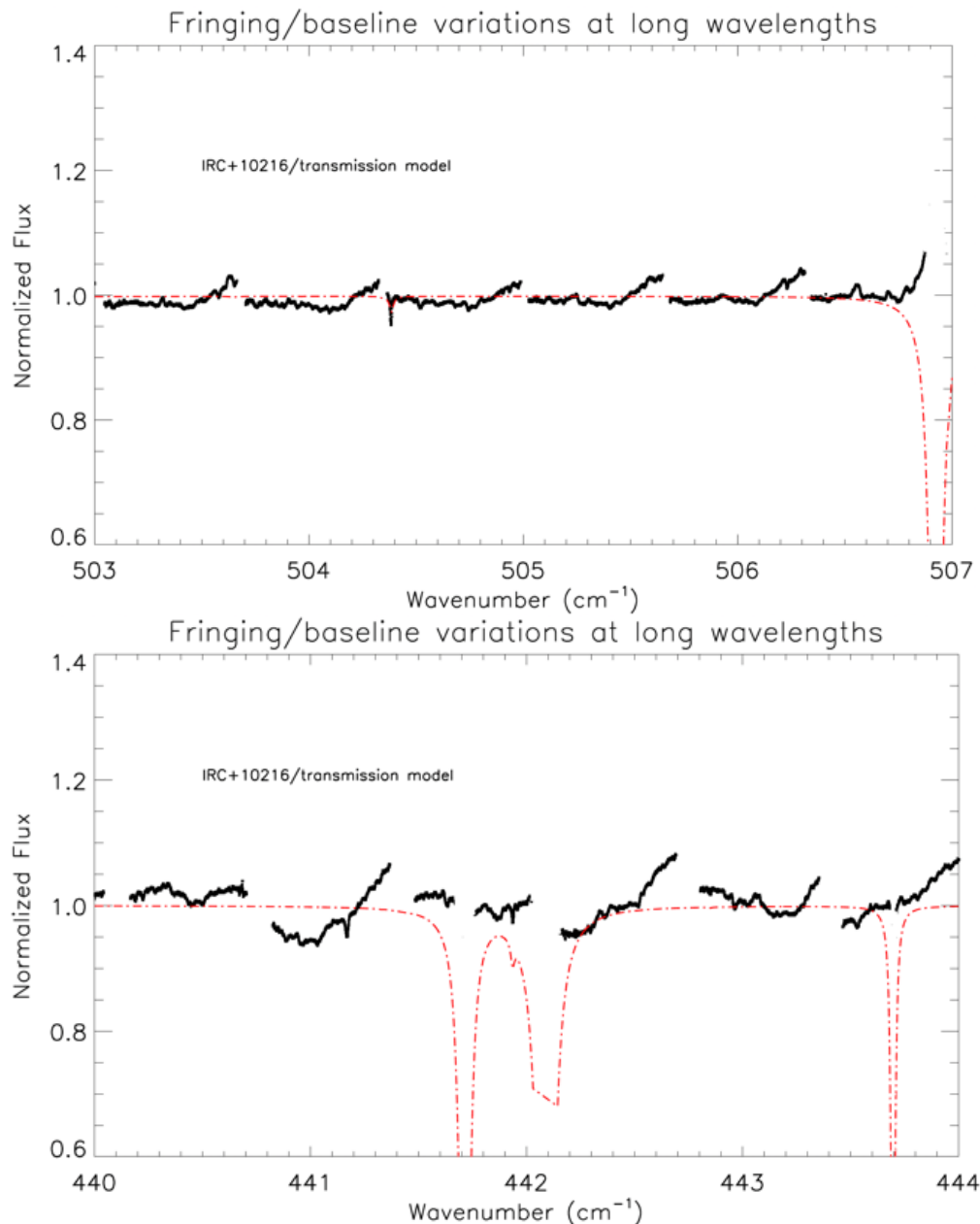
Figure 31 *IRC +10216 at 507cm^{-1} and 443 cm^{-1}. Instead of periodic fringing, there seems to be a repeating structure in the orders, like the upward curl on the higher wn side of the orders. There are many narrow molecular lines from the source in these spectra which are not really affected by the broad baseline variations.*
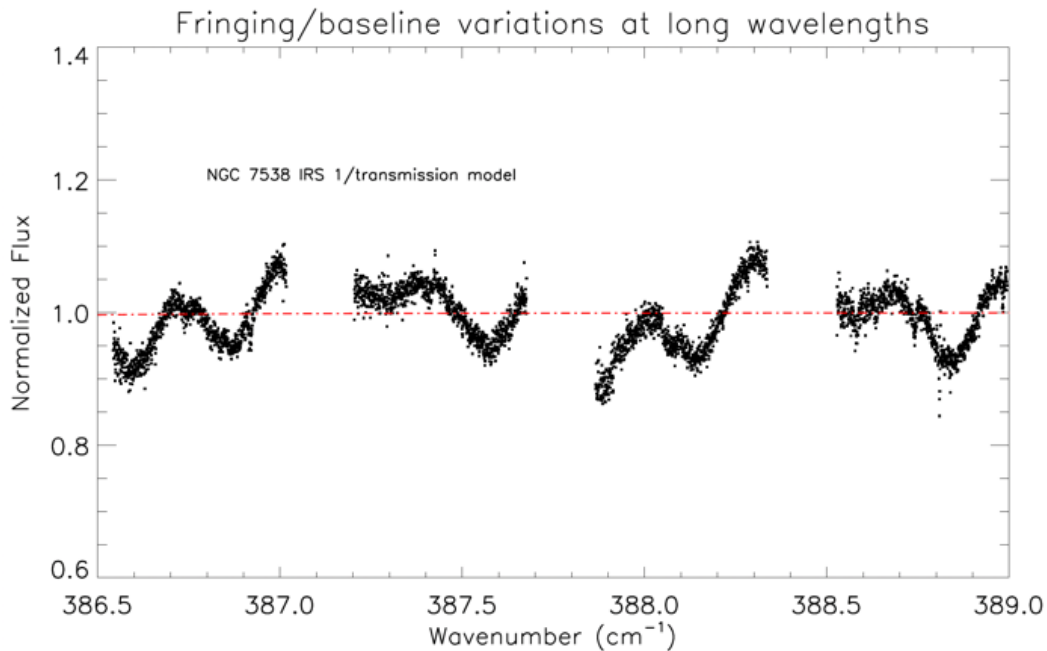
Figure 32 *NGC 7538 IRS 1, HIGH_LOW, 385 cm^{-1}, appears to show something more like standard fringing. Like IRC +10216, there are numerous narrow lines that can be analyzed despite the broad baseline variations.*

Figure 30, Figure 31, and Figure 32 are three representative examples of fringing or baseline irregularities in long wavelength observations of high-low or high-medium mode.

4.7.2. Real spectral features that look like fringing in high-resolution configurations

EXES observed many mass-losing stars with highly excited H_2O or hydrocarbon bands which superficially resemble fringing. Users will have to be alert to the details of their targets. Two examples of real source H_2O features in evolved stars are shown in Figure 33. Compared to Figure 30 which shows the typical instrumental fringing near these wavelengths, the H_2O line spacing is higher in frequency and has irregular spacings, which of course match to the known wavenumbers of a highly excited H_2O population.

4.7.3. Fringing in MEDIUM and LOW configurations

Medium and low-resolution configurations show fringing as well. The typical periods are 3-4 cm^{-1}, with amplitudes of 5-10 % in medium and 10-25% for low mode. Medium observations were usually taken with the target and calibrator of adjacent flight legs. In these cases, the calibrator was often effective as a direct divisor that removed both atmospheric absorption and fringing. Figure 34 shows an example of a medium configuration observation with typical fringing properties.

In low, the fringing is more severe than medium. The phase and amplitude were seen to vary with each new source acquisition. Thus, the telluric calibrators are unlikely to fully correct for fringes by simply dividing. However, the defringing tools written for JWST MIRI-MRS have been used successfully to fit and remove fringes from spectra taken in the EXES low configuration

(Pendleton et al., in prep). Figure 35 shows an example of a low configuration observation with typical fringing characteristics.
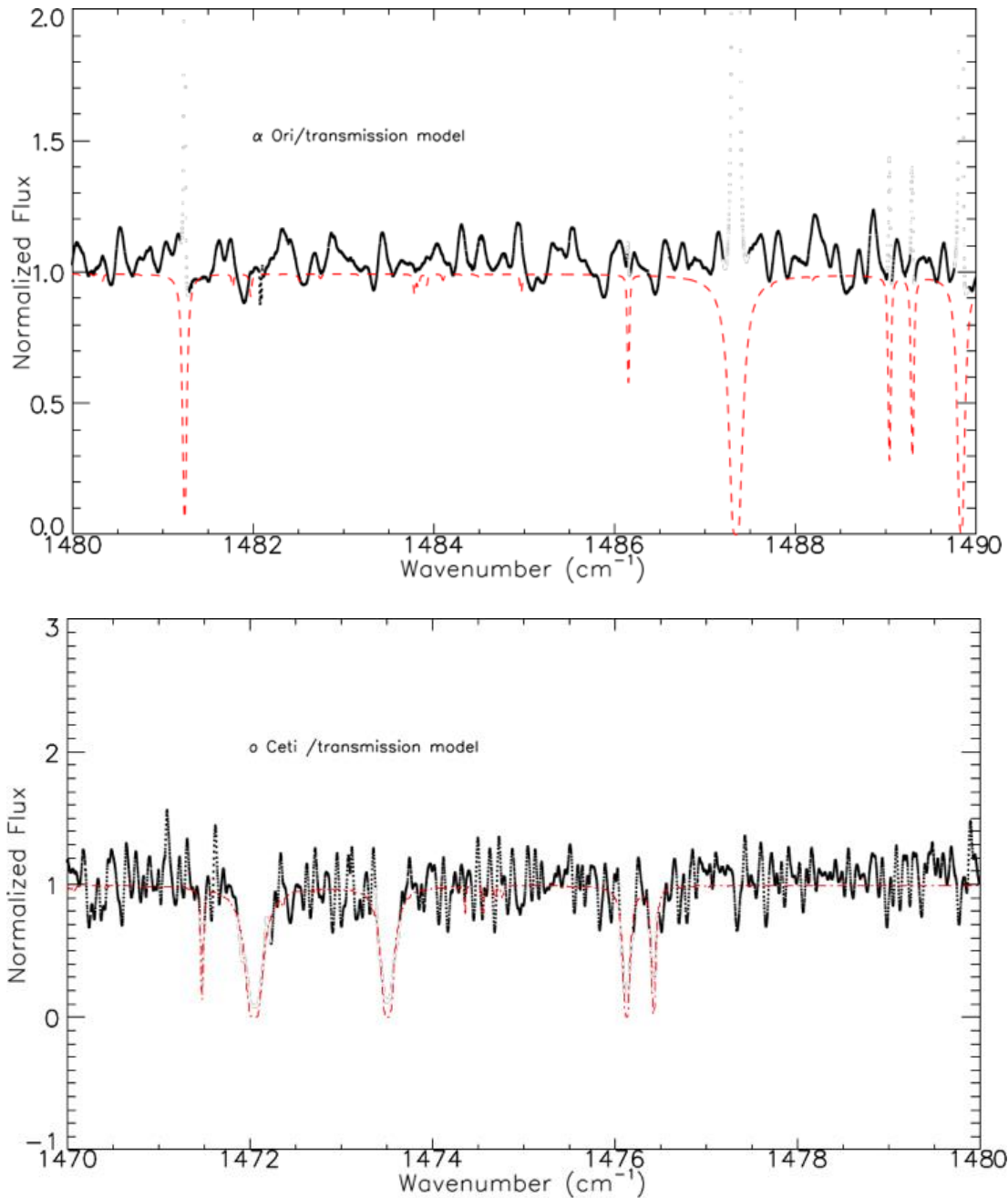

Figure 33 *Two examples of spectra with densely space H_2O P-Cygni lines. (Top) Betelgeuse (α Ori), M supergiant. (Bottom) Mira (o Ceti), symbiotic binary with mass-losing asymptotic giant branch star primary.*
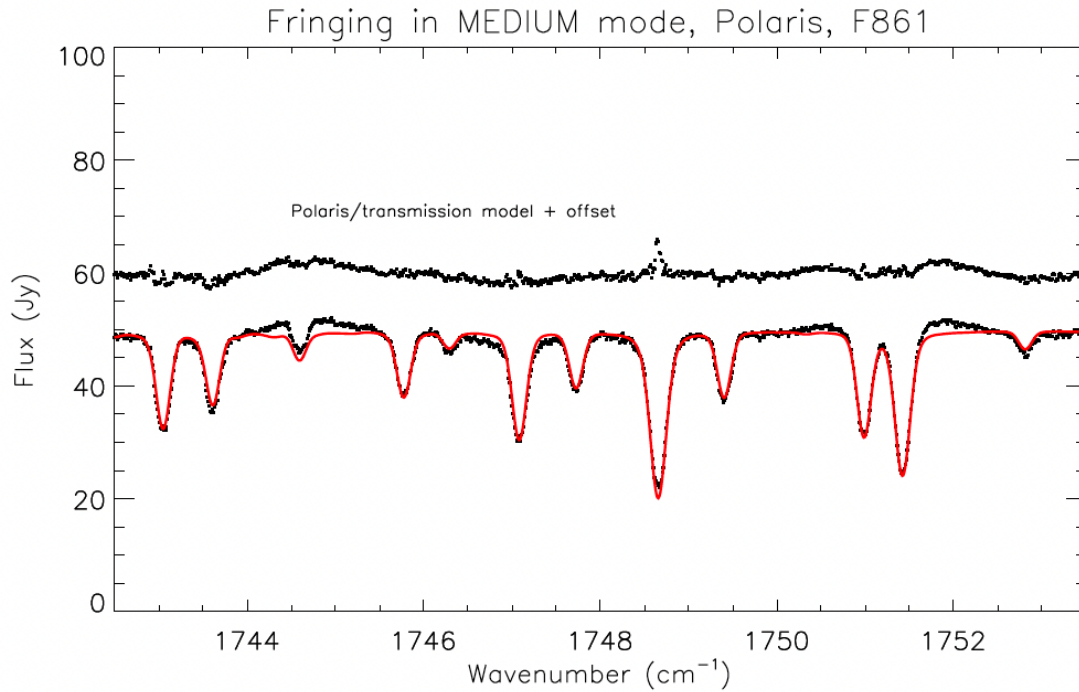
Figure 34 *The medium observation (R=13600) of Polaris has low amplitude fringing (8%) with a period of about 4 cm⁻¹. Medium mode observations almost always are accompanied by an adjacently observed telluric calibrator which is effective at removing the fringes.*
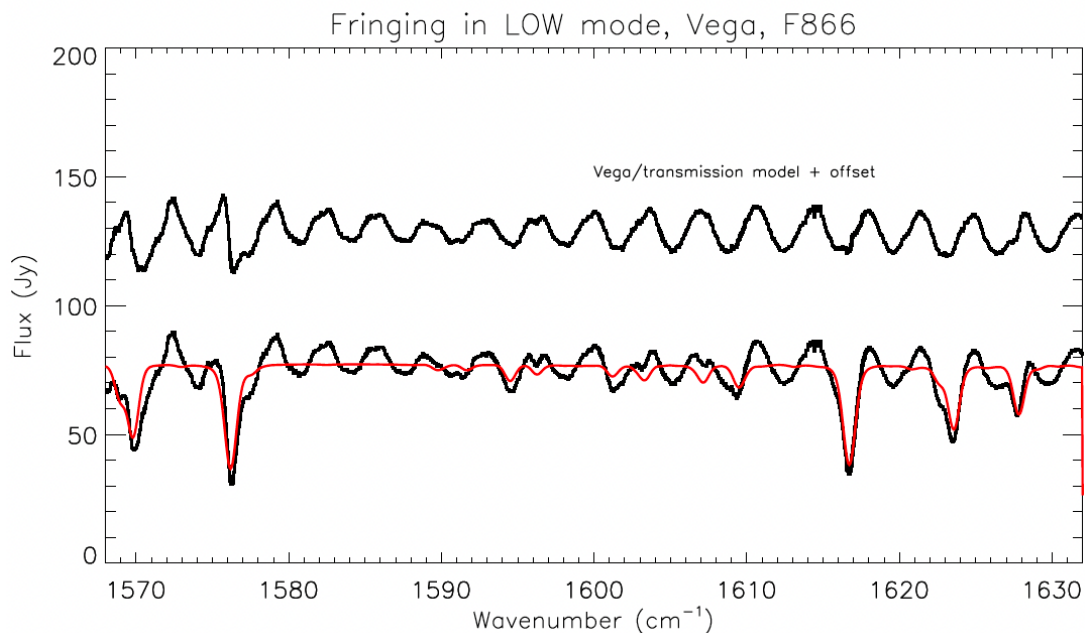
Figure 35 *Fringing in the EXES low mode seen in the example of Vega 3rd order, at 1600cm⁻¹ (6.25 μm). This observation was taken to be a calibrator for the science target, Cyg OB 2-12, but the phase and amplitude are seen to vary between the observations.*

5. SCIENTIFIC RESULTS

EXES is the first high-resolution spectrograph with nearly full access to the wavelengths in the thermal infrared. This unique capability enabled discoveries of the chemistry and kinematics in high-mass star forming regions, circumstellar envelopes of evolved stars, and direct observations of H_2 gas in a variety of astrophysical environments.

5.1. SURVEYING WARM GAS TOWARD MASSIVE PROTOSTARS

The first science paper from EXES was Indriolo et al. (2015), where 6 μm observations of the massive YSO AFGL 2591 was presented. The EXES observations spectrally resolved H_2O absorption first seen at low resolution with ISO/SWS.
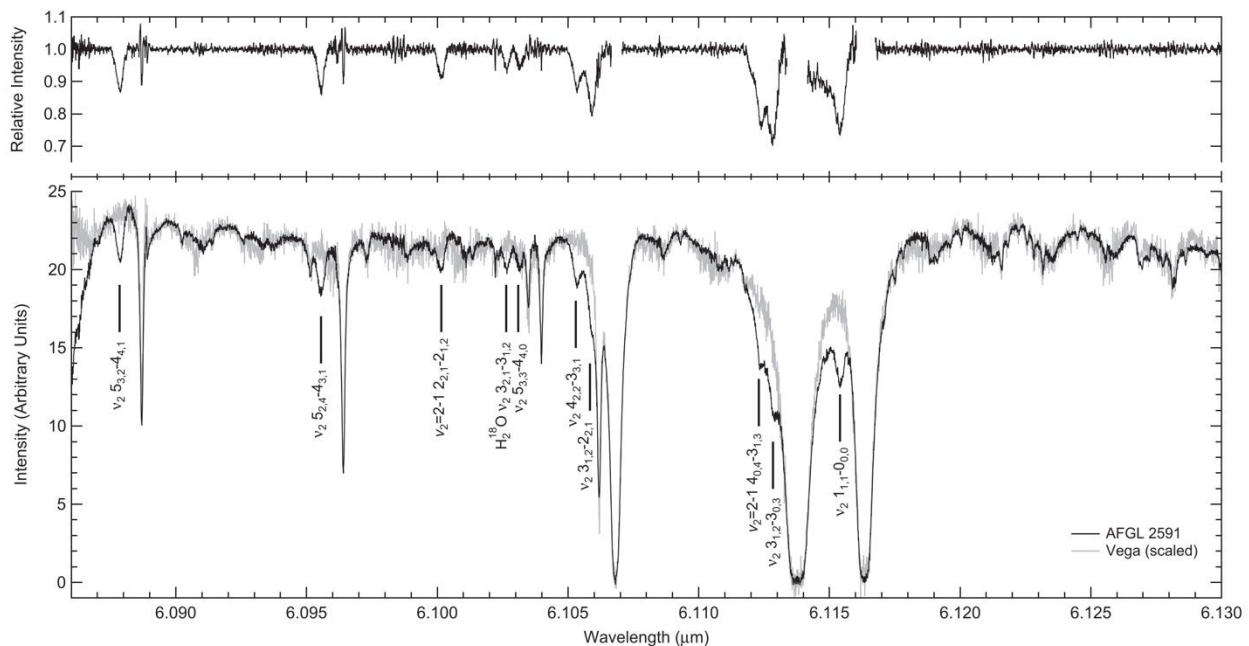
Figure 36 *Figure 1 from Indriolo et al. (2015). The bottom panel displays the EXES MRD product for both AFGL 2591 and the hot star Vega, which served as a telluric calibrator. Transitions from H_2O toward AFGL 2591 are labeled. The top panel contains the result of dividing the AFGL 2591 spectrum by a boxcar averaged Vega.*

This work demonstrated the power of EXES high spectral resolution at SOFIA altitudes for observing H_2O, a species which is normally impossible to study from the ground. The study confirmed warm and abundant water (T = 640 K, N(H2O) = 1.3 x 10^{19} cm^{-2}) toward this source but that there was a large scatter in the rotation diagram. They interpreted this as optical depth effects from the gas molecules being mixed with the continuum forming dust.

Nickerson et al. (2023) presented an inventory of molecules toward Orion IRc2, including isotopologues and isotopomers, detected in the EXES observation. These were HCN, $H^{13}CN$, HNC, SiO, SO_2, CH_4, NH_3, H_2O, $^{12}C_2H_2$, $^{13}C^{12}CH_2$, and H_2. Several of these species do not have permanent dipole moments, which means they can only be detected starting at mid-IR wavelengths and shorter. Most of the molecular lines showed two distinct kinematic components, dubbed the

"blue" and "red" clumps; the red component is only seen toward IRc2, but absorption from the blue component appears against many other IR sources toward BNKL.
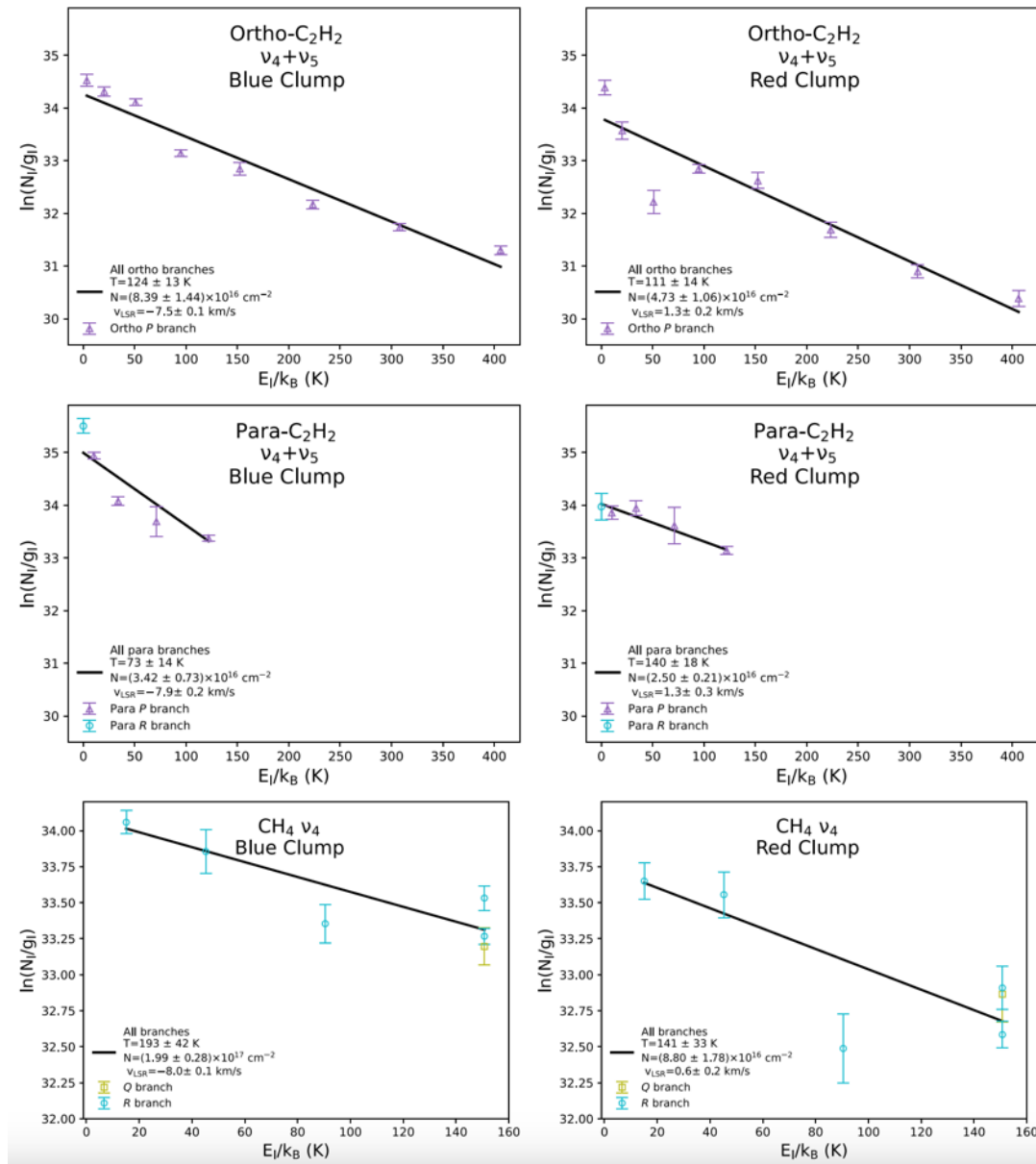

Figure 37 *A subset of the rotation diagrams presented originally as Figure 5 in Nickerson et al. (2023).*

Barr et al. (2018) presented the first ro-vibrational detections of CS towards AFGL 2591, which provides information deep into the hot core near the base of the outflow.

Barr et al. (2020) combined SOFIA/EXES, IRTF/TEXES, and IRTF/iSHELL to present a molecular inventory for both AFGL 2591 and AFGL 2136. The molecules detected were CO, CS (see rotation diagrams in Figure 38), HCN, NH_3, H_2O, and C_2H_2. These molecules were all detected in absorption and suggested to originate in the accretion disk thought to surround these sources.
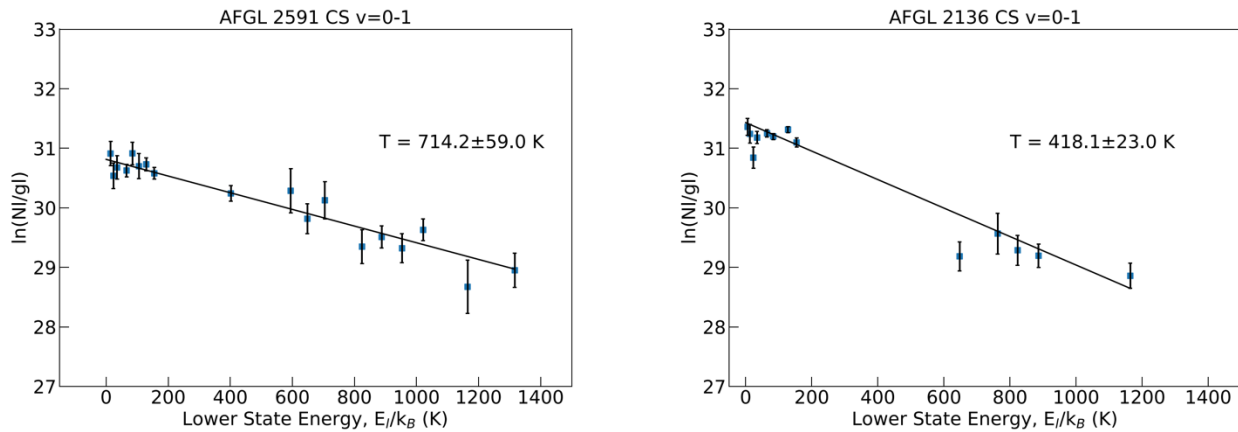
Figure 38 *Rotation diagrams for CS in both AFGL 2591 and AFGL 2136. Originally presented as Figure 5 in Barr et al. (2020).*

Barr et al. (2022) performed a detailed study of the H_2O absorption features in both AFGL 2591 and AFGL 2136. A new curve-of-method based on stellar atmosphere theory was deployed and used to show that the overall 5.5 – 8.0 μm water features are best explained if they arise in the atmosphere of a viscously-heated accretion disk.

Li et al. (2023) also studied ro-vibrational H_2O absorption from 5.5-8.0 μm in the high-mass binary YSO, W3 IRS 5. The complexity of this massive protostellar environment was revealed through multiple absorbing components with distinct temperatures and velocities, including: a hot H_2O population near both protostars, cold envelope gas, and warm absorption from the shocked clumps of gas that may be responsible for well-studied masers toward this source at millimeter wavelengths.

5.2. MOLECULAR HYDROGEN OBSERVATIONS

Molecular hydrogen (H_2) is the most abundant molecule in the universe. It also lacks a permanent dipole moment due to being homonuclear, which means it can only be studied in the mid-IR and shorter wavelengths. EXES has detected this molecule in a diverse set of astrophysical environments. This includes H_2 S(0) and S(1) maps of Jupiter during EXES' commissioning flights, the outflows of evolved stars, and different types of shocked environments.

Neufeld et al. (2019) observed H_2 S(4), S(5), S(6), and S(7) toward the protostellar bow shock, HH7. The velocity shift between the ortho- and para- hydrogen lines demonstrated the conversion from para- to ortho-H_2 for the first time within a shock, and at the same time gave the best evidence to date for the existence of non-dissociative continuous (C-type) shocks.

Reach et al. (2019) presented velocity resolved profiles of the H_2 S(5) line toward four different positions (Clump C, Clump G, and two positions in Clump B – labeled B1 and B2) of the supernova remnant IC 443. Detailed shock modelling showed that Clumps C and G are described well by C-type shocks, while Clump B2 was best described by a jump (J-type) shock. Clump B1 was found to be best described by a combined C- and J-type shock, which was used to infer a change in magnetic field direction between Clumps B1 and B2.
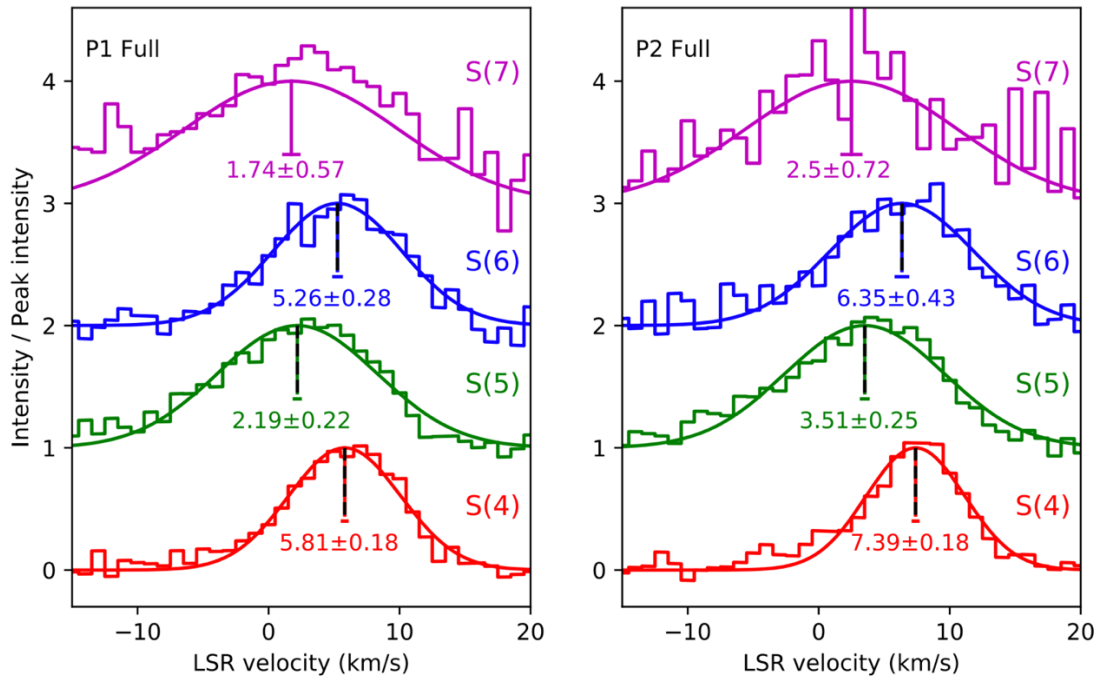
Figure 39 *Combined H₂ line profiles for both observed positions. The change in velocity centroids indicate the para-to-ortho conversion of H₂. This is reproduced from the bottom part of Figure 2 of Neufeld et al. (2019).*

Soam et al. (2021) presented observations of the S(1) and S(5) transitions of H₂ toward the photon dominated region (PDR) IC 63, which probed different UV irradiation levels from the star γ Cas. The observations allowed a direct measurement of the gas temperatures at these different positions, and elucidated how excitation temperatures respond to UV illumination.

Fonfría et al. (2022) presented the first direct detection of H₂, via the S(1) transition toward the outflow of an AGB star (IRC +10216). This allowed for the direct measurement of the mass-loss rate = $(2.43 \pm 0.21) \times 10^{-5}$ M$_\odot$ yr^{-1}, and ratio of CO to H₂ $(6.7 \pm 1.4) \times 10^{-4}$.
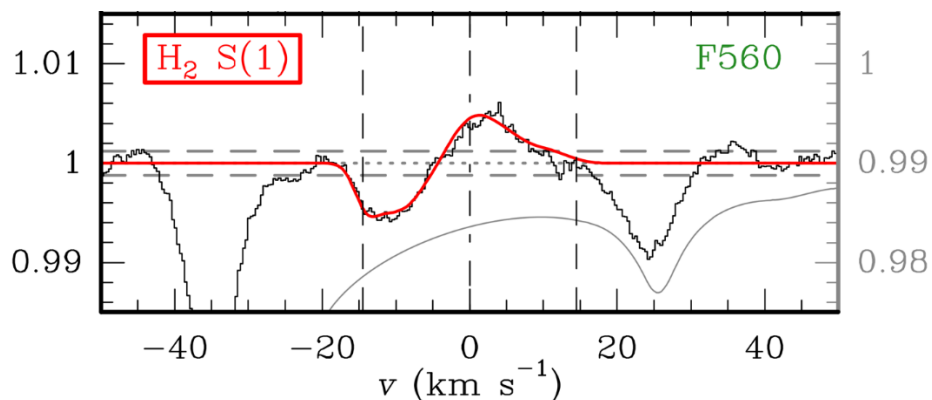
Figure 40 *The bottom panel of Figure 1 from Fonfría et al. (2022) with the detection of the S(1) transition of molecular hydrogen.*

6. REFERENCES

- Barr, A., et al. 2018, ApJ, 868, 2, doi: 10.3847/2041-8213/aaeb23
- Barr, A., et al. 2020, ApJ, 900, 104, doi: 10.3847/1538-4357/abab05
- Barr, A., et al. 2022, ApJ, 935, 165, doi: 10.3847/1538-4357/ac74b8
- Clarke, M., et al. 2015, Astronomical Data Analysis Software and Systems XXIV. 495, 355, website: https://articles.adsabs.harvard.edu/pdf/2015ASPC..495..355C
- Encrenaz, T., et al., 2013, A&A, 559, 65, doi: 10.1051/0004-6361/201322264
- Fonfria, J.P., et al. 2022, ApJ, 927, 33, doi: 10.3847/2041-8213/ac5a58
- Indriolo, N., et al. 2015, ApJ, 802, 14, doi: 10.1088/2041-8205/802/2/L14
- Li, J., et al. 2023, ApJ, 953, 103, doi: 10.3847/1538-4357/ace16e
- Lord, S.D. 1992, NASA Technical Memorandum, 103957, website: https://ntrs.nasa.gov/citations/19930010877
- Neufeld, D., et al. 2019, ApJL, 878, 18, doi: 10.3847/2041-8213/ab2249
- Nickerson, S., et al. 2023, ApJ, 945, 26, doi: 10.3847/1538-4357/aca6e8
- Reach, W., et al. 2019, ApJ, 884, 81, doi: 10.3847/1538-4357/ab41f7
- Richter, M.J., et al. 2018, JAI, 7, 1840013-1, doi: 10.1142/S2251171718400135
- Soam, A., et al. 2021, ApJ, 923, 107, doi: 10.3847/1538-4357/ac2eb7
- Sparks, W.B., et al. 2019, ApJL, 871, L5, doi: 10.3847/2041-8213/aafb0a
- Temi, P., et al. 2018, JAI, 7, 1840011-1, doi: 10.1142/S2251171718400111
- Villanueva, G., et al. 2018, Journal of Quantitative Spectroscopy and Radiative Transfer, 217, 86, doi: 10.1016/j.jqsrt.2018.05.023
- Woodward, C., et al. 2020, AJ, 159, 87, doi: 10.3847/1538-3881/ab67c2

APPENDIX

A. Using Telluric Calibrator Observations

EXES observed telluric calibrators for a small fraction of its projects. Due to the complexities of airborne observing scheduling, these telluric calibrators were costly to the observatory efficiency and proposers were encouraged to limit their calibrator requests in order to prioritize data collection of the science targets, and then rely on synthetic modelling of the atmospheric transmission.

An exception was made for medium and low-resolution observations because it was found to be difficult to disentangle instrumental baseline from spectroscopic features. Therefore, for such observations, a calibrator was usually observed adjacent to the science observation, without moving any instrument motors between the observations.

If there was a designated telluric calibrator for an observation, this is noted in the header COMMENT of the data which will include the AOR_ID of the calibrator so that it can be located in the archive.

The instrumental baseline and order shape are more likely to change over long times and with the adjustments made to the EXES internal optical alignment that happened between flight series. Because of this, the calibrator's usefulness is usually related to how close in time to the science target it was observed.

B. Wavenumber maps and spatial maps, order boundaries

In the 2D spectra after rectification the wavenumber channels are aligned in one dimension and the spatial channels are aligned in the orthogonal dimension. The wavenumber and spatial data planes can be viewed by loading extension 6 and 7 respectively of the UND, COA, or CAL files, (or their sky spectrum equivalents, see Section 4.1.8).

In the IDL pipeline (PIPEVERS = 1_0_2), UND and COA files only had one extension, which included all the flux plans and all the flux variance planes.

The wavenumber and spatial maps were located in a separate WVM file within the first plane and the second plane of the WVM, respectively.

The x, y coordinates of the order edges are recorded as a comma separated list in these header keywords:
>   ORDR_B: bottom edge of order
>   ORDR_T: top edge of order
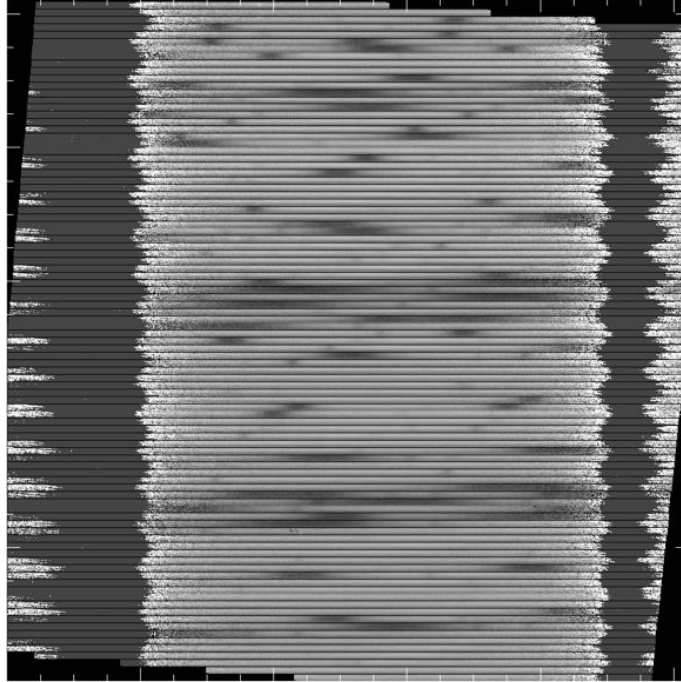>   ORDR_S: left edge of order
>   ORDR_E: right edge of order

Figure 41 *The COA (or CCR, UND, or CAL file) contains the 2D intensity of the cross-dispersed spectral orders, after steps like flat division, rectification, and coadding of the nod pairs are completed. It is in extension = 0.*
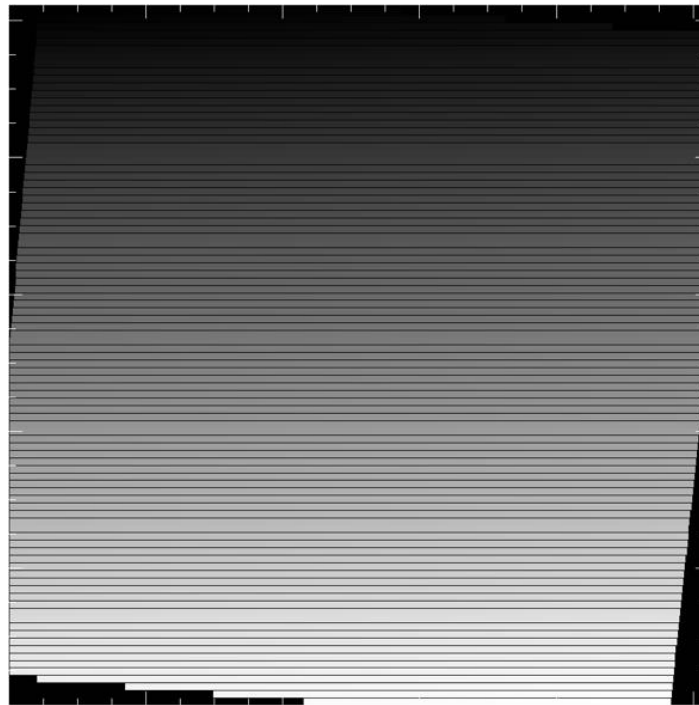

Figure 42 *The wavenumber map is aligned to the rectified order positions in the 2D intensity planes. It is located in extension = 6 of the 2D data for PIPEVERS =3_0_0dev. For PIPEVERS = 1.0.2, it is the first plane in the WVM file.*
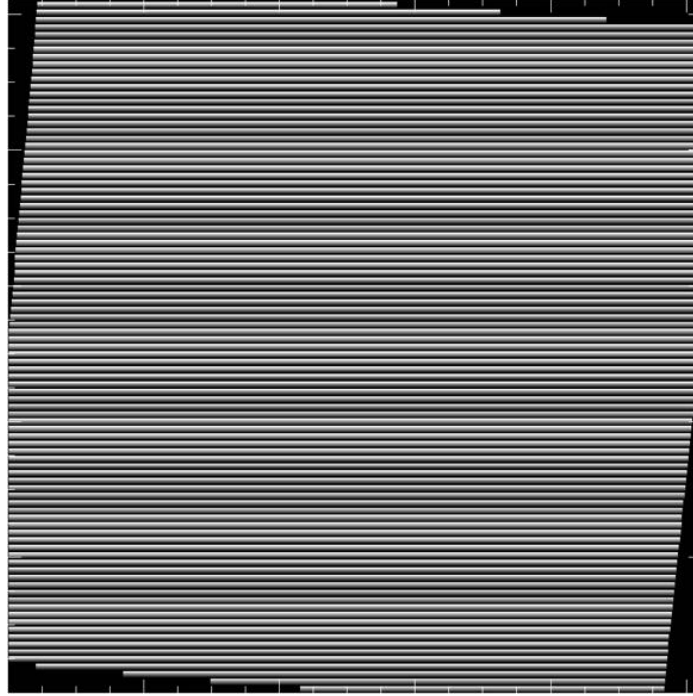
Figure 43 *The spatial map gives the relative spatial coordinate from the bottom to the top of the slit, in arcsec. It can be found in the extension =7 plane of the 2D spectra files for PIPEVERS =3_0_0dev. The pixel spacing of the spatial channels is PLTSCALE in the headers. For PIPEVERS = 1.0.2, it is the second plane of the WVM file.*

C. Custom extractions of extended source without the redux pipeline

All nodded observations have 1D extracted spectra included in the archive. However, users may not wish to be limited to the extraction region chosen for the archive spectra. This section guides the user to make their own custom extractions.

As an example, the Supernovae remnant IC 443 C was observed on F830 at 1447cm^{-1} for the sake of the H_2 S(5) line. The line is bright and there was no detectable continuum. Figure 44 shows the 2D spectrum from the CAL file of this observation, which shows that the H_2 emission is concentrated in the middle of the 9 arcsec slit.

The H_2 line appears in the in the 8th order of the archive SPC file, which is shown in Figure 45. It has been summed over a specified extraction region and converted to Jy. The extraction area is defined by three values: the spatial center, the spatial width and the slit width. These values are specified as the header keywords, APPOS**XX**, APRAD**XX** and SLTW_ARC, respectively. **XX** refers to the different orders but APPOS and APRAD are fixed to the same values for standard extractions.

In this example, APRAD = 4″ and SLTW_ARC = 2.11″. Thus, the solid angle of the extraction was:

$$\Omega = 2*\text{APRAD}*\text{SLTW\_ARC} = 2*(4.0″)*2.11″ = 16.9 \text{ arcsec}^2.$$

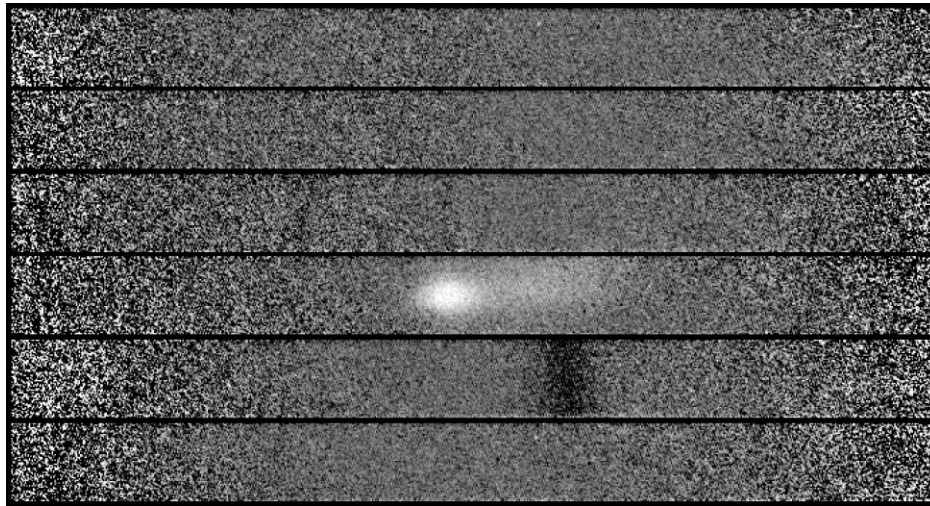To convert the spectrum to flux per solid angle, simply divide the SPC by Ω.

Figure 44 *A section of the COA file of an observation of IC 443 C with H_2 S(5) line emission. The dark line in the order below the H_2 line is due to residuals from sky subtraction.*
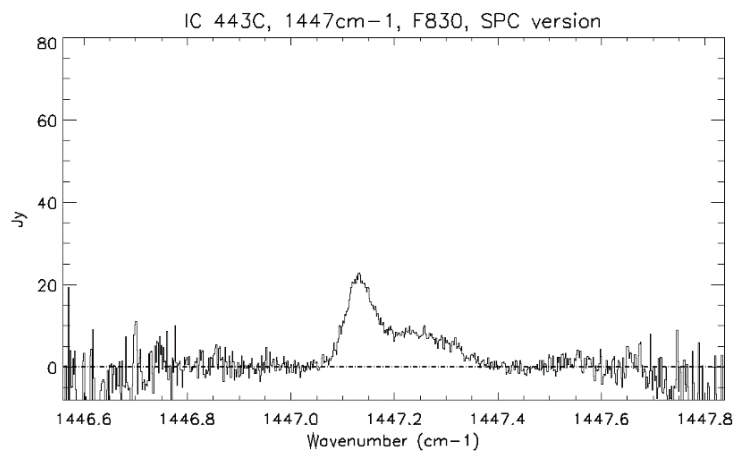

Figure 45 *The H2 S(5) detection of IC 443C as seen in the SPC file.*

Figure 46 shows that choice to extract +/- 4″ of the slit dilutes the emission. To make a custom extraction of the inner +/- 2 arcsec, simply take the sum of the CAL 2D spectrum. Find the order edge coordinates for the order with the H_2 line emission. In this example the relevant order is the 8th order which is highlighted in the header entries below. The relevant header entries are printed below, with the 8th order highlighted in blue:

    ORDERS = 1,2,3,4,5,6,7,8,9,10,11,12,13,14,15,16
    ORDR_B = 929,867,806,744,682,621,559,498,436,374,313,251,190,128,66,5
    ORDR_T = 986,924,863,801,739,678,616,555,493,431,370,308,247,185,123,62

The 2D wavelength scale can be loaded from extension = 6 of the CAL or COA frame. The wavelength along the order is a constant value along columns, so this 1D array can be extracted

with array[*, *X*], where *X* is any value 498 ≤ *X* ≤ 555. The central pixel along the slit will be ORDR_B + 29, approximately, at y = 527. Each pixel along the slit has a spatial size PLTSCALE, which in this case is PLTSCALE = 0.17119371".

For the +/- 4" extraction, one can simply compute $\sum$ CAL[*, 498+29 − 23: 498+29 + 23]. The beam area is Ω (±4″) = 16.9 arcsec². For an alternative extraction that sums the inner +/- 2", compute $\sum$ CAL[*, 527 − 12: 527 + 12]. The beam area is Ω(±2″) = 8.4 arcsec².

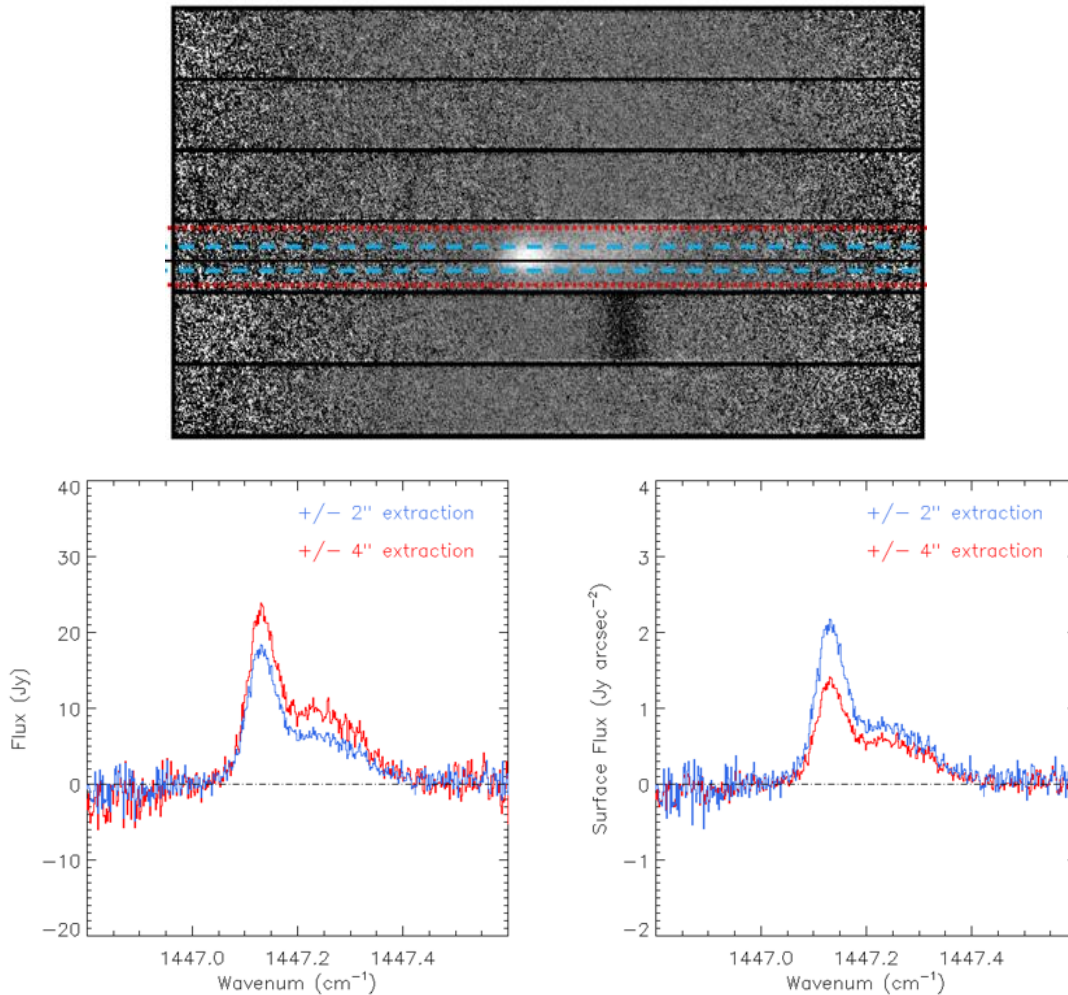<u>Figure 46</u> shows the differences between these two extractions.

Figure 46 *The default SPC file in the archive sums over +/- 4″, which is marked with the red lines on the 2D spectrum, and in blue on the 1D spectra. A custom version that sums over +/- 2″ is shown in blue. The total extracted flux is shown in the lower left panel, and the flux per solid angle is shown in the lower right panel.*